The Hope Fault at Hossack Station east of Hanmer Basin, North Canterbury

A thesis
submitted in partial fulfilment
of the requirements for the degree
of Master of Science in Engineering Geology
in the
University of Canterbury
by

T.J. McMorran

University of Canterbury
1991

THESIS with 3 separate items in back pocket.

Frontispiece Erosion of intensely fractured Torlesse basement within the Hope Fault Zone immediately west of the Boundary Stream locality.

Abstract

Oblique convergence of the Pacific and Australian Plates is accommodated in the northern South Island by the Marlborough Fault System. The Hope Fault is the southern of four major dextral strike-slip faults of this system. Hanmer Basin is a probable segment boundary between the Hope River and Conway segments of the Hope Fault. The Conway segment is transpressional and shows increasing structural complexity near the segment boundary at Hanmer Basin, with multiple Late Quaternary traces, and fault-parallel folding in response to across-fault shortening.

Between Hossack Station and Hanmer Basin a crush zone in excess of one kilometre wide is exposed in incised streams and rivers. The crush zone has an asymmetrical geometry about the active trace of the Hope Fault, being only 100-300 metres wide south of the fault, and more than 500 metres wide north of the fault. The most intense deformation of Torlesse bedrock occurs at the south side of the fault zone, indicating that strain is accommodated against the fault footwall. North of the fault deformation is less intense, but occurs over a wider area. The wide fault zone at Hossack Station may reflect divergence of the Hanmer Fault, a major splay of the Hope Fault.

At Hossack Station, the Hope Fault has accommodated at least 260 metres of dextral displacement during the Holocene. Dating of abandoned stream channels, offset by the Hope Fault, indicated a Late Holocene dextral slip-rate of 18 ± 8 mm^{-1} for the west end of the Conway segment.

Using empirical formulae and inferred fault parameters, the expected magnitude of an earthquake generated by the Conway segment is M6.9 to M7.4; for an exceedence probability of 10%, the magnitude is M7.7 to M7.9. Effects associated with coseismic rupture of the Conway segment include shaking of up to MMIX along the ruptured fault and at Hanmer Basin.

Uplift at the east end of Hanmer Basin, in conjunction with subsidence at the southwest margin of the basin, is resulting in the development of onlapping stratigraphy. Seismic reflection profiles support this theory. Possible along-fault migration of the basin is inferred to be a consequence of non-parallelism of the master faults.

Acknowledgements

Dr Jarg Pettinga supervised this thesis, and arranged for funding as part of the North Canterbury Active Tectonics Group; I would like to express my thanks to him for all his help throughout this project.

I would like to thank Andy Nicol for many interesting and useful discussions about this project, for help with fieldwork in Hanmer Basin and for most helpful editing. Thanks also to Hugh Cowan for his excellent editing.

The trenching programme that was undertaken late in 1990, involving several hours in cold, muddy water. Thanks go to those who helped with this work: Jarg Pettinga, Jocelyn Campbell, Hugh Cowan and Andy Nicol.

I am very greatful to Mick Gray for his terrific hospitality at Hossack Station; what a beautiful place it is! Thanks also to Laurie Ray for some interesting discussions.

Thanks to Rich Little and Patrick McMorran for help with fieldwork at Hossack Station on various occasions.

I would like to thank Dr Ray Wood for providing me with the included seismic profiles, and for helpful comments. Thanks also to Dr Alan Hogg at the Radiocarbon Dating Laboratory, Waikato University, for very rapid calculation of calibrated radiocarbon ages.

Special thanks to Karen Paterson for encouragement, especially at the thesis production part of the project, and for taking the excellent photographs.

Finally, thanks to two anonymous donations, for the production of this thesis.

Table of contents

Chapter one

INTRODUCTION

Chapter two

GEOLOGY AND GEOMORPHOLOGY OF THE HOPE FAULT ZONE: HOSSACK STATION TO EAST HANMER BASIN

Chapter three

LATE QUATERNARY DISPLACEMENTS AND RATES OF SLIP ON THE HOPE FAULT AT HOSSACK STATION

Chapter four

THE EVOLUTION OF HANMER BASIN

Chapter five

Summary and Conclusions

Table of Figures

CHAPTER ONE

Introduction

1.1 Study objectives

The objectives of this thesis are to detail the structural geometry and rate of Late Quaternary displacement on the Hope Fault between the eastern end of Hanmer Basin and Little Lottery River (Figure 1.1). Studies of Late Quaternary displacements on the Hope Fault and structures relating to fault displacements have previously been carried out by looking at surface trace morphology and displaced features at a number of localities (Freund 1971; Knuepfer 1984; Van Dissen 1989; Cowan 1989,1990). However the basement deformation associated with movement of the Hope Fault and the rate of Late Quaternary slip at eastern Hanmer Basin have not been extensively studied. To describe the three-dimensional structure of the exposed Hope Fault Zone at eastern Hanmer Basin is an intension of this study. Specific objectives undertaken by this thesis are as follows.

1. To map the Hope Fault Zone in the area of Hossack Station, east Hanmer Basin, in order to produce neotectonic maps showing detailed geological, structural and geomorphological data - suitable for incorporating with other similar maps compiled by the North Canterbury Active Tectonics Group. To use this data to establish a structural model for the west end of the Conway segment (Bull et al. 1991) of the Hope Fault and discuss the implications of the model for the Hope Fault as a whole.

2. To determine fault displacements, movement history and slip-rates for this segment of the fault, using the age and displacement of offset geomorphological features, determined by strategic trenching and surveying.

3. Following assessment of fault geometry and fault movement history, to evaluate seismic

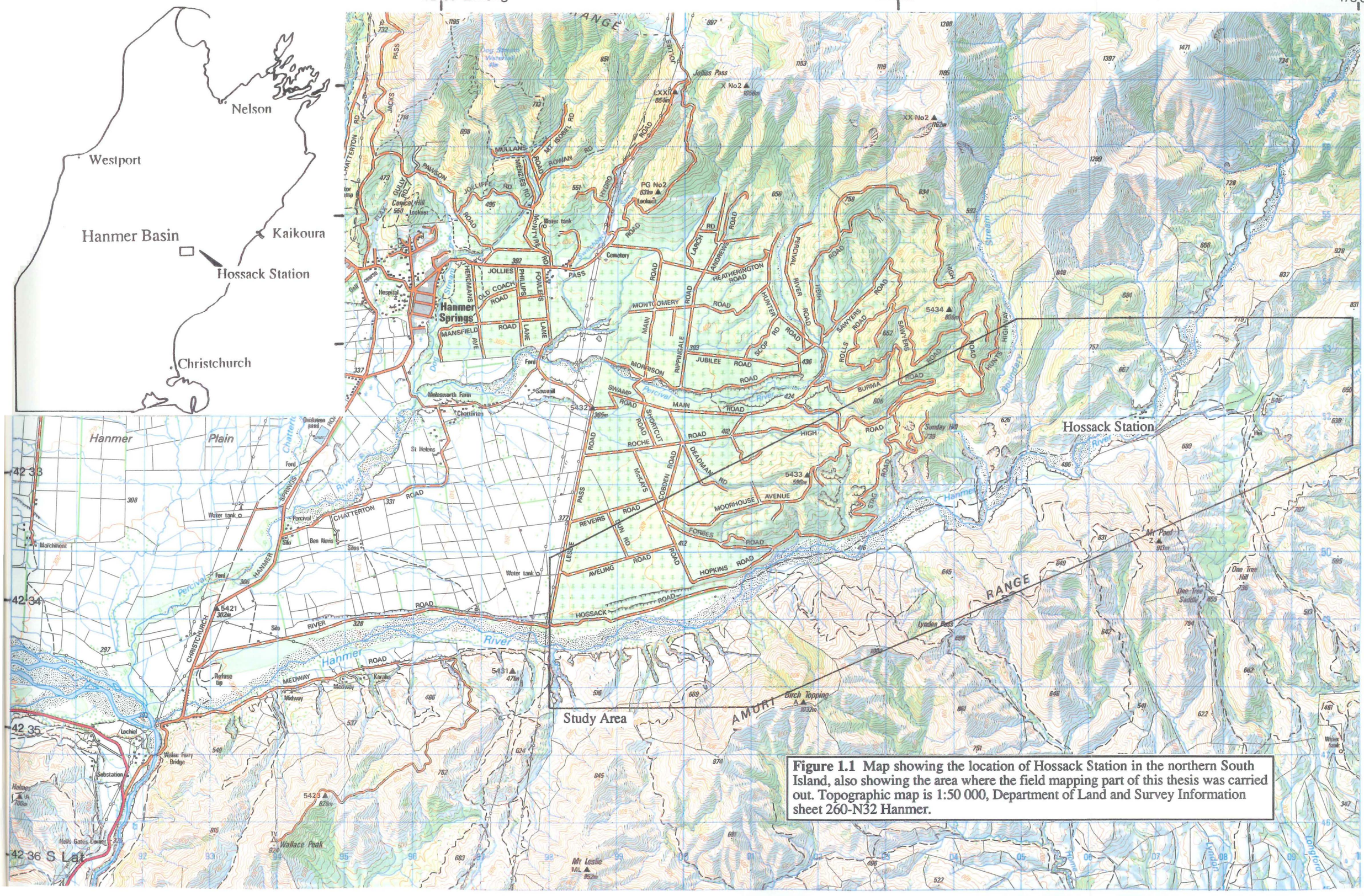

Figure 1.1 Map showing the location of Hossack Station in the northern South Island, also showing the area where the field mapping part of this thesis was carried out. Topographic map is 1:50 000, Department of Land and Survey Information sheet 260-N32 Hanmer.

hazards associated with this segment of the Hope Fault using empirical formulae that relate inferred fault parameters, such as fault displacement per event and fault segment length, to earthquake magnitude. The predicted effects of an earthquake generated by this fault are based upon accounts of the 1888 Amuri earthquake which ruptured the Hope Fault west of Hanmer Basin.

4. To present an interpretation of the structural history of Hanmer Basin based on the geological and structural information gathered from the Hossack Station and east end of Hanmer Basin.

1.2 Thesis organisation

This thesis is arranged to fulfil objectives one to four, presenting and discussing the data from the fieldwork with reference to earlier work carried out by other authors. The thesis has been compiled to facilitate access of information. Where possible, lengthy descriptions have been replaced by diagrams or appropriate referencing. The detailed structure and associated geomorphology of the Hope Fault Zone at Hossack Station is presented in Maps 1&2 (Map pocket). Chapter two discusses the structural, geological and geomorphological data relating to the Conway segment gathered during the study. Chapter three discusses the Late Quaternary slip-rates, fault movements at Hossack Station and a seismic hazard assessment for the Conway segment. Chapter four discusses data pertaining to the history of development of Hanmer Basin.

1.3 Regional tectonic setting

New Zealand lies across the boundry between the Pacific and Australian Plates (Walcott 1984a) (Figure 1.2). Oceanic crust of the Pacific Plate is being subducted westwards beneath the North Island and northern South Island, along the Hikurangi Trench (Fitch 1972; Walcott 1984a; Bibby 1981). In the northern South Island, the oblique plate motion is accommodated across the transpressional Marlborough Fault System. At the southwest end of the Alpine Fault the Australian Plate is being subducted eastwards beneath the Pacific Plate along the Puysegur Trench (Walcott 1984a). The present plate boundary configuration is thought to have developed about 10 Ma^{-1} ago

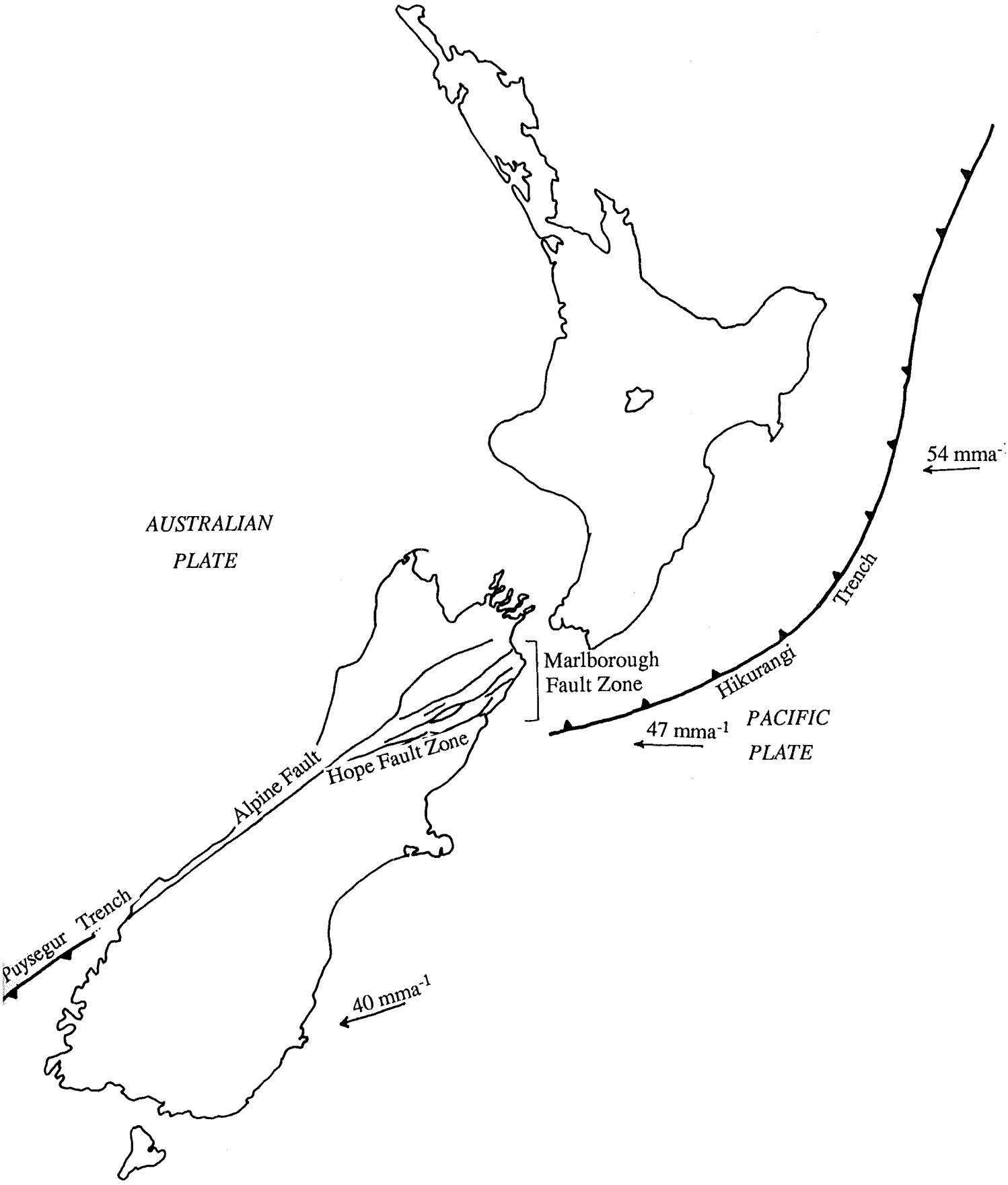

Figure 1.2 New Zealand's plate tectonic setting showing the Hope Fault in relation to other important elements of the Australian-Pacific Plate Boundary.After Walcott (1984a); plate convergence rate after Bibby (1981).

in response to a shift in the pole of plate rotation (Walcott 1984a).

Intermediate depth earthquake focii (>33 kilometres) delineate the upper surface of the subducting Pacific Plate beneath the North Island (Adams and Ware 1977; Reyners 1980). Deformation of the crust above the subduction zone dominates the structure of the North Island, eg. back-arc spreading, volcanism and plate convergence (Walcott 1978; 1984b). Intermediate depth earthquake activity on the subducting plate diminishes south of Kaikoura, indicating the southern limit of the subduction zone (Bibby 1981). The subduction zone is limited by the northern edge of the Chatham Rise, as this continental crust inhibits subduction (Walcott 1984).

The velocity of relative plate convergence at the southern end of the Hikurangi Trench has been estimated as 54 ± 9 mma^{-1} at an azimuth of $084\pm10^{\circ}$ (Bibby 1981). Near the subduction zone, deformation is dominantly thrusting normal to the trough axis. To the west, strike-slip faulting predominates (Bibby 1981). The complex transition from the Alpine Fault to the Hikurangi Subduction Zone occurs across the 150 kilometre wide Marlborough Fault System. In the northern South Island, regional strain is concentrated along four major subparallel dextral faults. From north to south, these the: Wairau, Awatere, Clarence and Hope Faults.

1.4 The Hope Fault Zone

The Hope Fault extends for 230 kilometres, from the Alpine Fault to the Kaikoura Coast, although a single major fault trace is visible for the central 150 kilometres only; from Harper Pass to Cribb Creek (Freund 1971) (Figure 1.3 and Map No.3 in the map pocket). Each end of the fault consists of diverging splays. where dextral displacement is dissipated as oblique-slip and thrusting (Freund 1971, 1974; Van Dissen 1989, 1991). Offshore, there is little evidence of the Hope Fault on seismic reflection profiles (Barnes pers. comm. 1991).

Two major changes in strike divide the Hope Fault into three distinct, relatively straight segments. In the Taramakau valley, near the Alpine Fault, the Hope Fault forms numerous smaller faults. Between the the Alpine Fault and the Hope River the Hope Fault has a strike of 075°. The Hope River segment has a more easterly trend of 083°. East of the Hanmer Plain the Hope Fault

Figure 1.3 Satellite image of North Canterbury. The Hope Fault strikes at about 070° across the top left of the photograph, with Hanmer Basin visible immediately right of centre at the top of the picture. The conspicuousness of the Hope Fault exemplifies the high rate of strain accommodated by the fault.(NASA 1976).

trends roughly 065° as far as the Kaikoura coast. The strike of the Hope Fault is consistent with the other major faults of the Marlborough Fault Zone. The other faults also have similarly segmented traces (Gregg 1964). East of Hanmer Basin the Hope Fault dips to the north, as shown by many active trace exposures (Freund 1971, Van Dissen 1989), and by the preservation of Tertiary sediments on the downthrown side of the fault.

The Hope Fault last ruptured in 1888, during a large (M7-7.3) earthquake (McKay 1890, Cowan 1991) centred west of Glynn Wye. One month after the earthquake, the effects were studied and documented by Mckay (1890). Mckay's observations of dextral offsets (1.5 to 2.4 metres) of fencelines crossing the fault, constitute one of the first records of strike-slip faulting (Sylvester 1988).

Cotton (1947) recognised that the Hanmer Plain was subsiding, and attributed this to vertical movement on the Hope, and Kaikoura Faults (the name given to the eastern section of the present Hope Fault). Following the widespread availability of aerial photographs, Wellman (1953) documented dextral offsets at a number of localities. Clayton (1966) and Freund (1971) described tectonic depressions along the Hope Fault, caused by right-stepping of the main fault trace. Hanmer Basin is the largest of several pull-apart basins on the fault, and defines the eastern end of the Hope River segment (Cowan 1989, 1990). A right step occurs across the basin with a separation of 6 kilometres between the major faults. Seismic reflection and gravity anomaly surveying indicate that the subsurface Hanmer depression is a relatively simple basin with a maximum depth of 850 metres (Anderson 1987; Wood pers. comm. 1990).

Recent studies by Knuepfer (1984), Cowan (1989) and Van Dissen (1989), have provided accounts of the Hope Fault trace morphology and slip-rates: on the Hope River segment at Glynn Wye (Cowan 1989,1990) and on the Kahutara and Mount Fyffe segments at Sawyers Creek and Hapuku River (Van Dissen 1989,1991). Estimates of slip-rate vary considerably between sites and authors. The geometry and structure of the Hope Fault at Hossack Station, was discussed by Freund (1971), but detailed mapping and the measurement of slip-rates have not been carried out.

Cowan (1989; 1991) suggests that the Hope River segment is ruptured by characteristic

earthquakes similar to the 1888 event, with a recurrence interval of 90 to 170 years, based upon the identification of five pre-historic earthquakes.

1.5 Study area

The study area comprises a corridor up to four kilometres wide between Hanmer Forest and Little Lottery River, an area largely occupied by Hossack Station. This region varies in altitude from 350 to 1000 metres above sealevel and is geograpically dominated by Hanmer River, which flows west along the Hope Fault Zone. The Hope Fault trace is exposed in several meanders of Hanmer River. Deeply incised tributaries, particularly to the north of Hanmer River, also provide exposure of the fault zone. Access to the field area is normally limited to four wheel drive vehicles, but only at times of low flow! Outside the area covered by the 1:10 000 maps (Nos. 1 and 2), field work was concentrated along road cut exposures (which are numerous) in the Hanmer Forest and at Karaha Station, on the south bank of the Hanmer River.

1.6 Local geology

The stratigraphy of the Hossack Station area consists of Mesozoic Torlesse Supergroup basement rocks and a cover of Pleistocene and Holocene deposits. The intervening Tertiary sequences, found throughout Canterbury, are not exposed in the area of this study.

1.6.1 Basement rocks

Torlesse Supergroup basement rocks in northern Canterbury consist mainly of well indurated, quartzofeldspathic sandstones and mudstones, metamorphosed to zeolite facies (Bishop et al. 1985). Torlesse rocks at Hossack Station form part of the Pahau Subterrane (Silberling et al. 1988), and are Late Jurassic to Early Cretaceous in age (Bishop et al. 1985). They are divided into two lithological associations (Bradshaw and Andrews 1980). (i) The Flysch-type association consists of interbedded sandstones and mudstones up to ten centimetres in thickness, of probable submarine fan origin. (ii) An alluvial delta-marginal marine association that contains many

lithologies, including massive sandstones and conglomerates derived from older Rakaia Subterrane Torlesse, and interbedded sandstones and mudstones (Bradshaw and Andrews 1980). Torlesse rocks experienced several periods of intense deformation (faulting and folding) prior to the initiation of the present plate boundary (Whitehouse and Bradshaw 1988).

1.6.2 Quaternary deposits

The deposition of thick gravel units in Hanmer Basin is interpreted during this study as having occurred during the Quaternary. Where exposed the gravels are consolidated, moderately to poorly bedded, poorly sorted, and subangular to angular. Postglacial gravels occur as veneers up to several metres in thickness deposited by the Hanmer River.

1.7 Methodology

The production of neotectonic maps was carried out using aerial photographs and field investigation. Data from field work was recorded on aerial photograph overlays and then compiled onto 1:10 000 base maps drawn from enlargements of NZMS 270 N32/A, contoured at 100 metre intervals. The aerial photographs included New Zealand Aerial Mapping: 1796/14-27; 1797/17-28; 1798/10-22; 1799/1-18. These photographs were taken in 1950, and show a landscape clear of vegetation, much of which is now covered by self-seeded exotic forest tree species. Aerial photographs at a scale of 1:25 000 taken during the early 1980's provided a useful comparative tool interpretation of geomophological features. Geomorphological features were measured by EDM surveying, 100 metre tape and/or aerial photographs. Scale corrections were applied to account for relief errors when estimating distances from aerial photographs.

1.7.1 Radiocarbon dating

High-precision dating of offset geomorphic features was crucial in establishing Late Quaternary slip-rates on the Hope Fault. Identification of the stratigraphic relationships between

wood samples and measurable fault offsets enabled slip-rates to be determined based upon the absolute radiocarbon age of the wood samples from a site at Hossack Station (Section 3.2). Dating of the organic material was carried out by the Radiocarbon Dating Laboratory at the University of Waikato, Hamilton (Appendix 1).

The conventional age of a sample using the radiocarbon dating technique is calculated using the half-life of 5568 years determined by Libby in 1949 (Bowman 1990) which enables the standard error to be incorporated into all age determinations. Appendix 1 shows the results of radiocarbon dating of the samples determined by the Radiocarbon Dating Laboratory.

Chapter two

Geology and geomorphology of the Hope Fault Zone: Hossack Station to east Hanmer Basin

2.1 Introduction

Along the southeast side of the Hanmer Basin, between the Waiau Gorge and Little Lottery River, the Hope Fault can be readily mapped both on aerial photographs and in the field. Where the Hope Fault enters Hanmer Basin from the east, the morphology of the fault zone becomes complex and is typically manifest as an array of splays, and structures relating to changes in the orientation of the master fault. Hanmer Basin forms the boundary between two segments of the Hope Fault Zone: the Hope River segment (Cowan 1989,1990) and the Conway segment (Bull et al. 1991).

The Conway segment of the Hope Fault consists of a zone of deformation up to several kilometres wide, associated with one or more active traces. The term Hope Fault Zone will be used to describe the wider zone of deformation associated with the active Hope Fault traces. In the east end of Hanmer Basin the Hope Fault Zone is well exposed in Torlesse bedrock. This permits investigation of the relationships between the active Late Quaternary traces and the associated fault zone.

In this chapter I will describe the morphology and geometry of the active traces within the fault zone at the eastern end of Hanmer Basin, and discuss their relationship to the basin.

2.2 Active traces associated with the Hope Fault Zone

Late Quaternary traces of the Hope Fault are relatively straight and strike at between 068° and 080° along the Hanmer River valley and are repeatedly exposed in the walls of incised meander loops (Figure 2.1). A single active trace occurs at the eastern edge of the study area near Little Lottery River, but becomes progressively more complex towards the Hanmer Basin as several active faults splay from it. The fault bifurcates 1.5 kilometres west of Hossack Station homestead,

and two distinct traces continue for at least two kilometres down the Hanmer River valley (Figure 2.1). Further west the fault forms a single trace, represented by a 20 metre-high scarp with the north side upthrown, in Hanmer Forest north of Hossack Road (Figure 2.1). The trace is continuous for two to three kilometres through Hanmer Forest and terminates at Leslie Pass Road at a bulge or pressure ridge (this feature is discussed in Section 2.2.5).

The general strike of the Conway segment is 065°, but the strike changes to 070-075° immediately east of the study area. The Hope Fault has two distinct changes in strike within the area of this study (Figure 2.1). An abrupt change of 5-8° occurs as the fault enters the Hanmer River valley from the east. Upwarping of a Holocene river terrace on the north side of the fault, immediately west of the bend, is due to compression caused by displacement across the bend (Figure 2.2). Sibson (1989) noted that such "isolated fault bends", demonstrate the effect of earthquake directivity. As fault rupture approaches, from the east in this case, the fault will tend to experience increased compression at the bend (Figure 2.3a). The terrace warping may also indicate that the fault motion vector is oriented south of the fault strike (Figure 2.3b). If this were not the case, extension would be evident east of the bend. The orientation of the fault motion vector is consistent with evidence of transpression across the fault at Hossack Station.

The second bend is a gentle curve, concave to the north, from Hanmer Forest, west to the Waiau Gorge. Consistent with this observation, Freund (1971) reported that much of the Hope Fault can be divided into "segments" up to several kilometres in length, that are broadly concave to the north and separated by abrupt bends to the south.

Good exposure of the fault plane has enabled several dips of the Hope Fault to be recorded (Figure 2.4). Dips are steep and consistently to the north (78°, 71° and 75°) (Map 1), as far west as the pressure ridge at Leslie Pass Road. The fault plane is only exposed where the fault forms a single surface trace (between Boundary Stream and the Little Lottery River). The measured dips are consistent with those reported by Freund (1971) for the Hope Fault between the Hanmer Basin and the Kaikoura Coast. Dips of less than 60° are indicated by fault scarps for the twin active traces near Boundary Stream, (Freund 1971), but these dips should not be considered reliable,

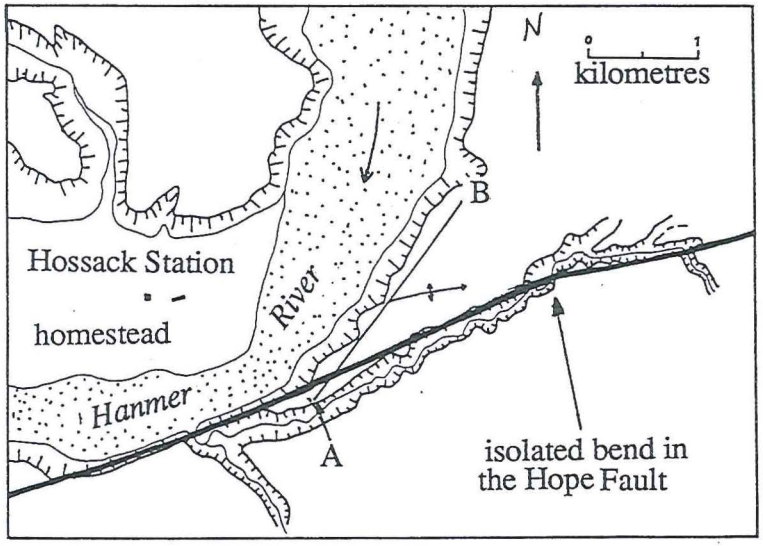

Figure 2.2 Locality map (A) and cross-section (B) of warping in a Holocene river terrace caused by compression at an isolated fault bend of 5-8° in the Hope Fault active trace at Hossack Station. Vertical exaggeration of the cross-section is 10x.

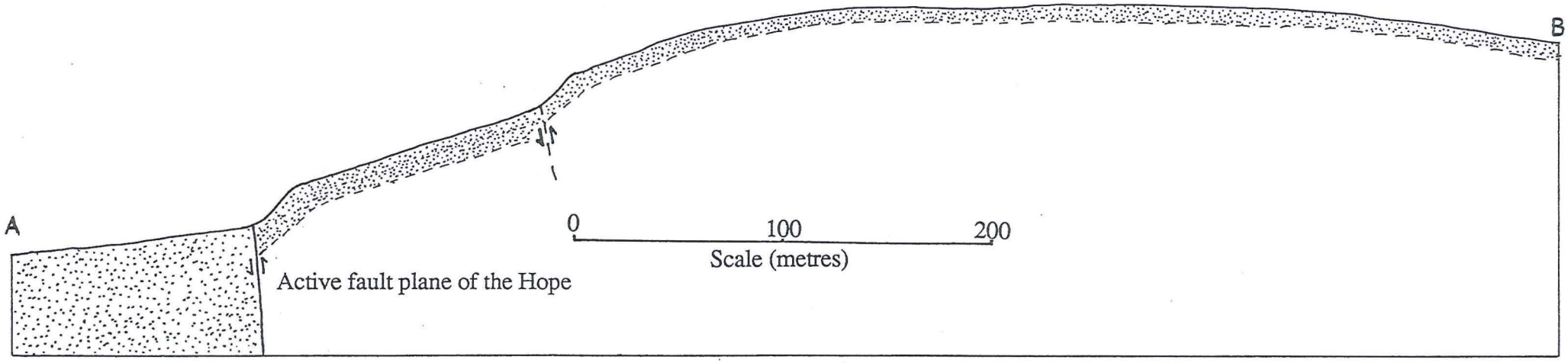

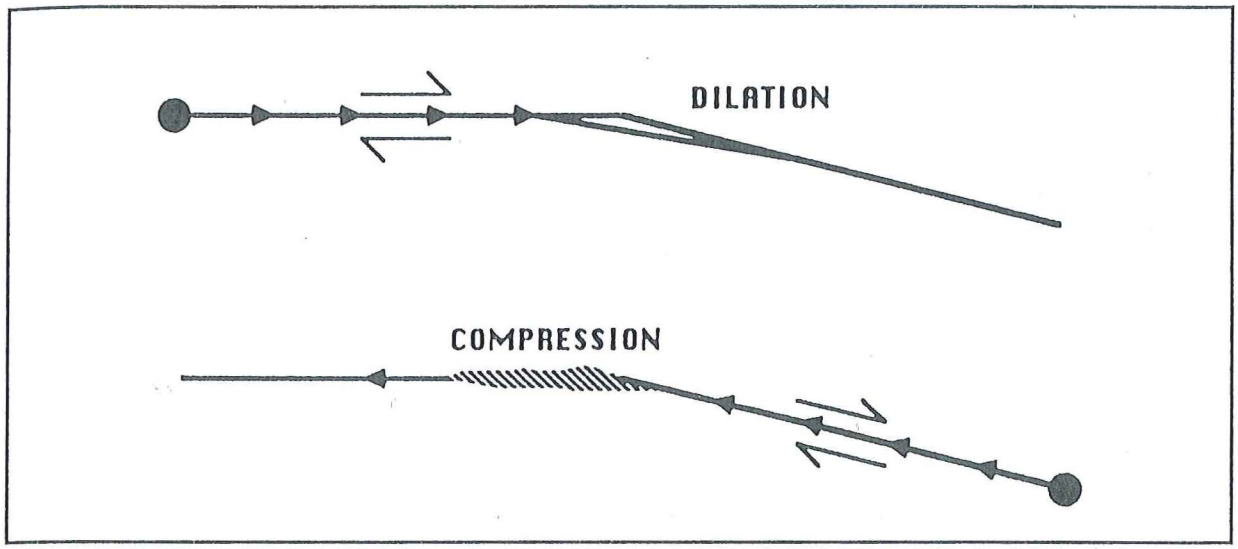

Figure 2.3a Cartoon map illustrating the changing response of an isolated fault bend to rupture directivity on a right-lateral strike-slip fault. Solid circles represent earthquake epicentres (Sibson 1989).

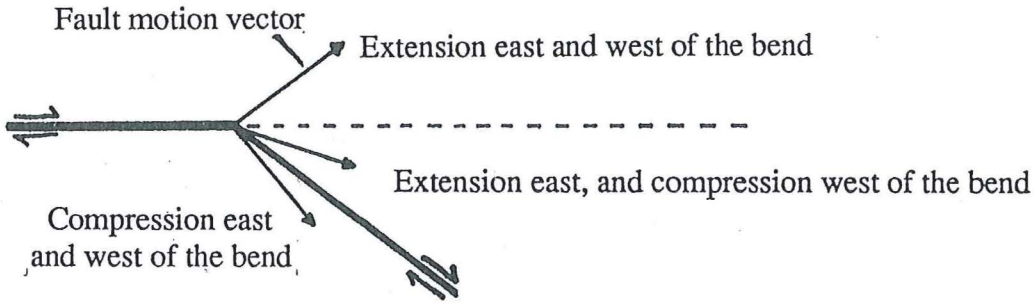

Figure 2.3b Effect of varying the fault motion vector at an isolated fault bend. If the fault motion vector is oriented to the convex side on the bend, extension will occur at the bend. If the fault motion vector is oriented to the concave side of the bend, compression will occur at the bend.

because the relationship between the fault plane orientation and fault scarp geometry is uncertain. In other localities the dips are unknown and must be inferred from the geology and geomorphology.

2.3 Basement geology of the Hope Fault Zone

Freund (1971) reported a crushed zone up to 2600 feet (800 metres) wide for the section of the Hope Fault east of the Hanmer basin. The width of the fault zone is difficult to define because a gradation, over several hundred metres, occurs from pulverised greywacke adjacent to the major traces to less fractured and shattered rock. This gradation can occur over a distance of more than a kilometre from the fault trace and is not uniform. Within the crushed zone, some pods of rock still have bedding preserved, but these are isolated blocks. The crushed zone shown on Map 2, is the area where Torlesse is devoid of any visible bedding. In this zone, the largest fragments of intact Torlesse are 2-3 centimetres across. The rock has a white or pale grey colour due to alteration and recementation. Often the crushed zone rock is well indurated. Immediately adjacent to the active fault trace the "fault pug" is very soft and can be remoulded or broken by hand.

Outside the crushed zone, the sedimentary structures (such as bedding) are visible, but the rock shows a high degree of shattering: blocks are frequently 1-2 centimetres across and large scale scree development is common on steep slopes (see Map 1).

The northern limit of the Hope Fault Zone is indistinct. Much of the Torlesse north of the crushed zone (as defined by Map 2) shows fracturing into centimeter sized blocks, but without the level of deformation found closer to the active trace. Faults and locally sheared Torlesse are exposed as far north as the edge of the mapped area, two kilometres north of the Hope Fault master trace.

The best exposures of Torlesse occur in the deeply incised streams within the fault zone, north of the active trace of the Hope Fault (Map 1). At a distance of more than one kilometre north of the active fault trace, bedding strikes at approximately 035°. Fault drag has caused deformation of Torlesse bedding so that closer to the fault trace bedding bends to become fault-parallel (Map 2). A

Figure 2.4 Exposure of the active fault plane of the Hope Fault (arrowed). Outcrop is 200 metres up a small stream opposite Hossack Station homestead. Grid reference 260 N32 073518. Dip of the fault plane is 71° north. Photograph shows Torlesse (highly sheared fault pug) faulted over Pleistocene gravel. Outcrop of fault plane is 4-5 metres high; viewed looking west.

similar pattern has been documented southwest of the Waiau river (Bradshaw and Andrews, 1980) (Figure 2.5) where the strike of Torlesse bedding swings from about 040° to 080° to parallel the fault. This phenomenon may be due to fault drag. Torlesse bedding at the Waiau Gorge is oriented nearly parallel to the Hope Fault and has a steep dip to the south. The change in Torlesse bedding orientation close to the fault must be considered in estimates of the total fault offset using stratigraphic markers (eg. Freund (1971;1974) uses chert and conglomerate beds). Freund considered that approximately 19 kilometres of strike-slip displacement has occurred on the Hope Fault, based on the matching of various chert and conglomerate beds across the fault. Freund may have underestimated the total fault offset by as much as 2-3 kilometres. The total offset indicated by matching the sedimentological change from the flysch-type association to the alluvial-deltaic association, from the south side of Hanmer Basin (Figure 2.5, Bradshaw and Andrews 1980) to Hossack Station (Map 2), is 20±2 kilometres.

2.4 Relationship between active traces and the basement crush zone.

An important feature of the fault zone is that its dimensions are asymmetric in relation to the present Hope Fault active trace. At Boundary Stream the crushed zone (as defined by Map 2) is only 150 metres wide on the south side of the fault, whereas over 400 metres of crushed zone appears on the north side. Two kilometres north of the active trace, Torlesse still shows considerable shattering and has been subject to extensive gully erosion, landsliding and scree development. The southern margin of the crushed zone has a well defined edge in contrast to the north side of the zone. The edge of the crushed zone appears to dip steeply to the north, as does the active trace.

Often an active fault trace will be located on one side of its associated fault zone (Sibson pers. comm. 1991) and this asymmetry may reflect strain concentration on the footwall of the fault. Asymmetry of the crushed zone has been inferred elsewhere within the Hope Fault Zone. Freund (1971) noted that the Quaternary trace of the Hope Fault at the Charwell river occurs 800 metres north of a large, apparently fossil crushed zone. The switching of activity from one active trace to

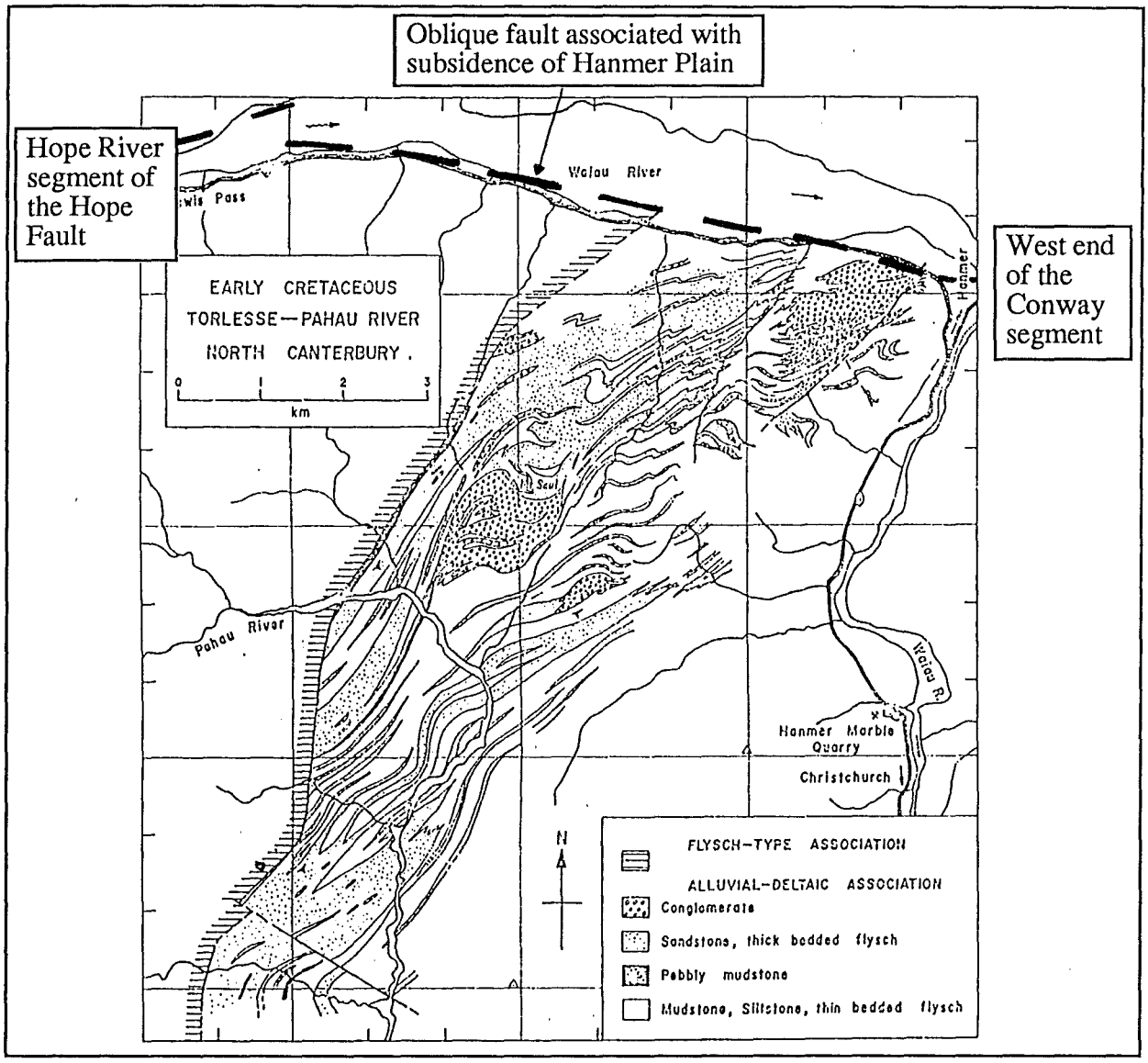

Figure 2.5 Map showing the effect of fault drag in Torlesse close to the Hope Fault. Distortion in bedding occurs within a zone up to three kilometres from the fault. Map also show change in Toresse lithological association. (Bradshaw and Andrews 1980).

another can be inferred at Boundary Stream (see Section 3.3).

Another explanation for the wide fault zone at Hossack Station is that the Hanmer Fault splays north from the Hope Fault in that area. The Hanmer Fault is not traceable from Hossack Station to Hanmer Springs, where the Hanmer Fault is most clearly delineated as a continuous Holocene trace (refer Section 2.5.2).

2.5 The relationship between the Hope Fault and Hanmer Basin

The Hanmer Basin is a pull-apart basin formed at a right step-over or releasing bend (Crowell 1974) in the Hope Fault. The Conway segment of the Hope Fault enters the basin from the east and bounds the south side of the Hanmer Plain. The Hope River segment of the Hope Fault exits the Hanmer basin from the west corner after stepping six kilometres to the north, across the basin. The Hope River segment splays into many fault traces as it enters the Hanmer Basin (Pettinga pers. comm. 1991). The Conway segment of the Hope Fault also shows splaying as it enters the basin, but the style of faulting is compressional rather than extensional.

The section of the Hope Fault in Hanmer Forest terminates at Leslie Pass Road. The fault displaces the highest terrace level (the surface of Hanmer Plain), as a 20 metre-high riser that bounds the north bank of the Hanmer River (Figure 2.1). Lower-level terraces to the west of Leslie Pass Road have not been displaced by the fault. The river terraces on the south side of the fault have been upwarped in the form of a pressure ridge (Figure 2.6). Progressive upwarping of the terrace and deflection of the river around the growing bulge, is inferred by tracing each terrace riser across the structure.

The Hope Fault steps to the southwest across the Hanmer River and does not cut the youngest terraces. In crossing the Hanmer River the fault appears to make a left (restraining) stepover (Figure 2.1). Uplift resulting from the stepover is not apparent in the river terraces on the south side of the Hanmer River. It is unlikely that the pressure ridge at Leslie Pass Road results from shortening at the apparent step-over, because the uplift is concentrated at the end of the fault trace on the north side of the Hanmer River, rather than being spread over a larger area between the

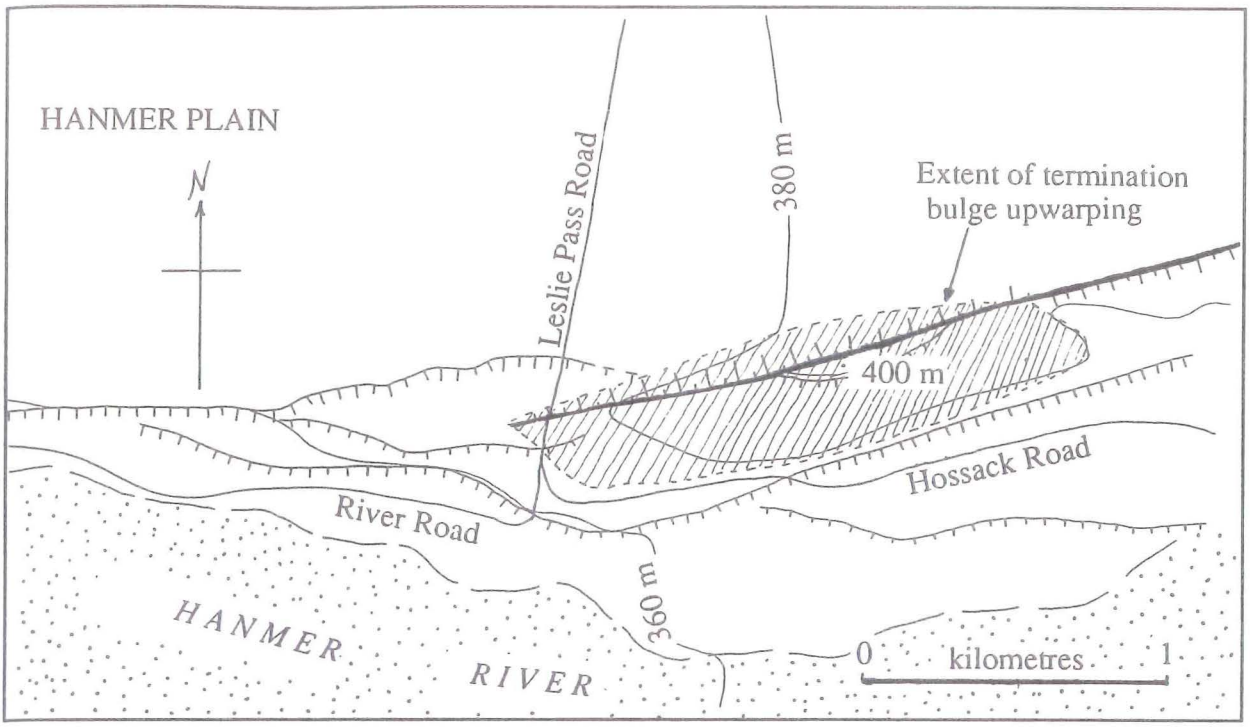

Figure 2.6a Plan of pressure ridge or termination bulge on the Hope Fault in Hanmer Forest. The active fault trace is not evident on the lower river terraces west of Leslie Pass Road. Hanmer Plain surface is upwarped by 25-30 metres. The Hope Fault dips to the north (indicated by upthrown north side on a transpressional fault segment).

Figure 2.6b Photograph of bulge or pressure ridge adjacent to the Hope Fault in Hanmer Forest. Uplifted terrace risers are visible across the bulge. Leslie Pass Road marks the edge of the forest.

traces. The pressure ridge seems to be a consequence of postglacial uplift as a consequence of termination of this section of the fault segment.

2.5.1 The Hope Fault from Karaha Station to Waiau Gorge

The Hope Fault can be traced for 3 kilometres along the river terraces between Karaha Station and the Waiau Gorge (Figure 2.1). Sense of movement for the fault is difficult to determine, as the terrace risers cut by the Hanmer River are parallel to the strike of the fault. Aerial photographs (Photo run 1799/13) indicate that the fault has dextrally offset several stream channels flowing north-south across the fault. The fault appears to be upthrown to the south along this section. Also consistent with dextral fault movement is the development of a small graben at a 200 metre right stepover in the fault trace (Figure 2.7).

Exposure of Torlesse basement in this area is sufficient to delineate the crushed zone, with the Waiau Gorge providing an excellent cross-section. A crushed zone is also visible in the road cut of the Lewis Pass Road (SH 7), on the west bank of the Waiau River (Figure 2.1). The crushed zone here is about 500-600 metres wide south of the fault, much wider than the south side of the fault at Hossack Station. A transition occurs from totally intact Torlesse 300 metres south of the Waiau Ferry Bridge, to totally crushed Torlesse near the Hanmer River bridge. South of the fault, bedding in Torlesse dips at moderate to steep angles to the south and strikes between 60° and 110° (subparallel to the Hope Fault).

The dip of the Hope Fault along the southeast side of the basin is uncertain. Freund (1971) reported dips to the north and south for the active fault trace between Karaha and Medway Stations. If the fault is transpressional there, the fault may dip to the south, as implied by the apparent throw at the locality (south side up). The orientations of the crushed zone and Torlesse bedding may reflect a south dip for this part of the fault.

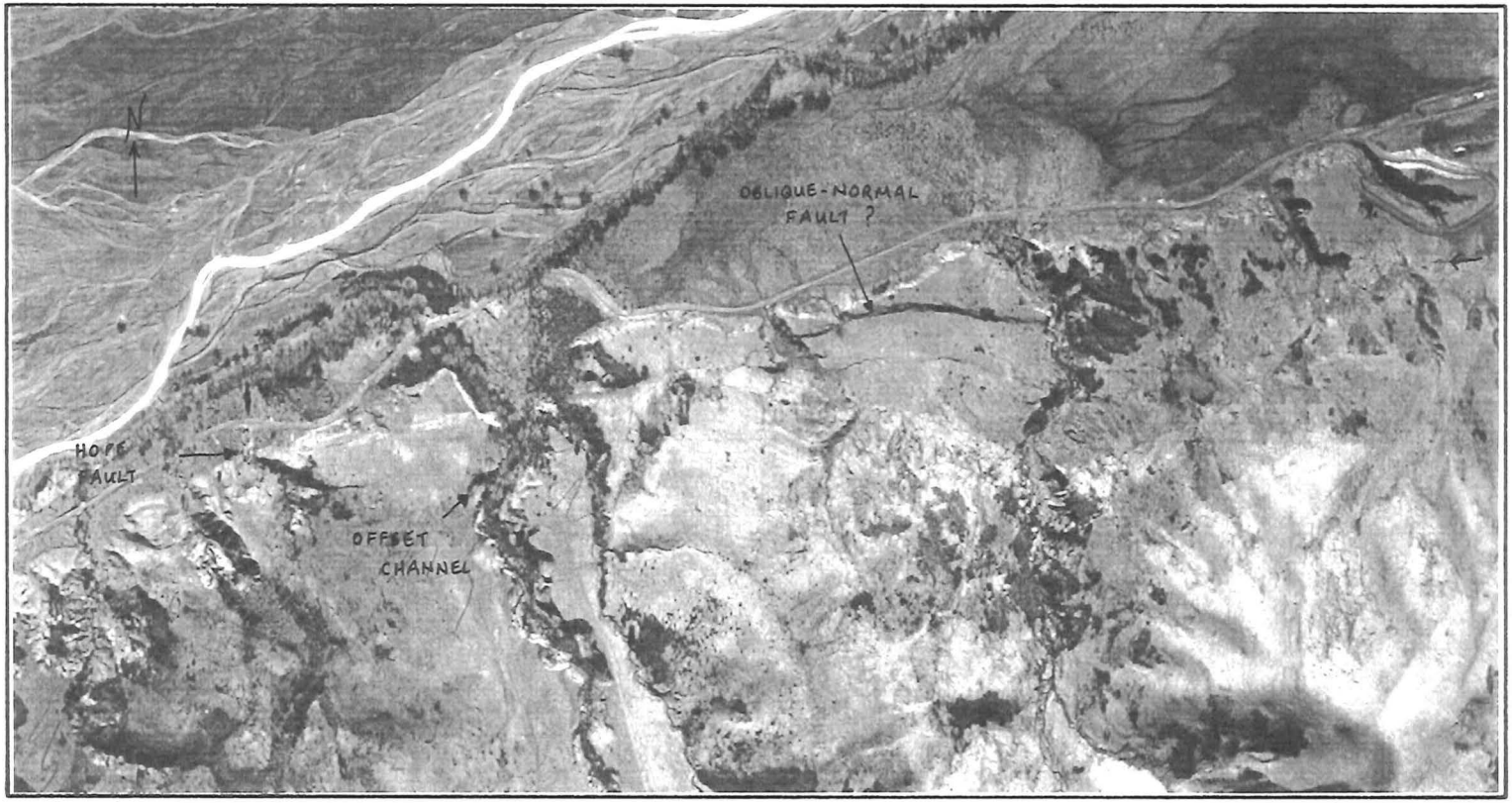

Figure 2.7 Aerial photograph of pull-apart basin developed at a 200 metre right step-over or releasing bend in the Hope Fault at Midway Station. Prominent arcuate fault scarp is probably an oblique-normal fault associated with extension at the step-over. Note the dextral offset of a channel immediately west of the graben. Scale is approximately 1:8000.

2.5.2 Hanmer Fault

The Hanmer Fault splays from the Hope Fault near Hossack Station, and is mapped as a series of discontinuous Late Quaternary traces on the north side of the Hanmer Plain, striking 110° through Hanmer Springs. The active trace is complex around Hanmer Springs, and comprises a series of en echelon restraining stepovers. Observations from a trench across the fault near the Hanmer Hospital, indicate that the fault dips steeply to the north (Pettinga pers. comm. 1991). The fault vertically displaces the basement by about 50 metres under Hanmer Springs township (Leech 1988) and the overlying alluvial fan surface by up to ten metres between the Percival River and the Rogerson River. A dextral component of displacement is possibly indicated by apparently offset channels crossing the fault at Hanmer Golf Course.

To the east of Hanmer Springs, the Hanmer Fault surface trace extends as far as Hanmer Forest, where it becomes indistinct. Further east in Hanmer Forest, intense faulting and deformation within a zone at least 300 metres wide was observed in the Torlesse (Figure 4.2), but without an active surface trace. Several faults are exposed in Boundary Stream and an important splay extends as far east as the Hossack homestead, and is marked by a series of large landslides. This fault strikes at 100° and dips 50° to the south. At the Hossack Station, this splay is exposed in Torlesse basement, but does not cut Holocene gravel. Movement of the Hanmer Fault appears to have been dissipated by many splays in a wide shear zone in the Boundary Stream-Hossack Station area. The Hope Fault Zone is in excess of 1000 metres wide at Boundary Stream which may reflect a convergence of the Hanmer Fault Zone in this area.

Between the active Hanmer Fault trace and the zone of deformation in the Hanmer Forest, the fault is not exposed, but may be inferred to exist at depth below folded Pleistocene gravel deposits (Section 4.5). These folds are coincident in orientation with the Hanmer Fault and presumably indicate reverse faulting at depth. The inference that folding is the surface expression of displacement of the Hanmer Fault at depth, is supported by the observation that the active fault trace is most prominent near the Hanmer Springs Township where Quaternary gravels are relatively thin (Torlesse basement was encountered 60 metres below the ground surface, in a well

drilled in Hanmer Springs township (Anderson 1987)).

The Hanmer Fault has not moved in historic times.

2.5.3 Marble Point Fault

The Marble Point Fault splays southwest from the Hope Fault approximately four kilometres east of Karaha Station (Figure 2.1). Several fault traces strike approximately southwest on the south side of the Hanmer River, between Boundary Stream and Karaha Station. Associated with these faults is a zone of deformed Torlesse up to 500 metres wide, striking 045^{o} and roughly coincident with Broom Stream. The zone of faulting marks the line of the Marble Point Fault, which is exposed as a zone of shearing, 45 metres wide, in the east bank of the Waiau River immediately south of the Marble Point limestone quarry (Syme pers. comm. 1991). The shear zone at Karaha Station shows a well defined northwest margin and an indistinct southeast margin; in a similar fashion to the geometry of the Hope Fault Zone at Hossack Station, only in reverse. The concentration of strain against the footwall of the fault may lead to a sharper transition from sheared to non-sheared rock as is seen on the south side of the Hope Fault zone at Hossack Station. The geometry of the shear zone suggests that the Marble Point Fault dips to the southeast. No recent fault traces have been attributed to the Marble Point Fault near the Waiau River, but at the Hanmer River end of the shear zone, several Late Quaternary fault traces are visible, and these may be associated with a transfer of strain from the Hope Fault Zone to the Marble Point Fault. A large reverse component of movement is inferred for this fault as Torlesse basement is thrust over a sequence of Eocene and Oligocene volcanics, marine sandstones and limestones. Slickenside data are indicative of both reverse and strike-slip faulting (Syme pers. comm. 1991).

2.5.4 Secondary faults in Hanmer Basin

Steep, south-dipping faults outcrop along the north bank of the Hanmer River (Map 2). These faults splay from the Hope Fault into the Hanmer Basin and form a series of scarps in Hanmer Forest which are parallel to local river terraces. Seismic reflection data (Wood pers. comm. 1991)

confirms the existence of these faults at depth, but fluvial modification of the scarps cannot be discounted. Freund (1971) mapped these terrace risers as fault scarps.

The steeply dipping faults in Hanmer Forest are secondary to the main structure of the Hope Fault Zone and appear to be reverse faults, which have developed in association with folding and shortening on the north side of the active Hope Fault trace. This interpretation is confirmed by seismic reflection data (Wood pers. comm. 1991). Other faults are exposed in a road cut along the ridge running up to Sunday Hill (Figure 2.1). These are sub-parallel to the Hope Fault and are secondary faults relating to local folding. Folding along the north side of the Hanmer River is discussed in Chapter 4.

The drainage pattern north of the Hope Fault in Hanmer Forest is to the northwest, away from the Hanmer River suggesting that some backtilting of the basin floor has occurred. Backtilting may be indicative of a reverse component of movement of the active Hope Fault trace, consistent with the fault motion further east at the Hossack Station.

2.6 Geomorphology of the Hope Fault Zone at Hossack Station

2.6.1 The Hanmer River channel morphology

In general the Hanmer River follows a course on the northern side of the Hope Fault, where the Torlesse rocks within the crushed zone offer less resistance to erosion. The Hanmer River shows changes in channel form along its length. Upstream from Hossack homestead, it flows down a straight valley, incised into Torlesse and convergent with the Hope Fault (Figure 2.1). The river then occupies a meandering channel, also cut into Torlesse, for about 5 kilometres until it reaches Pleistocene gravels where it forms a 500 metre wide braided river bed. Variations in river gradient along its length are considerable (Figure 2.8) and coincide with changes in channel form.

The lowest gradient of the Hanmer River is the section upstream from the Hossack homestead. The suggested cause of the low gradient is uplift and backtilting on the north side of the Hope Fault. The steepest section of the river is the five kilometre meandering reach, cut in bedrock. The

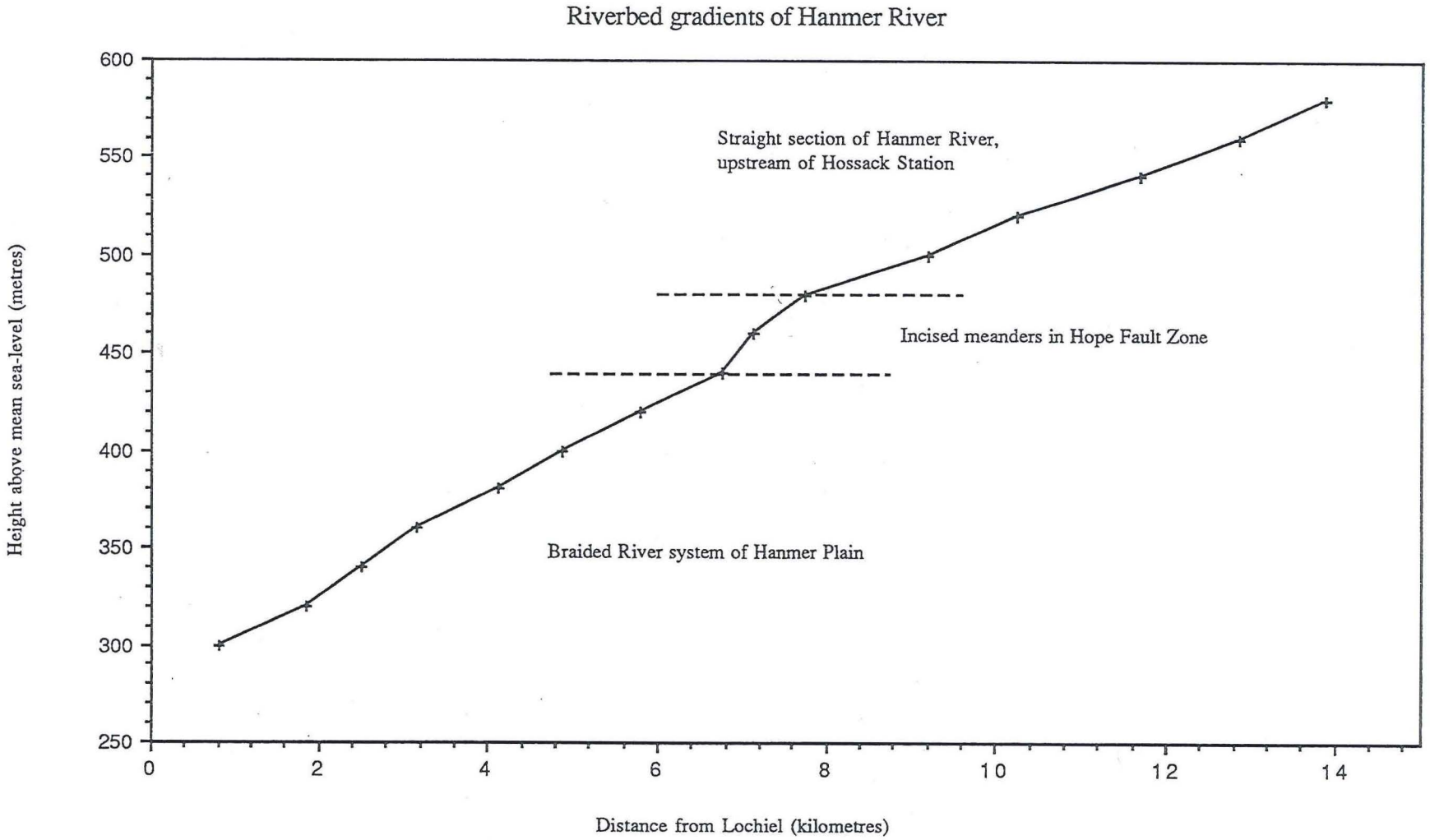

Figure 2.8 Graph showing the three distinct sections of the Hanmer River, corresponding to the straight section of the river above Hossack Station homestead and north of the Hope Fault; the meandering section along the Hope Fault Zone; and the lower reaches along the Hanmer Plain, south of the fault. Note that the steepest gradient is through the Hope Fault Zone.

gradient reduces again where the river encounters basin fill deposits near the Hanmer Plain. The meandering channel form may have resulted from "choking" of the river by an overabundance of sediment from the three major tributaries: the Little Hanmer River; Shingly Creek; and Boundary Stream, all of which currently discharge large amounts of sediment. Where the rivers are flowing on crushed bedrock within the fault zone, incision appears to have been rapid. This rapid downcutting is evident in many streams at Hossack Station where waterfalls or steps have formed at the Torlesse/Holocene gravel unconformity.

2.6.2 Effects of faulting on geomorphology

The presence of a broad zone of deformed Torlesse along the Hope Fault has resulted in large scale landsliding and ridge renting during earthquakes. The highly crushed Torlesse has a low cohesive strength, and its high permeability, can effect potentially high pore water pressures. The slope stability is further reduced during seismic shaking. The rapid downcutting that has occurred in streams traversing the highly crushed rock also decreases slope stability by removal of support. Large scale scree development is typical along the incised streams north of the Hope Fault. The screes often extend from streambed to ridge crest and introduce considerable volumes of coarse-sediment to the drainage system.

2.6.3 Ridge renting or "sackung"

The large scale gravitational spreading of steep sided ridges has been attributed to sackung or ridge renting (Savage and Varnes 1987). Ridge rents up to 2-3 metres in height and hundreds of metres in length are evident on many ridges in the area immediately adjacent to the Hope Fault (Figure 2.9). Faulting has conditioned the basement rocks for the development of ridge rents.

The common orientation of ridge rents is steeply dipping and ridge parallel. In the case of the study area, this orientation closely reflects bedding strike of the Torlesse. The steep bedding orientation of the Torlesse may encourage the development of ridge rents.

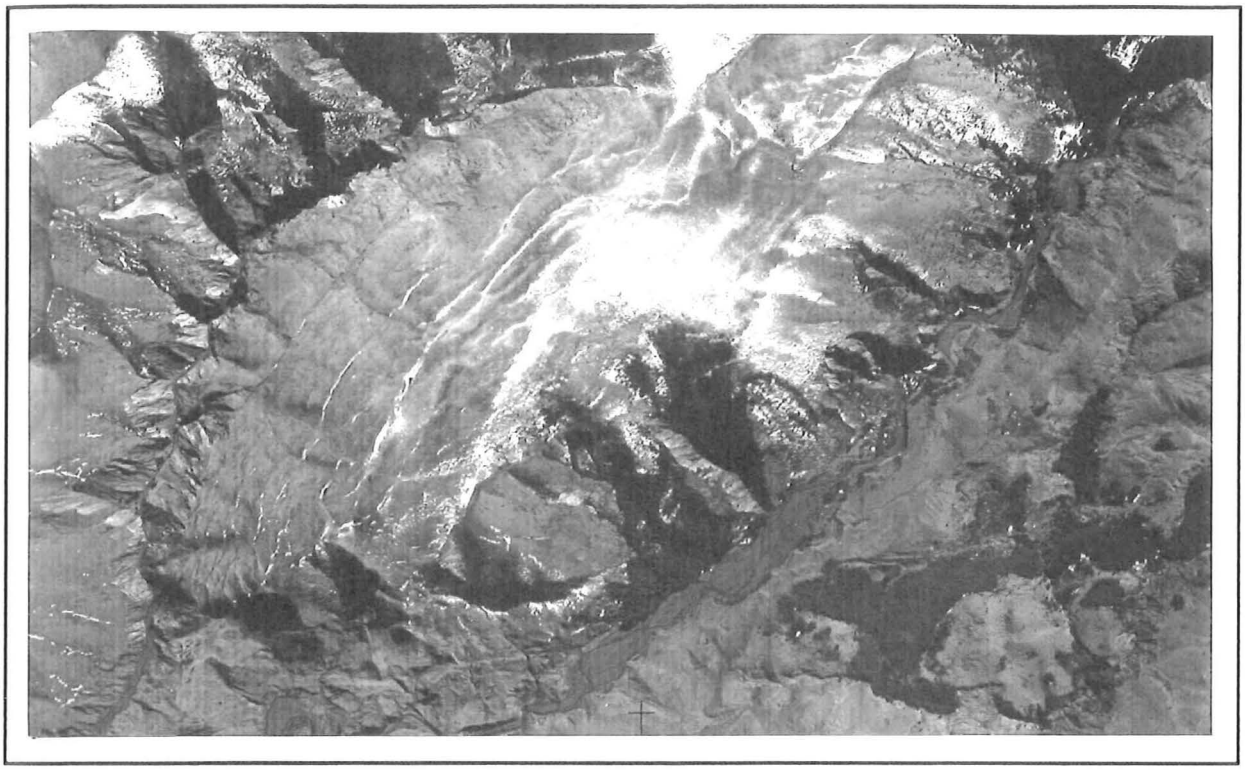

Figure 2.9 Aerial photograph showing the development of ridge-rents within the Hope Fault Zone. The active trace of the Hope Fault is visible crossing Little Lottery River at the lower edge of the photograph. Scale is approximately 1:8 000.

2.6.4 Landsliding

Several large prehistoric landslides are evident at Hossack station. The landslides occur on the north side of the fault, within the crushed zone. As with ridge renting, the steep bedding dips in the Torlesse may have affected some of these landslides.

An impressive landslide 200 metres west of Hossack homestead is the result of a block of Torlesse being isolated between a splay from the Hanmer fault, and the weak highly sheared Torlesse bedding planes (Figure 2.10). This landslide overlies a terrace two metres above the present floodplain of the Hanmer river. This terrace may be approximately 1000 years old (see section 3.3 for discussion). The landslide was encouraged by prior trimming of the slope toe by the river on its then active floodplain. The landslide must be younger than the estimated 1000 year B.P. age for the terrace. A buried soil "A" horizon which developed on the terrace, now beneath the landslide, indicates that the slide probably occurred a considerable time after the terrace formed, and is likely to be younger than 1000 years.

Two more landslides have occurred on this splay fault, one in Boundary Stream, the other in Shingly Creek. The landslide into Boundary Stream dammed the incised channel. A tightly meandering section of the stream is evidence of incision into the dam. Both slopes had been undermined by deep stream incision, both Boundary Stream and Shingly Creek having formed canyons 150-200 metres deep.

A large landslide southeast of Sunday Hill, is evident from Boundary Stream (grid reference:260 N32 043515). The failure plane dips at approximately 8 degrees to the east, and is visible in a cliff face about 5 metres above present river level. A tree trunk protrudes from beneath the landslide and provides an excellent opportunity for dating the event, but is unfortunately inaccessible.

Dating large landslides such as those described above, provides an opportunity to estimate the ages of prehistoric earthquakes on this segment of the Hope Fault.

Figure 2.10 Landslide developed in Torlesse immediately east of Hossack Station homestead. The slide block has been isolated between bedding in the Torlesse and a fault trace which is possibly a splay from the Hanmer Fault. Bedding orientation strikes NE-SW and dips steeply to the SE. Fault trace strikes ESE and dips to the southwest. The Hope Fault is visible cutting Holocene river terraces south of the Hanmer River. Photograph from NZ Aerial Mapping 1797/24.

2.7 Conclusions

The Hope Fault Zone comprises a corridor of deformation several kilometres wide which is associated with an active fault trace. At Hossack Station the active trace is relatively straight and dips to the north. As the Hope Fault Zone approaches the Hanmer Basin from the east, the active trace becomes more complex, splaying to the north and south and changing in strike and dip.

The relationship between the Hope Fault Zone and its active trace is asymmetrical: the active trace is located at the southern edge of the fault zone. The well defined south margin of the fault zone and an indistinct north margin, are indicative of a north dip probably due to the concentration of strain against the fault footwall.

The vertical throw of the Hope Fault's active trace is north side up, indicating that the fault is transpressional. The presence of compressional features; such as secondary reverse faults, and folds that trend parallel to the fault strike, also indicate transpression.

Secondary reverse faults, oblique-reverse faults and fault parallel folds are evident at the east end of Hanmer Basin, and accommodate local north-south shortening.

The wide fault zone at Hossack Station may reflect the divergence of the Hope Fault Zone and the Hanmer Fault Zone. The Hanmer Fault is a major splay of the Hope Fault and strikes at 110^{o} along the northeast side of Hanmer Basin. It is an oblique-slip fault and shows indications of being a reverse fault at the east end of Hanmer Basin.

The Marble Point Fault splays south from the Hope Fault Zone four kilometres east of Karaha Station. It has a strong reverse character, but may be transpressional. Movement on the Marble Point Fault has caused the tight folding of Tertiary sediments at Marble Point.

Geomorphic features such as landslides, ridge-rents and the development of screes, reflect the inherent weakness of the Torlesse within the fault zone.

CHAPTER THREE

Late Quaternary displacements and rates of slip on the Hope Fault at Hossack Station

3.1 Introduction

The Hope Fault east of Hanmer Basin is active, with estimated dextral slip-rates of between 20 mma^{-1} and 40 mma^{-1} for the Conway and Kahutara segments (Van Dissen 1988; Bull pers. comm. 1991). These slip-rates are higher than the 14 ± 3 mma^{-1} estimated by Cowan (1990) for the Hope River segment of the Hope Fault at Glynn Wye, west of Hanmer Basin. The purpose of this chapter is to present new data on fault displacements and slip-rates for the Hope Fault at Hossack Station, and to review existing data for the slip-rate of the Hope Fault Zone, for the purpose of comparing rates and styles of displacement.

In this study, estimates of slip-rate are based on the analysis of displacements at two sites along the fault: (1) east of Hossack Station, where three stream loops have been progressively offset by the fault; and (2) west of Hossack Station, where degradational terrace risers are offset across two traces of the Hope Fault. At the stream loops locality, radiocarbon dates import maximum and minimum slip-rates for the Late Holocene. At the second site, displacements and slip-rate are known with less certainty, but still provide useful information about the history of movement of the two traces during the Holocene.

Slip-rate is an indicator of long-term fault activity and represents a quantitative measure by which faults, or fault segments, can be compared. The slip-rates inferred for the Hope Fault at Hossack Station are compared with rates determined further to the east (Bull pers. comm. 1991), and to the west (Cowan, 1990). These slip-rates contribute to the understanding of the evolution of Hanmer Basin.

The seismic hazard posed by the Hope Fault east of Hanmer Basin can be assessed using

known or inferred parameters for that section of the fault. In this chapter an evaluation of the seismic hazard is made using empirical formulae that relate expected and maximum magnitudes of earthquakes to the length, width and displacement of the faults in question.

3.2 Stream loop locality

3.2.1. Site description

At the stream loop locality one kilometre east of Hossack Station homestead, the Hope Fault occurs as a single trace striking at 075 degrees (Figure 3.1). Although not exposed at this locality, the fault plane was observed to dip at 70 degrees to the north, approximately 500 metres to the west (Figure 2.4). As the Hope Fault passes from the Hanmer River valley to the Little Lottery River catchment, it crosses a small stream that drains along the fault before joining the Hanmer River. The stream catchment lies to the north of the fault. An incised channel crosses the fault approximately 700 metres to the east of the trench locality and is displaced by up to 240±30 metres (Figure 3.1). The vertical fault offset is less than two metres at this site, with the north side upthrown. The site selected for trenching to establish a slip-rate is located where the stream recrosses the fault, from south to north (Figure 3.1). At this locality the stream channel is incised 2-3 metres on the south side of the fault, and shows no evidence of meandering. Where the stream crosses the fault, three separate phases of channel development are evident from the presence of three incised stream loops (Figures 3.1 and 3.2). The stream loops are preserved on the northern, upthrown side of the fault. A fan is currently aggrading from the northeast. The fan is inferred to be active, and streams have contributed fine sediment to the swamp. A small catchment (0.2 km^2) means the streams lack the stream power to discharge coarse material across the swamp and into the stream loops. The abandoned stream channels are currently poorly drained, and carry a small flow from the swamp. Preliminary augering, indicated a carbonaceous and woody layer at depths of up to 2.5 metres in the swamp. This, in conjunction with the reducing swamp environment, indicated excellent potential for preservation of organic material suitable for radiocarbon dating.

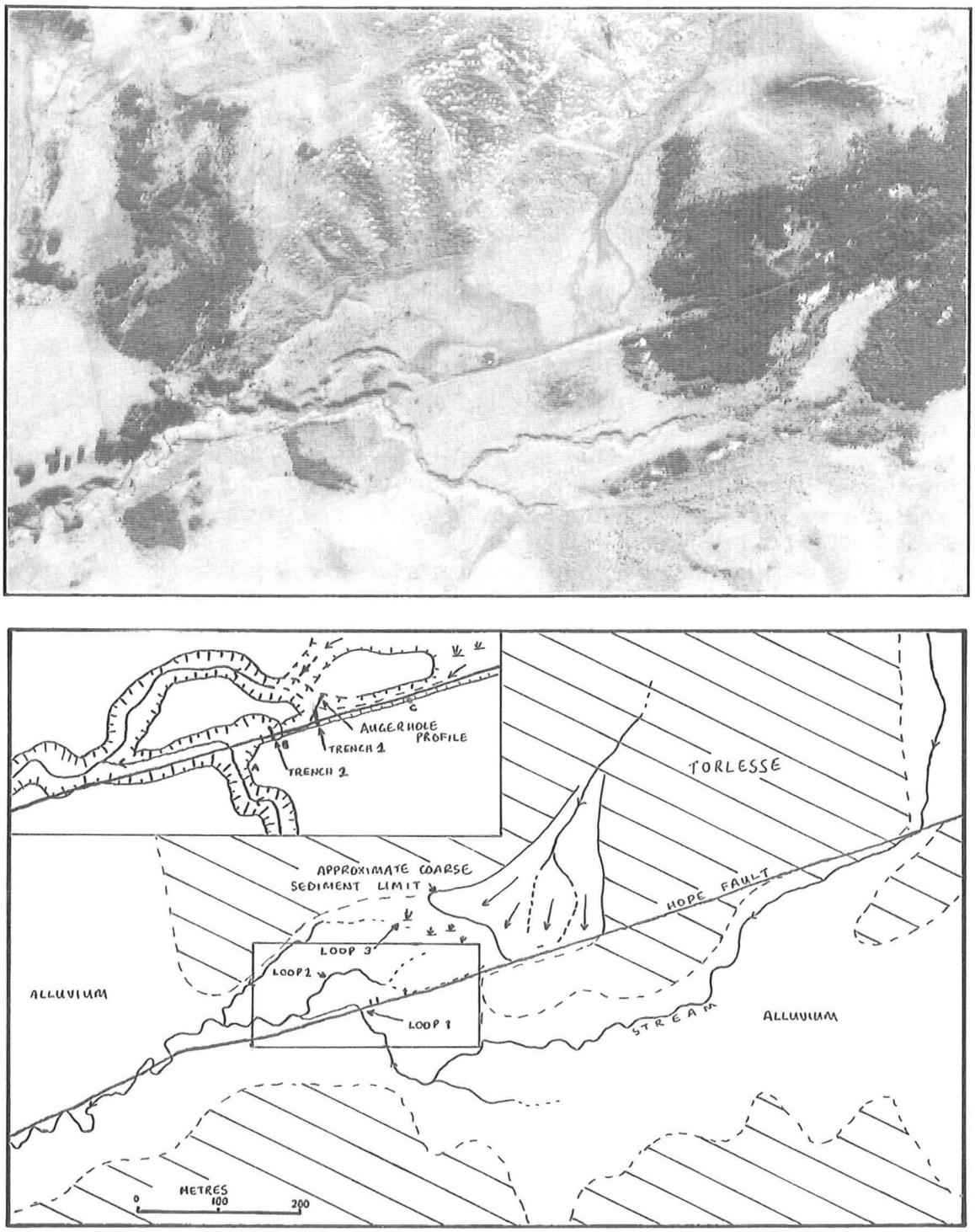

Figure 3.1 Stream loop locality at Hossack Station. The Hope Fault active trace strikes approximately 075°. Three phases of stream channel offsetting are evident north of the fault, with trench and augering locations shown on the inset. Crosshatching represents Torlesse exposed through alluvial gravels. Fan and swamp development are evident in the centre of the photo and map. AB is the maximum offset of the youngest stream loop; AC is the maximum offset of the second loop. Airphoto base NZ Aerial Mapping (1950) 1797/25. Scale is approximately 1:8000.

3.2.2 Trenching at the stream loops

In order to determine the fault rupture history, trenching of the organic-rich deposits adjacent to the fault was undertaken at the offset stream loops locality. Hand augering had broadly defined the subsurface stratigraphy and enabled the trenches to be located in the optimum positions. Figure 3.3 shows the seven auger holes, aligned across the second stream loop (Figure 3.1 for location). The augering indicated a buried channel cut in bedrock (Figure 3.2), with a thin cover of gravel overlain by silt to a depth of approximately two metres. Below a depth of one metre, blue-grey silt and abundant organic material, ranging from peat layers to wood samples several centimetres in diameter, was retrieved. The auger failed to penetrate below approximately two metres, where fine subangular gravels were subsequently exposed in the trench. This was assumed to be a bedrock contact.

Following the augering programme, three trenches were excavated. Each trench was dug across the fault and into the channel-fill deposits to a depth of two to three metres. Two trenches were located in the youngest loop, with one in the second loop (Figure 3.1), only the two trenches providing the most information were logged in detail (Figures 3.4 and 3.5). Both trenches provided organic material for radiocarbon dating of the deposits. Carbonaceous material was also taken from the third, unlogged trench, to further determine an age for the youngest offset stream loop.

3.2.3 Trench stratigraphy and fault related deformation

The stratigraphy beneath the first and second stream loops is illustrated in Figures 3.4 and 3.5 respectively. Each trench shows a one to two metre thickness of silt underlain by gravel (Figures 3.4 and 3.5). The gravel unit is poorly sorted and poorly bedded, and contains wood up to almost one metre in length (see Figure 3.4). The silt material contained scattered pebbles and abundant organic material, usually twigs up to two centimetres in diameter.

A clear division between two types of sediment is shown in the stratigraphy. The upper units of the stratigraphy are composed entirely of fine sediment (silt and clay) and the lower units are

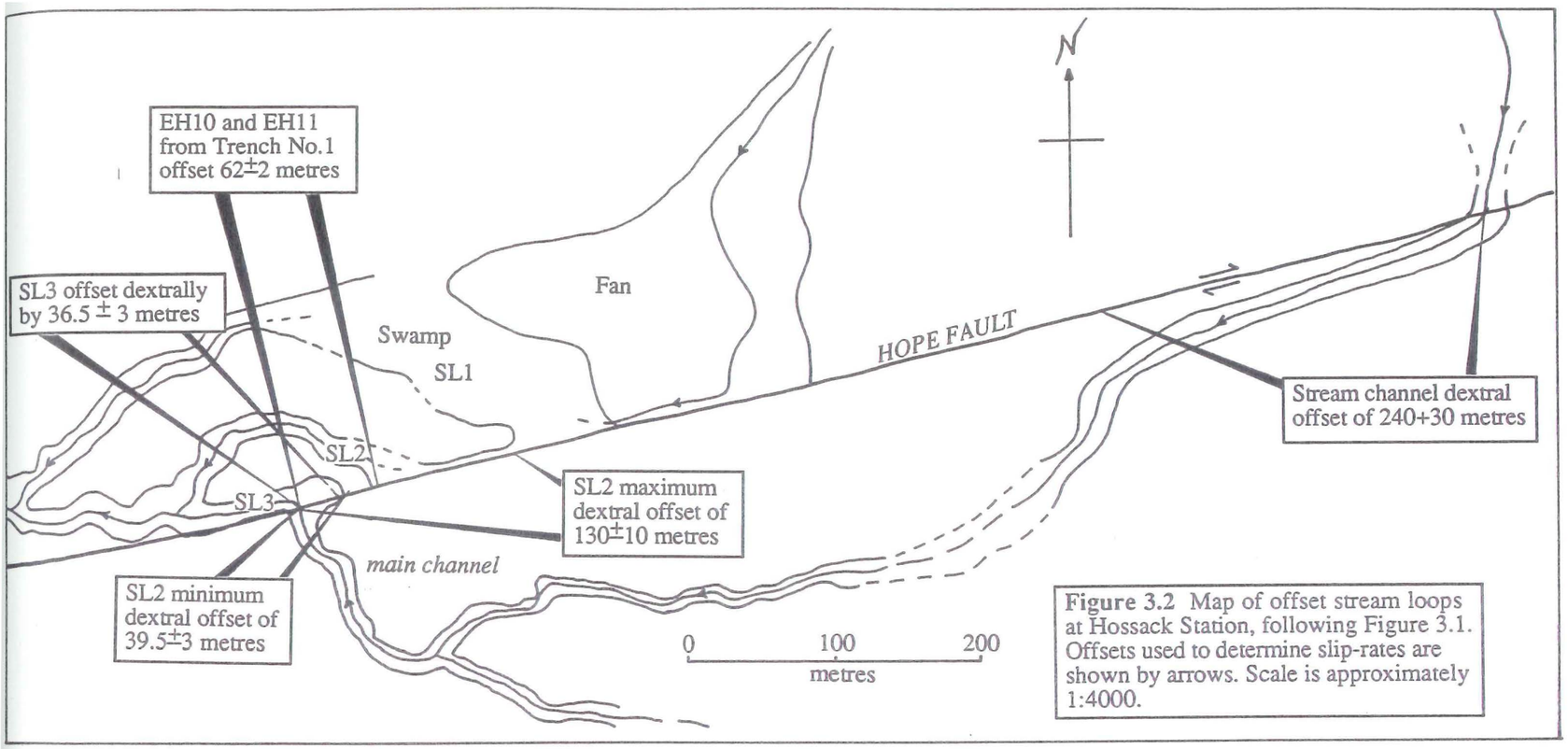

Figure 3.2 Map of offset stream loops at Hossack Station, following Figure 3.1. Offsets used to determine slip-rates are shown by arrows. Scale is approximately 1:4000.

Oblique elevated photograph of the stream loops site-looking south. The active channel crosses the fault at the centre of the view and flows off to the right.SL2 is apparent as a 'D'-shaped channel filled with scrub in the middle of the photograph. Bright green area at extreme left is the swamp, filling SL1. SL1 crosses the bottom of the view, beneath the photographer.

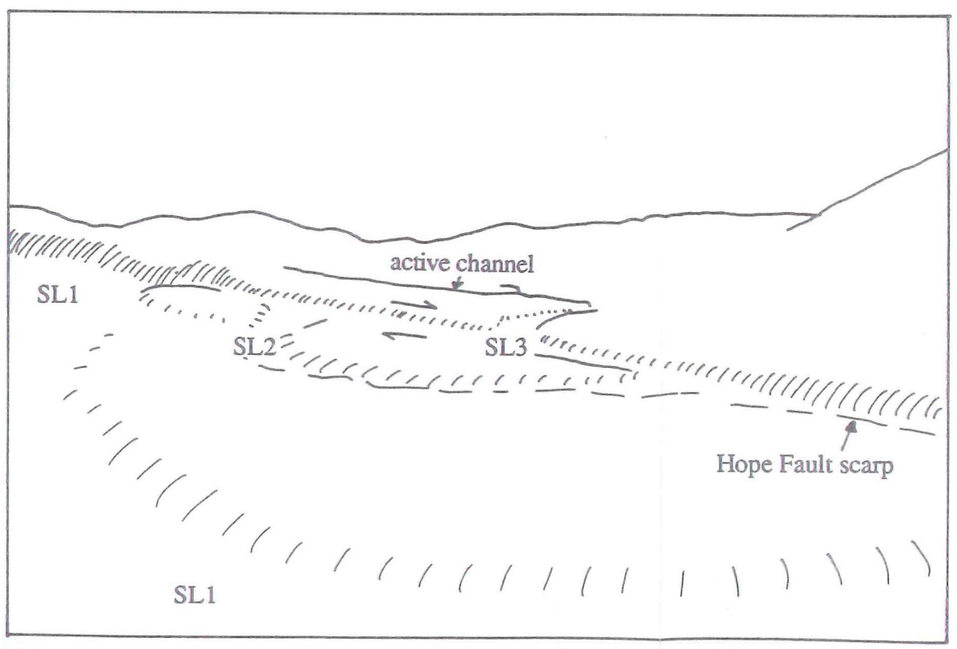

composed of angular gravels. The gravels are poorly sorted and poorly bedded, they are inferred to be debris flow materials deposited during periods of heavy rain. It is unlikely that these deposits came from the fan on the northeast side of the fault, as the stream on the fan lacks the power to transport coarse material as far as the trench sites. However, the main stream (Figure 3.1) has a catchment that is five times larger and a correspondingly higher stream power, suggesting that it is the probable source of the coarse materials. Auger logs from the swamp adjacent to the fan (Figure 3.1), showed only scattered pebbles in a silty matrix, to a depth of two to three metres. These logs indicate that the limit of coarse material derived from the fan is restricted to the area shown on Figure 3.1. The gravel exposed in the trenches is therefore likely to have been deposited by the large stream, rather than streams from the fan. This interpretation is also supported by the auger logs (Figure 3.3), which suggest that the gravels follow the topography of the present stream loop.

The fine sediments exposed in the upper part of the trenches are inferred to be overbank deposits which post-date the offsetting of the stream loop in which each trench is located. These deposits were probably laid down during flood events when the stream overflowed its channel, forming eddies behind the offset stream loop, which trapped suspended silt, clay and organic material.

In both trenches the fault zone is clearly defined by the presence of a soft, clay-rich pug, which is interspersed with fine angular chips of Torlesse sandstone. This material is: (1) mixed by fault movement with disturbed "A" horizon material (Figure 3.5), and (2) injected into the lithologies immediately adjacent to the fault (Figure 3.4). In Trench No.2, two fault shear gouge zones signify at least two different faulting events, and are separated by the deposition of gravels immediately south of the most recent trace. Units 5 and 6 immediately south of the active surface trace in Trench No.1, are tilted (30 degrees to the south). This tilting was not evident in either of the other trenches.

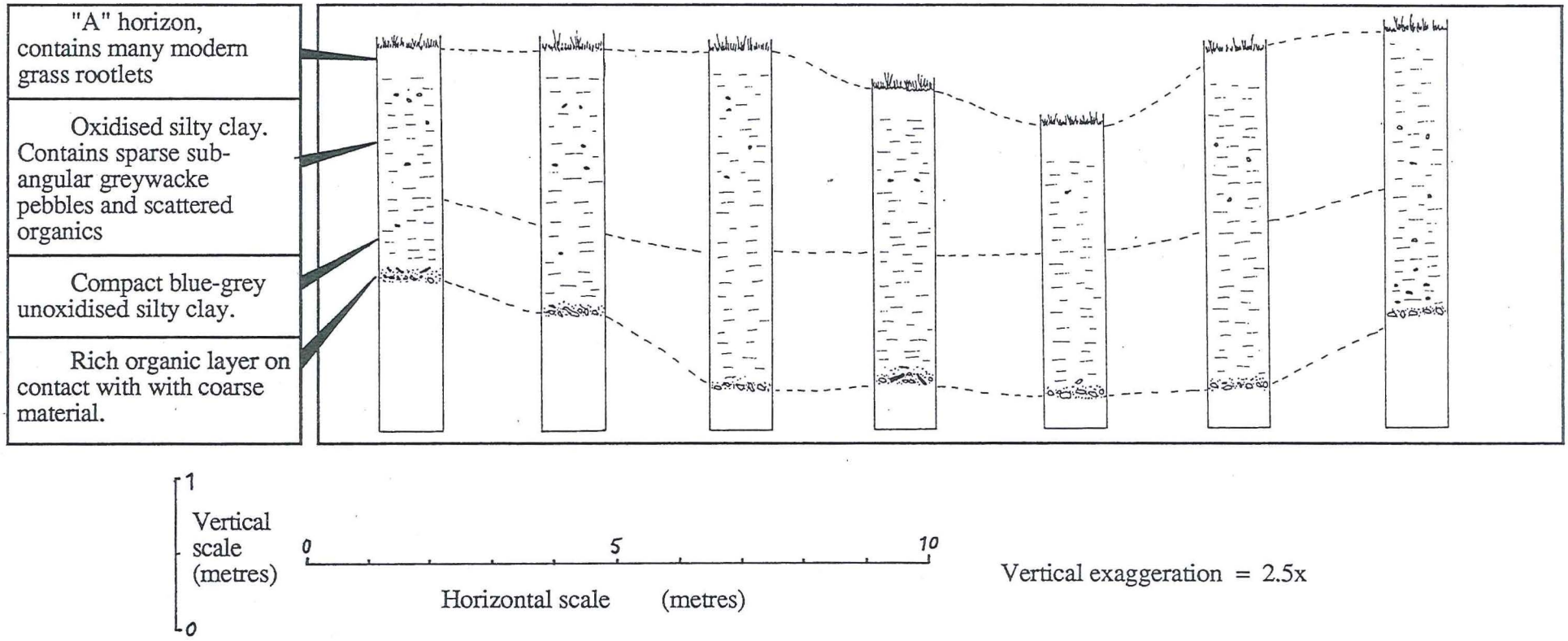

Figure 3.3 Auger stratigraphy compiled using a disturbed sample hand auger, forming a cross-section of SL2 at Hossack Station stream loops locality. Channel floor shown to mimic ground surface (inferred to be cut in bedrock as auger would not penetrate, however it was later proved to be gravel material).

Sample	Locality	Unit	Description	Weight	Age (conventional)	Age (calibrated)
EH8 (Wk 1992)	Trench 1	3: gravel	Nothofagus	82 g	3660 +/- 60	3630+/-60
EH10 (Wk 1993)	Trench 1	2: silt	Nothofagus	83.1 g	2410 +/- 50	2380+/-50
EH 11 (Wk 1994)	Trench 1	7: silt	Nothofagus	12.48 g	2420 +/- 40	2390+/-40
EH 15 (Wk 1995)	Trench 2	3: gravel	Nothofagus	25.8 g	930 +/- 40	900+/-40
EH 19 (Wk 1196)	Trench 2	2*: silt	Nothofagus	63.43	470 +/- 55	440+/-55

Table 3.1 Sample description and age determined by radiocarbon dating. A more detailed description is given in appendix B. * EH19 was sampled from with Trench No.3, but the silty sediment in which it was found was correlated between the trenches as being Unit 2 (see Figure 3.4). For calibration details refer to Appendix 2.

3.2.4 Radiocarbon dating of trench stratigraphy

Five pieces of wood were sampled from fine and coarse units in the three trenches, in order to bracket the age of stream channel abandonment (Table 3.1). The wood samples may be of the genus *Nothofagus*, the dominant indigenous forest tree in the area.

Samples EH10 and EH8 were selected for dating because they were located above and below the inferred stratigraphic boundary between gravel deposits of the active channel, and fine deposits representing overbank deposition after the stream loop had been offset. Sample EH11 was recovered from Unit 7, in Trench No.1, within disturbed deposits alongside the fault, having been incorporated during fault rupture. EH11 therefore predates the last rupture of the fault.

The deposits from Trench No.2 showed a similar relationship between fine overbank sediment and overlying coarse channel deposits. Sample EH15 was recovered from within gravel (Unit 3- Figure 3.5) and may have been deposited prior to the first increment of fault displacement of the channel associated with the youngest offset stream channel. No suitable sample was found in the overbank material from this trench.

The third trench, also situated in the youngest offset stream channel (Figure 3.1), showed the same stratigraphy as Trench No.2 and provided sample EH19 from within overbank silts.

3.2.5 Slip rate determination

The slip-rates determined during this study are based on the five radiocarbon dates from the trenches (Figures 3.4 and 3.5). Stream loop terrace risers and trench locations were measured relative to the active channel position, south of the fault, using EDM surveying. Table 3.2 shows a summary of slip-rate calculations.

3.2.5 (i) Interpretation of stream loop offsets

The abandonment of the second stream loop (SL2) and the establishment of the youngest stream loop (SL3) is interpreted have occurred in response to dextral faulting. Stream loop (SL2) (Figure 3.2), has been progressively uplifted by fault displacements relative to the channel on the south side of the fault. Relative uplift on the north side of the fault reduced the stream gradient,

Trench No.1 log

UNIT 1: Light, greeny grey, **clayey silt**, with some fine sub- angular gravel. Orangey brown mottling, and dark grey- brown, manganese staining at base. Overlain by organic- rich topsoil, containing abundant charcoal and rootlets.

UNIT 2: Massive, light greeny grey to blue grey, gleyed **silty clay**. Clear base to oxidised zone indicated by colour change. Rich organic layer along base of unit and scattered with roots below base of oxidised zone.

UNIT 3: Massive to crudely bedded, blue grey, medium **gravel**. Poorly consolidated, with abundant organic material, from fine, organic- rich mud, to 0.75 metre tree stump. Overlain by organic- rich, loose, medium to coarse gravel, near fault.

UNIT 4: Massive, poorly sorted, blue grey, angular, fine to medium **gravel**, in stiff, gritty clay matrix.

UNIT 5: Massive to crudely bedded, grey, gleyed, subangular to subrounded, medium **gravel**,in sandy matrix.

UNIT 6: Browny grey, fine **sand** to silt, with fine angular gravel bed and organic- rich silt bed. Overlain by oxidised, angular to subangular, medium to coarse sandy gravel.

UNIT 7: **Fault zone**. Dark grey silt with scattered organics. Wedges of colluvium, containing angular clasts up to 10 cms long. Injections of silt into coarser material are common.

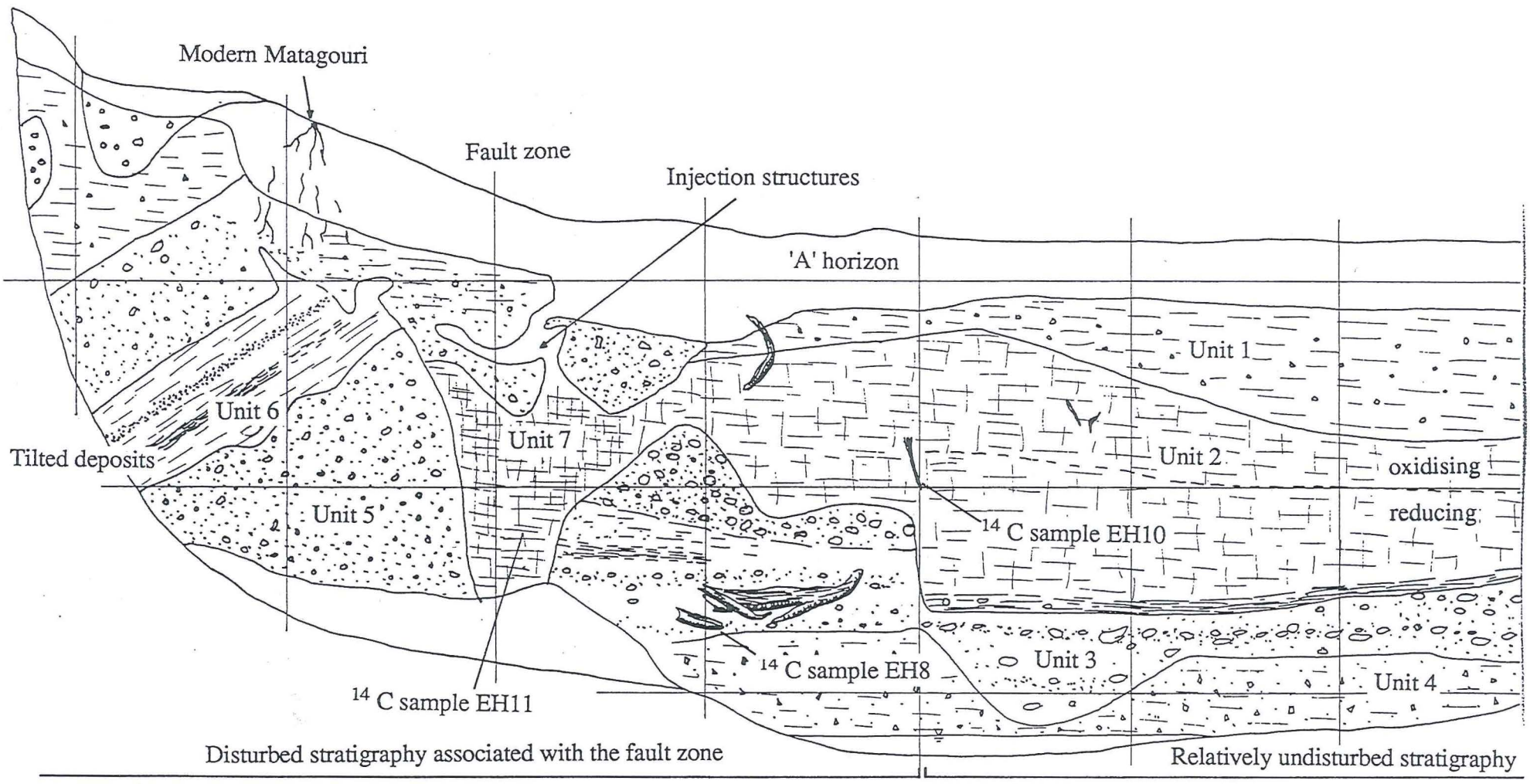

Figure 3.4 Trench log of Trench No. 1 Logged by H.A. Cowan, J.K. Campbell and T.J. McMorran

Trench No.2 log

UNIT 1: Massive, dense, grey brown, mottled, oxidised, silty, sandy, **clay**, with subangular to angular greywacke clasts (<3 cms) and rootlets. Below oxidising level, dark grey to greenish grey, crudely bedded, poorly sorted, subangular gravel with organic pods.

UNIT 2: Massive, dense, moist, grey green **clayey silt** with angular to very angular fragments of greywacke. Sparse rootlets below oxidising zone. Becomes more sandy in oxidising zone.

UNIT 3: Massive to crudely stratified, dark grey to dark greyish green, subangular to subrounded, poorly sorted, coarse **gravel** in silt and clayey silt with some sand, to sandy silt with some clay, matrix.

UNIT 4: Massive, dark brown to yellowish brown, mottled, moist, **clayey silt** with some sand and fine angular pebbles- transition to mottled subsoil and organic rich topsoil.

UNIT 5: Dark grey to greyish green, moist, plastic **silty clay**.

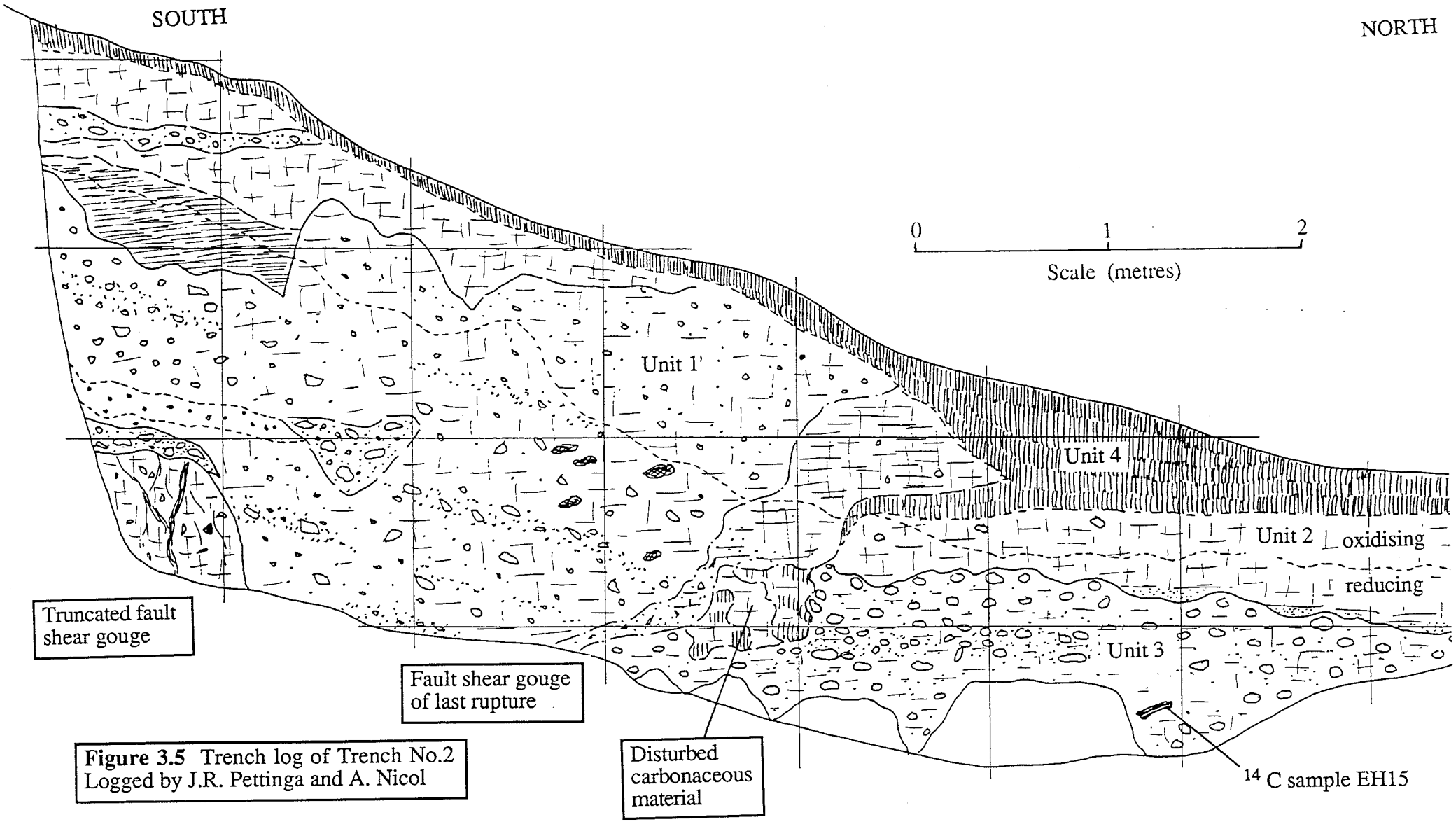

Figure 3.5 Trench log of Trench No.2
Logged by J.R. Pettinga and A. Nicol

presumably to the point where the formation of a new stream channel westward, along the fault, was easier than maintaining the old channel. The dextral offset of the youngest stream loop (SL3) is 36.5±3.0 metres, (distance 'A'-'B' in Figure 3.1 and Figure 3.2). This measurement was made between the centre of the present-day active channel, where it crosses the active fault trace, to the top of the riser (R3), also adjacent to the fault. The error associated with this measurement comes from the 3 metre width of the floor of the active channel south of the fault, and the uncertainty of the initial position of the channel relative to the riser (ie. the riser position marks a maximum eastward location for the new channel, but the stream may have been some distance (3 metres) west of the riser crest).

The position at which the oldest stream loop (SL1-Figure 3.2), was abandoned in favour of the second stream loop (SL2)(point 'C' in Figure 3.1), is inferred to be 130±10 metres from the main channel on the south side of the fault. The relatively large error associated with the position of establishment of the second stream loop (SL2), reflects the uncertainty in locating the position of the former stream channel- which flowed almost parallel to the fault scarp at this point (Figure 3.1). The lower limit of offset for the second stream loop (SL2); ie. the amount of horizontal fault displacement that has occurred since abandonment of that channel, is the maximum offset of the youngest stream loop (SL3), plus the displacement that occurred during the earthquake that caused the second channel (SL2) to be abandoned. The horizontal displacement that is likely to occur in association with an earthquake on this section of the fault is 3 to 5 metres (Section 3.5.3). Thus the minimum offset for SL2 is 33.5 metres plus 3 metres for the single event; a total of 36.5 metres. The minimum and maximum offsets of SL2 are thus 39.5±3 metres and 130±10 metres respectively (Figure 3.2). Sample EH8 (3630 ± 60 years- Table 3.2) was taken from within the gravel in Trench No.1, and represents a time prior to channel abandonment.

3.2.5 (ii) Slip-rate calculations

Following Knuepfer (1984) and Cowan (1989), slip-rate errors were calculated using: (a) the minimum offset divided by the maximum age (a lower bound); and (b) the maximum offset divided

Sample	Age	Loop displacement		Slip-rate	
		min.	max.	min.	max.
	(years B.P.)	(metres)		(mm per year)	
EH8(Wk1992)	3630 +/- 60	39.5+/-3	130+/-10	9.9	39.2
EH10(Wk1993)	2380 +/- 50	39.5+/-3	60+/-2	15.0	26.6
EH11(Wk1994)	2390 +/- 40	39.5+/-3	60+/-2	15.0	26.4
EH11(Wk1995)	900 +/- 40	-	36.5+/-1.5	-	37.2
EH19(Wk1996)	440 +/- 55	-	20+/-1.5	-	48.0

Table 3.2 Slip-rates estimated for the Hope Fault at the stream loops site at Hossack Station. Minimum slip-rates are calculated using minimum offset in maximum age and maximum slip-rates are calculated using maximum offset in minimum age. Ages are calibrated radiocarbon dates.

by the minimum age (an upper bound). The Late Holocene slip-rate implied by the age of SL2 (based upon the radiocarbon age of EH8) and the amount of fault offset, is a maximum of 39.2 mma^{-1} and a minimum of 9.9 mma^{-1} (Table 3.2).

The sediments from which samples EH10 and EH11 were recovered (Figure 3.4), were deposited after the abandonment of SL2. Trench No.1 was located 60.0 ± 0.5 metres east of where the active channel crosses the fault (Figure 3.2). Samples EH10 and EH11 determine the maximum amount of slip that can have occurred since their deposition, as they would have been removed by subsequent erosion had the stream been subsequently faulted past their position (Trench No.1 in Figure 3.1). Since EH10 an EH11 were deposited, 62.0±2 metres of fault displacement has occurred, suggesting a maximum slip-rate of 26.5 mma^{-1}.

Sample EH15 (900 ± 40 years- Table 3.1) is interpreted as having been deposited soon after the establishment of SL3. The amount of fault displacement that has occurred since the abandonment of the second stream loop is 36.5 ± 3.0 metres, as described above. The slip-rate determined from sample EH15 is a maximum of 37.2 mma^{-1} (Table 3.2). Sample EH19 (440 ± 50 years-Table 3.2), was taken from Trench No.3. After its deposition up to 22 metres of fault displacement has occurred. This represents a maximum slip-rate of 48.0 mma^{-1}.

3.2.5 (iii) Errors associated with radiocarbon dating

An important source of errors to be considered when using radiocarbon dates of organic material to date stratigraphic units or geological relationships, is that the age assigned to a sample represents the time at which that sample ceased to absorb atmospheric carbon; ie. the time of death of the sample. It is possible that a sample could be preserved, possibly buried and subsequently eroded and redeposited for some period of time before being deposited in the sampled position. Such events could explain an anomalously high age for a sample. An anomalously young age for a sample could be due to contamination by younger carbonaceous material. Contamination was not evident in the samples chosen from the Hossack Station trenches.

3.2.6 Interpretation of slip-rate results

The slip-rates that were determined during this study range from 9.9 mma^{-1} to 48.0 mma^{-1}. As the plate convergence rate is approximately 47 mma^{-1} (Bibby 1981) at this latitude, the latter slip-rate is certainly excessive. The slip-rates calculated for SL3 are significantly higher than those determined for SL2. Although values calculated for SL3 are maximum slip-rates; and the errors are proportionately higher for the small values of fault displacement relative to the active channel width (3 metres), the difference may reflect a Late Holocene increase in slip-rate.

The slip-rate determinations vary in reliability due to: (i) their stratigraphic position ie. how close to the boundary between the coarse and fine sediment the sample locality was: Figures 3.4 and 3.5; and (ii) the maximum and minimum fault displacement limits for the sample. Samples EH10 and EH11 probably provide the most reliable indication of slip-rate of 26.5 mma^{-1} for the past 2400 years. This maximum slip-rate is important because it is significantly lower than the slip-rates that have been determined east towards the Hikurangi Subduction Zone (eg. Van Dissen 1989; Bull pers. comm. (1991). Sample EH8 probably provides the most reliable minimum of 9.9 mma^{-1}. The inferred slip-rate for this locality is thus 9.9 to 26.5 or 18 ± 8 mma^{-1}.

3.3 Boundary stream locality

3.3.1 Site description

Immediately west of the junction of Hanmer River and Boundary Stream (Figure 3.6), a promontory of basement Torlesse covered by a veneer of Holocene river gravel is preserved within a meander loop of the Hanmer River. It is cut by two ENE striking active traces of the Hope Fault. Between the two fault traces a tectonic depression has formed; with the north side upthrown by 3-4 metres and the south side upthrown by 7 metres. The northern fault incorporates a right step-over or releasing bend of about 15 metres, which may have contributed to the development of the "graben", and made matching of the terraces across the fault traces difficult. North of the "graben", several fault scarps are evident that are inferred to reflect reverse faulting, being upthrown to the

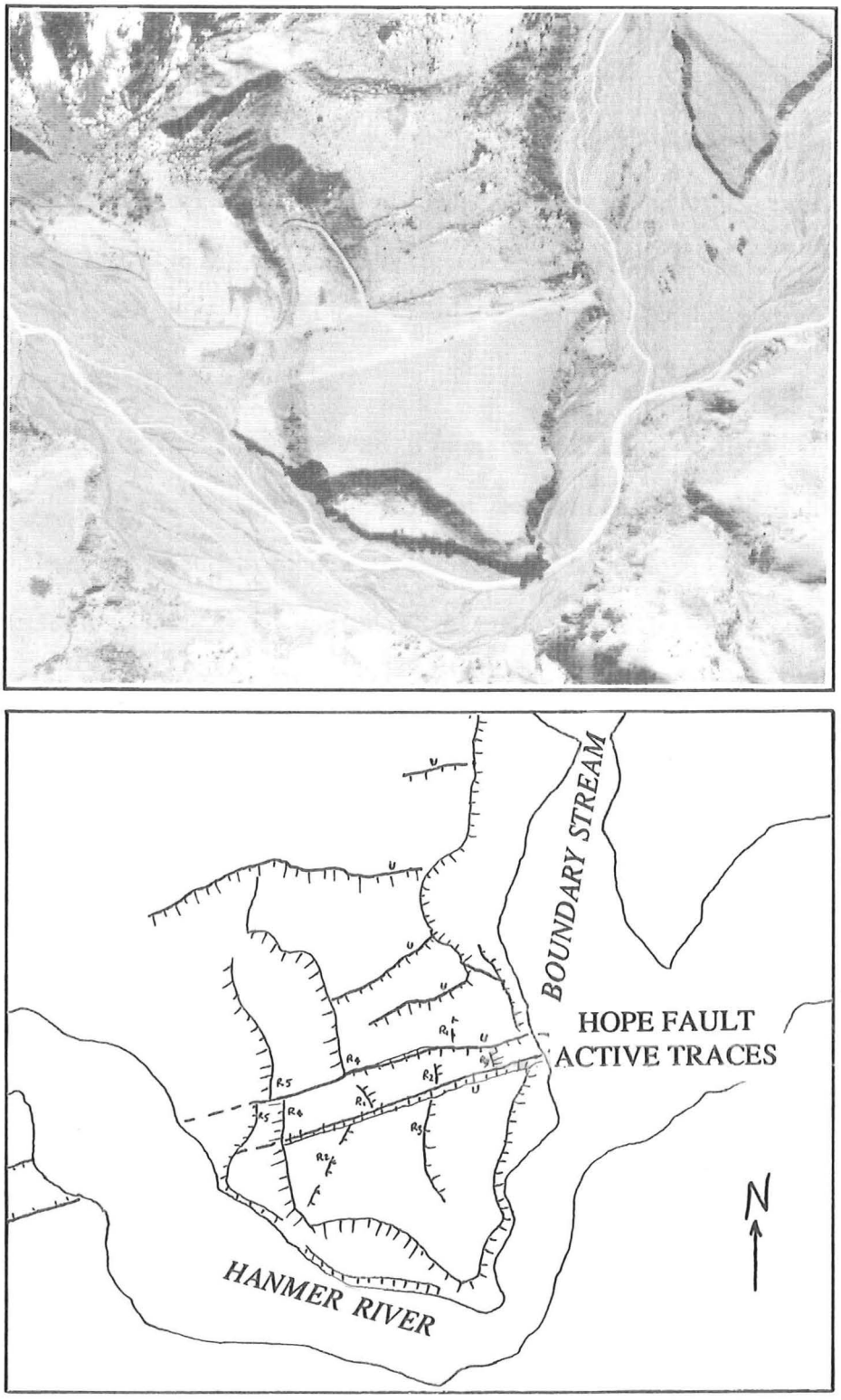

Figure 3.6 Boundary Stream locality at Hossack Station. Two traces are evident striking at 070°. Terrace risers (R_1-R_5) are dextrally offset by the faults. R_4 and R_5 are offset by the northern fault only. Dip-slip faults north of the dextral traces, are probably reverse and north-dipping, see text. Airphoto is from 1950 (1798-23), scale is approximately 1: 8000.

north. The site is between 20 and 30 metres above the present level of the Hanmer River and several former terrace risers show dextral of up to 260 metres. The terrace risers vary from 0.5 metres to about 20 metres in height and are poorly matched across the faults.

3.3.2 Fault movement history

Remnants of the terrace risers are used to interpret the Holocene history of faulting at the Boundary Stream site. The formation of the "graben" between Holocene traces of the Hope Fault may reflect different orientations of the two faults. Given that the Hope Fault is transpressional at this locality (refer to Chapter 2), the vertical offsets imply a north dip for the northern fault and a south dip for the southern fault. Freund (1971) following Lensen (1958) suggested that the "graben" has formed as a result of strike-slip movement of the northern fault, and dip-slip movement on the southern fault. This theory is untenable because terrace riser offsets at the site indicate that both faults are predominantly strike-slip in character.

A flight of five degradational terraces are offset by the two active traces (labelled R1 to R5, Figure 3.6). At least 260 metres of fault displacement has occurred since the first degradational terrace was formed during the Late Pleistocene or early Holocene. Risers R1, R2 and R3 have been displaced cumulatively by both fault traces (>260, 210±6, and >145+ metres respectively). The riser offsets at this site were initially mapped on aerial photographs (1797/20 and 1798/20), checked by field investigation, then measured by EDM surveying. Errors are estimated to be ±3 metres for horizontal displacements and ±0.5 metres for vertical displacements, based upon the uncertainty of matching the riser crests across the faults. Risers R4 and R5 have been displaced by the northern fault only, implying that activity has switched from the southern fault trace to the northern fault trace prior to the formation of riser R4.

Another promontory, opposite Shingly Creek, 1 kilometre east of Boundary Stream (Figure 2.1; Map 2), is traversed by two active traces that are both upthrown to the north. The transpressional regime inferred for the locality, based upon the relative fault throws as discussed in Chapter 1, suggests that both of these faults dip to the north. Both faults exhibit dextral

Locality	Author	slip-rate	h/v ratio	comments
Harper Pass	Hardy and Wellman (1984)	14		28 000yr BP riser? displaceed 200m
Glynn Wye	Clayton (1966)	15.25		20 000yr BP moraine displaced 305 m
	Freund (1971)	7.45		20 000yr BP moraine displaced 149 m
	Suggate et. al. (1978)	8.2		18 000yr BP moraine displaced 147 m
	Hardy and Wellman (1984)	17		20 000yr BP moraine displaced 336 m
	Knuepfer (1984)	20.9		16 630 +/- 3230yr BP moraine displaced 347 +/- 7 m
	Knuepfer (1988)	19.5		18 680 +/- 3780yr BP moraine displaced 347 +/- 7 m
	Wellman (1985)	13.3		15 000yr BP moraine displaced 200 m
	Cowan (1989)	16.8		17 000 +/- 1000yr BP moraine displaced 286 +/- 6 m
	Cowan (1990)	14+/-3*		17 000 +/- 2000yr BP moraine displaced 230 +/- 20 m
Manuka Creek	Knuepfer (1984)	8.2		4 010 +/- 520yr BP riser displaced 32.7 +/- 3 m
		14.8		1 220 +/- 100yr BP riser displaced 18.1 +/- 3.5 m
	Wellman (1985)	20		1 800yr BP riser displaced 36 m
	Cowan (1989)	10.6+/-0.3*	15-17	3 482 +/- 77yr BP riser displaced 36 +/- 0.5 m
Hossack Station	This study	18+/-8	30-33	162 +/- 2 m h.& 5 +/- 1 m v. displacement of riser (see section 3.2.5)
Sawyers Creek	Van Dissen (1989)	28 +/- 8		2 780 +/- 560yr BP riser displaced 78 +/- 2 m
		33 +/- 13	13.6	4 570+/-910yr BP riser displaced 150+/-20m h. & 11m v.
Goldmine Creek	Van Dissen (1989)	16		14 375+/-2000yr BP fan displaced 230+/-20m
Hapuku River	Knuepfer (1984)	2	1.5	6 290+/-950yr BP riser displaced 30+/-10m h. & 10-12m v.
	Van Dissen (1989)	4.8	3	6 290+/-950yr BP boulder bar displaced 12.6m h. & 8.5+/-0.3m v.

Table 3.3 Slip-rates (mma^{-1}) calculated for the Hope Fault, showing the general trends in variation of h/v ratio and slip-rate.* denotes best estimate.

displacements. The southern fault offsets a terrace riser by 56±16 metres (the large uncertainty reflects the measurement of this displacement from an aerial photograph (1797/23), and the acute angle between the fault trace and the terrace riser). Perpendicular to the northern fault, two abandoned stream channels 48±4 metres apart, suggest that dextral displacement has occurred, but an accurate total displacement cannot be measured due to uncertainty about the relative position of the stream source. Continuity of these fault traces with the active traces at Boundary Stream is unknown due to a lack of exposure between the sites where the faults cross the active Hanmer River floodplain.

3.4 Slip-rates for the Hope Fault.

The dextral slip-rate (18±8 mma^{-1}) determined at the stream loops site, accounts for a large percentage of the total strain (45±5 mma^{-1}) estimated by Bibby (1981), to be presently accommodated by the Marlborough Fault System. Thus the Hope Fault accounts for a significant component of plate boundary deformation of the Marlborough/North Canterbury area. Table 3.3 and Map 3 present slip-rate data for the Hope Fault determined by several workers. Three significant trends of these data are:

(1) The slip-rates are higher on the Conway segment northeast of Hanmer Basin, than along the Hope River segment to the west of the basin.

(2) The Holocene dextral slip-rate on the main strands of the Hope Fault appears to decrease towards Hanmer Basin, both from the east and west.

(3) The dextral slip-rate decreases sharply at the northeast end of the Hope Fault, near the Kaikoura Coast.

The highest slip-rate is along the Kahutara Segment of the fault (Van Dissen 1991) near Charwell Basin, (approximately 35 mma^{-1}, Bull pers. comm. 1991; 20-25 mma^{-1}, Van Dissen, 1991). This may reflect the proximity of the strike-slip Hope Fault to the Hikurangi Subduction Zone. The Mount Fyffe and Seaward Segments (Van Dissen 1991) of the Hope Fault have a more oblique nature as discussed below. The slip-rates on the Mount Fyffe and Seaward segments are

lower than the Kahutara and Conway segments, and slip from the Hope Fault may be accommodated by transfer to the Jordan Thrust and the Fyffe Fault and by folding within basement rocks (Van Dissen 1991). The Seaward Segment is inferred to have been inactive during the Holocene (Van Dissen 1989).

The drop in dextral slip-rate at Hanmer Basin presumably reflects the complex dissipation of strain to the ends of the adjacent fault segments. Cowan (1989;1990) inferred that the apparent drop in Late Quaternary slip-rate between Glynn Wye and Manuka Creek was matched by a proportionally similar decrease in horizontal displacement that occurred during the 1888 earthquake.

The horizontal/vertical (h/v) ratio is a measure of the obliquity of displacement across a fault. A strike-slip fault has a high h/v ratio, while a dip-slip fault has a low h/v ratio. The h/v ratios shown in Table 3.3 show that the obliquity of slip on the Hope Fault decreases from the Kaikoura Coast westwards to Hanmer Basin. The h/v ratio at Manuka Creek is lower than at Glynn Wye or at Hossack Station and may indicate the effect of local transtension on the Hope Fault.

The azimuth of principle horizontal shortening (PHS) is approximately 120 degrees in North Canterbury and Marlborough (Nicol pers. comm. 1991). Assuming that this is consistent at Hossack Station, the PHS direction differs by about 50° from the strike of the Hope Fault and implies that this section of the fault is likely to be transpressional. The Hope River Segment of the Hope Fault strikes more easterly (approximately 085°) and differs from the regional principle horizontal compression direction by only $30\text{-}35^{\circ}$, consistent with Cowan (1989,1990) where he suggests that this section of the fault is undergoing transtension. The Mount Fyffe Segment of the Hope Fault shows a low h/v ratio, consistent with an oblique fault motion vector. There, the principle horizontal compression direction is at about 65° to the fault strike.

3.5 Seismic hazard assessment of the Conway Segment

The object of seismic hazard assessment in the context of this study is to evaluate the likely magnitude and effects of coseismic rupture of the Conway segment of the Hope Fault. The

assessment follows empirical guidelines for estimating earthquake magnitude using the inferred fault length, fault plane area and maximum fault displacement; Wyss (1979), Slemmons (1982) and Bonilla et al. (1984). The formulae calculated by these workers are used to determine the likely earthquake magnitude for the Hope Fault, east of Hanmer Basin.

3.5.1 Probable rupture length

The Hope Fault east of Hanmer Basin comprises at least four segments: the Conway segment (Bull et al. 1991), the Kahutara segment, the Mount Fyffe segment and the Seaward segment (Van Dissen 1991). Van Dissen (1991) describes the Kahutara segment as being continuous from the Kowhai River to Hanmer Basin. For the purposes of seismic hazard evaluation in this study, I shall divide this section of the Hope Fault into the Conway and Kahutara segments, with a segment boundary at Charwell Basin. The Charwell Basin, 17 kilometres west of the Kowhai river, is formed by a one kilometre right stepover or releasing bend in the Hope Fault. Given that Lake Glynn Wye graben reduced the fault displacement by approximately 42% during the 1888 Amuri earthquake, as rupture propagated through it (Cowan 1989, 1990), it is possible that the Charwell Basin could arrest rupture on the Hope Fault (Bull, pers. comm. 1991). Maximum rupture lengths east of Hanmer Basin for the Hope Fault are thus 50 kilometres for rupture halted by Charwell Basin, and 67 kilometres for rupture from Hanmer Basin to the Kowhai Rivers. The boundary between the Kahutara and Mount Fyffe segments is located at the Kowhai River (Map 1). There the Fyffe Fault branches northward, accommodating much of the right-lateral slip from the Hope Fault (Van Dissen, 1991). The Jordan Thrust similarly accommodates movement from the Mount Fyffe segment and splays from the boundary between the Mount Fyffe and Seaward segments of the Hope Fault. Movements of both the Mount Fyffe and Seaward segments of the Hope Fault have occurred during the Quaternary. The Seaward segment has been active in the Late Pleistocene and the Mount Fyffe segment during the Holocene (Van Dissen 1989). Estimated slip-rate for the Mount Fyffe segment is 2.1-7.5 mma^{-1}, the drop in slip-rate from the adjoining Kahutara segment

(Table 3.3) is thought to be accommodated by the Fyffe Fault (Map 1), distributed shear within Torlesse, and folding of the Kaikoura Ranges (Van Dissen 1991).

3.5.2 Rupture width

Wyss (1979) proposed that more accurate estimates of earthquake magnitude can be achieved by considering the area of the fault plane that can rupture. Fault plane area can be inferred from the distribution of microearthquake aftershocks which delineate the ruptured fault plane. In New Zealand the modelled rupture depth for shallow earthquakes is 12 kilometres (New Zealand Seismological Observatory 1988).

3.5.3 Fault displacement

No single event fault displacements are evident at Hossack Station. The 1888 earthquake on the Hope Fault (Section 3.5.6) did not rupture east of Hanmer Basin (Cowan 1991). Near Charwell, single or multiple event offsets suggest 3-5 metre horizontal displacements (Bull, pers. comm. 1991) for rupture of the Conway segment. Comparison of slip-rates (Table 3.3) indicates that horizontal displacement is likely to be less at Hossack Station, than further east on the Conway segment or on the Kahutara segment. Therefore the maximum fault displacement likely to occur during rupture of the Conway segment is inferred to be five metres.

3.5.4 Recurrence interval for earthquakes generated on the Conway segment.

Using the estimated size of fault displacement for a single seismic event on the Conway segment (2-5 metres) and the averaged slip-rate estimate at Hossack Station determined earlier in this chapter, the likely return period for coseismic fault rupture can be estimated. An uniform rate of slip is assumed for the purpose of estimating the return period. Maximum and minimum inferred displacements for the fault are 5 metres and 2 metres, respectively. By dividing the minimum fault displacement (2 metres), by the maximum slip-rate (26.5 mma^{-1}), a minimum return period of 77 years is calculated. The estimated maximum return period is calculated by dividing the maximum fault displacement (5 metres) by the minimum slip-rate (9.9 mma^{-1}), to get a return period of 500

Equation (	Fault length (kms)	Fault area (km sq)	Max. displacement (m)	magnitude
1:Ms=4.15+logA	50	640	-	6.9
1:Ms=4.15+logA	67	657.6	-	7.1
2:Ms=1.404+1.169logL	50	-	-	6.9
2:Ms=1.404+1.169logL	67	-	-	7.1
3:Ms=6.974+0.804logD	-	-	3	7.4
3:Ms=6.974+0.804logD	-	-	5	7.5
4:Ms=6.24+0.619logL	50	-	-	7.3
4:Ms=6.24+0.619logL	67	-	-	7.4
5:Ms=7.00+0.748logD	-	-	3	7.4
5:Ms=7.00+0.748logD	-	-	5	7.5

Table 3.4 Earthquake magnitudes calculated using empirical formulae from: (1) Wyss (1979); (2) & (3) Slemmons (1982); (4) & (5) Bonilla et al. (1984).

years. Dating of earthquake-generated rockfalls using lichenometry techniques suggests that the last rupture of the Conway segment was about 1838 A.D. (Bull, et al. in press).

Accurate determination of a return period for this section of the fault depends upon better knowledge of the average amount of slip that is likely to occur during an earthquake. Lack of historical precedents makes this estimation difficult. However, the likelihood of a large earthquake being generated by rupture of the Conway segment is high, as based upon the figures given above, as the time elapsed since the last event is well above the estimated minimum return period.

3.5.5 Estimation of probable earthquake magnitude

Earthquake magnitude calculations for an individual fault are based on empirical relationships between earthquake magnitude, fault length, and maximum fault displacement. Table 3.4 was compiled using equations from Wyss (1979), Slemmons (1982) and Bonilla et al. (1984).

As the relationships used in Table 3.4 are derived by regression, the magnitudes determined by each formula is a "best fit" answer that is expected to be exceeded in 50% of cases. It is statistically possible to determine an expected magnitude which will be exceeded in a smaller percentage of cases. The maximum magnitude ($M_{a(L)}$) is determined for an exceedence probability (a)

$M_{a(L)} = M_{(L)} + t_{(1-a)} s[{}^{1}/_{n}+1]^{0.5}$ where a=exceedence probability; s=standard deviation; t=critical value from t-distribution for (n-2) statistical degrees of freedom; n=number of earthquakes in sample. The results for 1,5 and 10 percent exceedence probabilities are given in Table 3.5.

3.5.6 The 1888 Amuri earthquake

The 1888 Amuri earthquake, centred on the Hope River segment west of Glynn Wye (Mackay 1890; Cowan 1989,1990), is the only rupturing event to have occurred on the Hope Fault since European settlement. Assessment of the effects of the 1888 earthquake are based upon historical reports and field investigations. Isoseismal maps, based on felt intensities reported from central New Zealand - especially around the Hope Fault Zone, show strongly elliptical isoseismals,

Ms(L)	s	n	d.f.		t		M (L)
				1%	5%	10%	
7.3	0.293	23	21	1.323	-	-	7.7
7.3	0.293	23	21	-	1.721	-	7.8
7.3	0.293	23	21	-	-	2.518	8.1
7.4	0.293	23	21	1.323	-	-	7.8
7.4	0.293	23	21	-	1.721	-	7.9
7.4	0.293	23	21	-	-	2.518	8.2
Ms(D)							M (D)
7.4	0.331	18	16	1.337	-	-	7.9
7.4	0.331	18	16	-	1.746	-	8
7.4	0.331	18	16	-	-	2.583	8.3
7.5	0.331	18	16	1.337	-	-	8
7.5	0.331	18	16	-	1.746	-	8.1
7.5	0.331	18	16	-	-	2.583	8.4

Table 3.5 Earthquake magnitudes (Ms(D) and Ms(L)) calculated using emperical formulae from Bonilla et al. (1984). M(D) and M(L) are magnitudes that are adjusted to the exceedence probabilities of 1,5 and 10 %. Students t-distribution values are from Mendenhall (1983).

parallel to the Hope Fault Zone, indicating rapid attenuation north and south of the fault. These factors suggest a very shallow focus for the 1888 earthquake (Cowan 1991). Modified Mercalli intensities of MMIX were experienced along the fault and at Hanmer Plain. Cowan suggests that fault rupture initiated beneath the Hope River-Boyle River junction (the inferred epicentre), and propagated eastwards before being arrested by Hanmer Basin, a distance of 30±5 kilometres. Aftershock activity was concentrated at the Hanmer Plain for more than a month. The halting of rupture and concentration of aftershock activity at Hanmer Basin, is consistent with other examples of rupture arrest at releasing bends or stepovers, where suctional forces arise from the rapid opening of extensional fractures within fluid-saturated crust, and soak up the strain at the rupture tip (Sibson 1985,1986).

Shaking intensity was strongly influenced by subsurface geology. Hanmer Springs township was shaken at an intensity of about MMVI, whereas Woodbank and St Helens Stations, on the Hanmer Plain, experienced intensities of up to MMIX (Cowan 1989). This variation of intensity over a small distance reflects differences in subsurface geology. The depth of basin fill beneath Hanmer Springs is 60 metres, as opposed to several hundred metres closer to the centre of the basin (refer to Chapter 4).

3.5.7 Likely effects of coseismic rupture along the Conway segment

An earthquake associated with coseismic rupture of the Conway segment of the Hope Fault is likely to show similar effects to the 1888 Amuri earthquake. Felt intensities associated with an earthquake of magnitude 7.0 to 7.5 are likely to locally reach MMIX. Rupture arrest and the concentration of aftershock activity at the Hanmer Basin is likely to lead to some of the highest felt intensities, especially at the eastern end of the basin. High felt intensities would be expected to occur in a narrow zone adjacent to the ruptured fault segment, as was the case during the Amuri earthquake. Eiby (1966) describes the effects of MMIX shaking as leading to severe damage to masonry buildings. Damage to foundations, underground services and reservoirs is likely. Cracking of the ground may be conspicuous but damage to paths and roadways minor.

Sympathetic rupture of the Hanmer Fault, associated with coseismic rupture of the Conway segment, is probable and could lead to higher intensity shaking of Hanmer Springs than was experienced during the 1888 earthquake. Building damage associated with ground renting in a 100-200 metre wide zone along the fault trace should be expected (Pettinga pers. comm. 1989). Whether or not the Hanmer Fault will rupture in association with the Conway segment, and the detailed effects of rupture of the Hanmer Fault, are uncertain as no historic events have occurred.

The presence of many prehistoric landslides at Hossack Station suggests that seismically generated landslides would occur in response to ground shaking. The possible damming of streams and rivers along, or near the fault, should also be considered. The presence of remnants of a landslide dam in Boundary Stream is a good example. Eastward along the Conway segment at Mount Lyford, landsliding is also evident (Bell pers. comm. 1990). Reactivation of existing landslides, and the triggering of new ones should be considered likely in the event of an earthquake generated by movement of the Conway segment.

3.6 Summary and conclusions

The Hope Fault enters the study area from the Little Lottery River catchment to the east, where only one strike-slip fault trace is evident. A stream, dextrally displaced by approximately 260 metres, has formed a series of stream loops which have been progressively offset by dextral faulting.

Trenching of two of the offset stream loops at Hossack Station led to the recovery and dating of organic-rich overbank sediments, deposited after the former channels were abandoned. The dates indicate the timing of movements on this section of the fault, and imply a slip-rate of 18 ± 8 mma^{-1} for the last 3700 years. A slip-rate of about 35 mma^{-1} from the youngest offset stream loop (SL3) may imply a non-uniform rate of movement for the fault, or merely less certainty associated with the measurement of the stream loop offset.

The slip-rate for this section of the fault is lower than the slip-rate established for the Hope Fault further east at Charwell where it is inferred to be approximately 35 mma^{-1} (Bull pers. comm.

1991). The lower slip-rate at Hossack Station signifies the proximity of the fault segment boundary, represented by the Hanmer Basin. The slip-rate at Hossack Station is higher than that at Glynn Wye (14 ± 3 mma^{-1}), and at Manuka Creek (10.3 ± 0.6 mma^{-1}), (Cowan 1989, 1990). The higher slip-rate east of Hanmer Basin may reflect the proximity to the Hikurangi Subduction Zone.

The investigation of active traces at three localities (Stream Loops, Boundary Stream, and opposite Shingly Creek) all suggest that the activity has migrated from one trace to another during the Holocene. The best example (Boundary Stream locality) shows that since the initiation of postglacial downcutting of the Hanmer River, two fault traces have been active. The offsetting of the degradational terraces suggests that the currently active trace (the northern trace) became active during the Holocene and since that time has accommodated the dextral slip. The southern trace has been inactive since the inception of the northern fault.

The comparison of h/v ratios shows that the highest documented h/v ratio for the Hope Fault occurs at Hossack Station. The high h/v ratio indicates that east of Hanmer Basin, the angle between the fault motion vector and the strike of the Hope Fault is at its smallest value. Movement across the Hope Fault is more transpressional towards the Kaikoura Coast and the Hikurangi Subduction Zone, yet becomes transtensional along the Hope River Segment.

Assessment of the seismic hazard posed by the Conway segment of the Hope Fault was made using empirical formulae that relate earthquake magnitude to fault length, fault area, and maximum fault displacement. The expected magnitude associated with rupture of the Hope Fault east of Hanmer Basin, is M6.9 to M7.4 (Table 3.4)- depending on the choice of formula, and whether the rupture propagates across the Charwell basin. The maximum likely earthquake magnitude based on statistical analysis of past strike-slip generated earthquakes by Bonilla et al. (1984), for an exceedence probability of 10%, is M7.7 to M7.9 (Table 3.5). The associated ground shaking for the expected event (M6.9-7.4) would be locally at least MMIX. Rupture would be arrested by Hanmer Basin, where intense shaking and aftershock activity would be expected. In Christchurch, felt intensities of at least MMVII are likely (following the effects of the 1888 Amuri earthquake

described by Cowan 1989, 1991). The return period for earthquake ruptures on the Conway segment, based upon the slip-rate calculated at Hossack Station, and an inferred single-event rupture, is between 77 and 500 years. The last coseismic fault rupture on this segment of the fault was approximately 1838 A.D. (Bull et al. 1991), based upon lichen age data from local sites near the Conway segment.

CHAPTER FOUR

The evolution of Hanmer Basin

4.1 Introduction

Hanmer Basin is a pull-apart basin developing about half way along the Hope Fault Zone. It has formed as a consequence of strike-slip movement across a 6 kilometre right step-over or releasing bend in the Hope Fault. Earliest mention of a causal relationship between the Hope Fault and Hanmer Basin was by Cotton (1949) who attributed subsidence of the southwest side of the basin to displacement along the Hope Fault. He inferred that vertical displacement is the dominant type of movement along the fault. Acknowledgement that Hanmer Basin is developing within a major strike-slip fault zone gave rise to proposals that it is a pull-apart basin ("tectonic depression" Clayton 1966) or ("rhomb-shaped graben" Freund 1971).

Since these authors studied the Hope Fault, further work has been carried out: gravity anomaly surveying (Anderson 1987); recognition of Hanmer Basin as a probable segment boundary (Cowan 1989,1990); mapping of faults within the basin (Pettinga in prep.); and seismic reflection surveying (Wood in prep.), but details of the basin morphology and evolution still remain unclear. The purpose of this chapter is to discuss new data collected from the east end of Hanmer Basin to better define the basin's geometry and evolution. In particular this data adds to existing information regarding the thickness of basin fill, and augments the understanding of the geometry and kinematics of the Hope Fault at the east end of Hanmer Basin.

Hanmer Basin features prominently in the literature of pull-apart basins (eg. Mann et al 1983; Aydin and Nur 1982; Hempton and Dunne 1984; Freund 1974). Pull-apart basins develop at releasing bends and step-overs (Crowell 1974) in strike-slip faults, ie. a right bend or stepover for a dextral fault, or a left bend or stepover for a sinistral fault. At such discontinuities, a section of the fault is oblique to the general fault motion vector. Movement of the oblique, linking section of the fault may be accommodated by secondary faults. Secondary fault patterns have been predicted for releasing step-overs, by mathematical modelling and shear box experiments

(Rodgers 1980; Segall and Pollard 1980) (Figure 4.1a). These models predict the formation of oblique faults, linking the master faults. The development of secondary faulting patterns in field situations can often be similar to the patterns predicted by modelling: examples are shown in Figure 4.1b.

Hanmer Basin is situated at a major northward bend in the Hope Fault. East of Hanmer Basin the Conway segment strikes approximately 065 degrees and is a transpressional fault, while west of the basin the Hope River segment strikes 080 degrees and accommodates transtensional strain. The deepest part of the basin appears to be beneath an axis striking approximately east-west, linking the two segments of the Hope Fault (Anderson 1987, Figure 4.2). Basin geometry is determined by faults on all sides. The north side of the basin is bound by the Hanmer Fault (Section 2.5.2); the northwest side, by splays of the Hope River segment. The Conway segment of the Hope Fault traverses the south side, east of the Waiau Gorge. The southwest side of the basin is controlled by a major fault, currently hidden beneath the active floodplain of the Waiau River. This fault has a large component of vertical throw and is probably an oblique-slip normal fault.

The Hanmer Plain is the present upper surface of Quaternary basin fill deposits of Hanmer Basin. It is rhombahedral in shape, being sixteen kilometres from west to east and seven kilometres from north to south. The edges of the Plain are defined by steep greywacke ranges that rise to 1000 metres above the Plain, except at the eastern end of the basin, where basin fill is folded into low hills. The existence of faults in the mountains north of Hanmer Plain may suggest that the basin is defined by the range crest rather than the limit of Quaternary fill (Pettinga pers. comm. 1991).

4.2 Tilting of the Hanmer Plain

The Hanmer Plain is tilted to the south. Seismic profiles show that basin deposits also dip to the south and become progressively steeper with depth (Wood pers. comm. 1991). The major rivers (the Waiau and Hanmer Rivers), closely follow the south side of the plain and reflect tilting

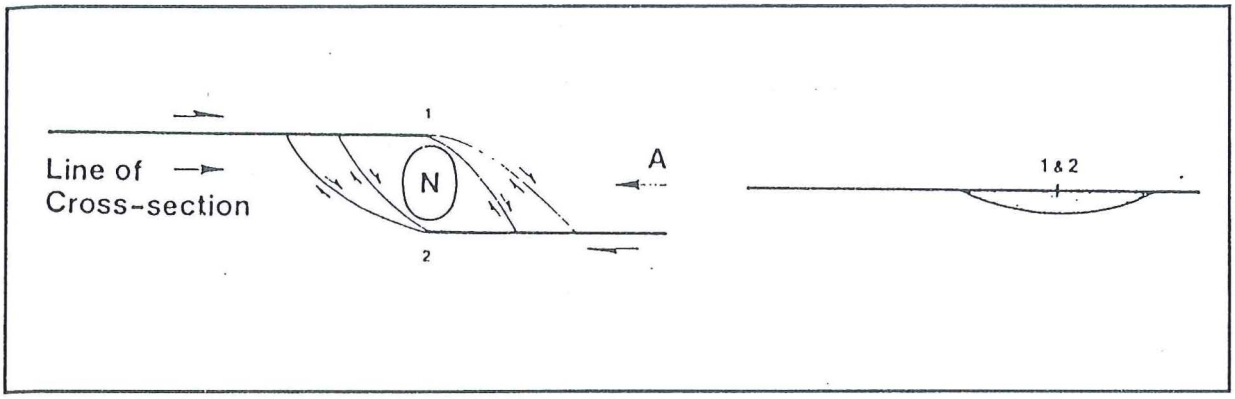

Figure 4.1a Sketch of the likely distribution of secondary faults that develop at a right stepover in a dextral fault. Area labelled N is zone of predicted normal faulting. Right side is a vertical cross-section, parallel to the master faults, through the centre of the basin. Source- Rodgers (1980).

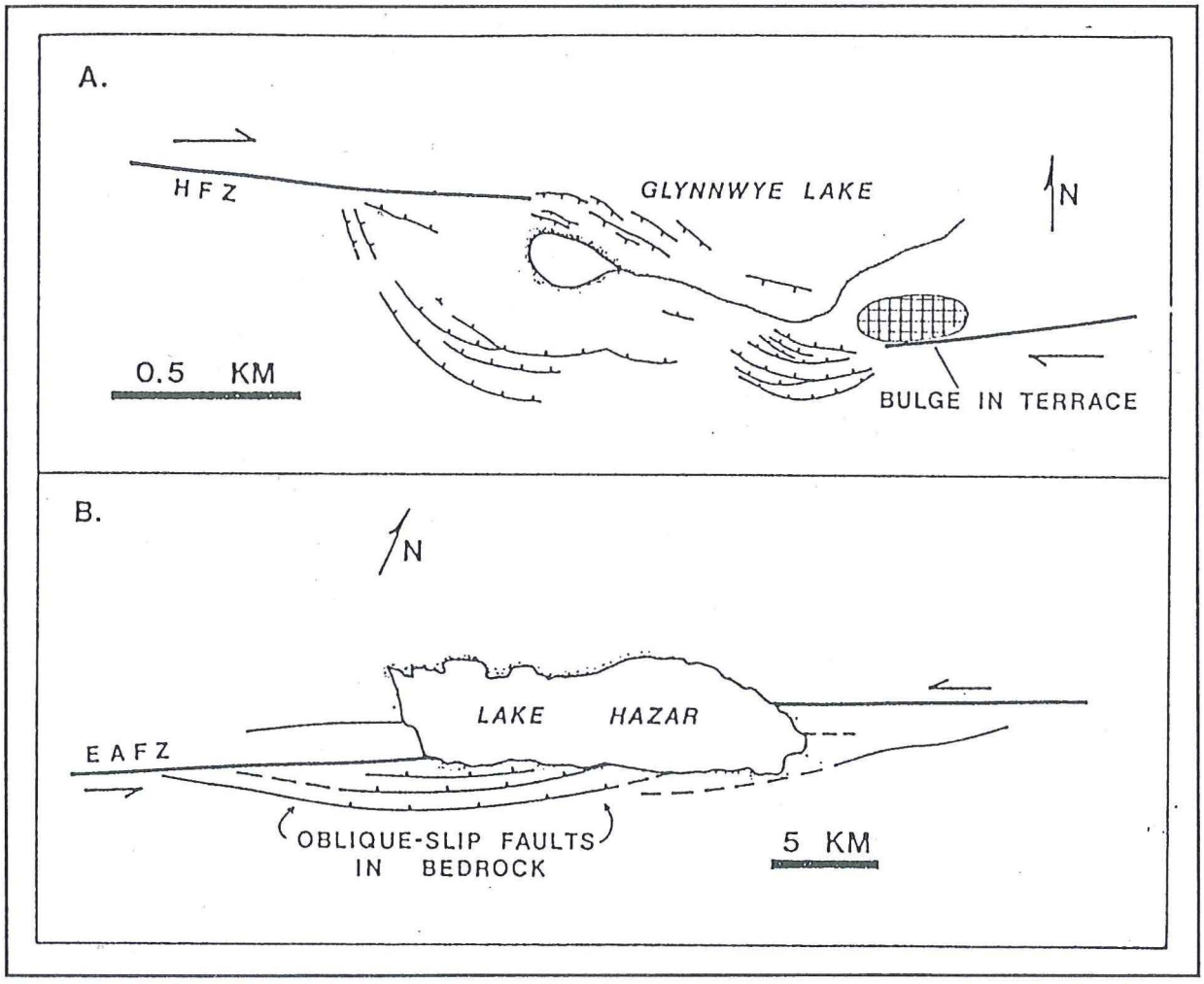

Figure 4.1b The development of secondary faults in response to extension at a dilational fault jog. **A** is a map of the graben development at Lake Glynn Wye on the Hope Fault Zone. Note the development of a bulge in the terrace in response to the non-parallelism of the master faults, in this case the Hope Fault active traces. **B** is a map of the active Lake Hazar Basin, Turkey. The master faults are the East Anatolian Fault Zone. Source- Mann et al. (1983).

of the basin floor. A Late Pleistocene terrace on the south side of the Waiau River is approximately 60 metres above present river level. West of Hanmer Basin downcutting of the Waiau River has formed a flight of Late Quaternary terraces. As the Waiau River enters the basin, the terraces on the north side of the river dip eastward under fans developed by the Grantham River (Pettinga pers. comm. 1991), and disappear 2-3 kilometres east of the western corner of the basin. The terraces on the north bank of the Hanmer River, similarly dip westward into the Hanmer Plain 3-4 kilometres east of the Waiau Gorge. This suggests that the Waiau and Hanmer Rivers are not actively downcutting within Hanmer Basin - in fact within the basin the rivers may be aggrading. The terraces on the south bank have been trimmed by the river, but have formed in response to differential vertical movement. The 60 metre terraces therefore represent a minimum vertical, postglacial offset and imply that fault-related subsidence is concentrated on the south side of the basin.

4.3 Depth of Hanmer Basin

The subsurface geometry of Hanmer Basin has been inferred from gravity data (Anderson 1987). Contoured bouguer anomalies imply that the deepest point of the basin (approximately 850 metres deep) is south of Hanmer Springs, and that the Torlesse/Quaternary unconformity dips gently towards that point (Figure 4.2).

In the north bank of the Hanmer River near Hossack Station, along the southern boundary of Hanmer Forest, weakly bedded Pleistocene gravels are exposed and dip at approximately southwest at 25^{o} (Figure 4.3). Exposure of these gravels along a three kilometre section of the Hanmer River reveals a minimum thickness of 1000 metres. This is somewhat more than the 850 metres estimated from the Bouger gravity anomaly (Freund 1971; Anderson 1987). As will be discussed below, the presence of a large stratigraphic thickness in the basin may reflect an early stage in the development of an onlapping accumulation of strata typical of pull-apart basins (eg. Sylvester 1988).

The same Pleistocene gravels are exposed further north in Hanmer Forest where they dip

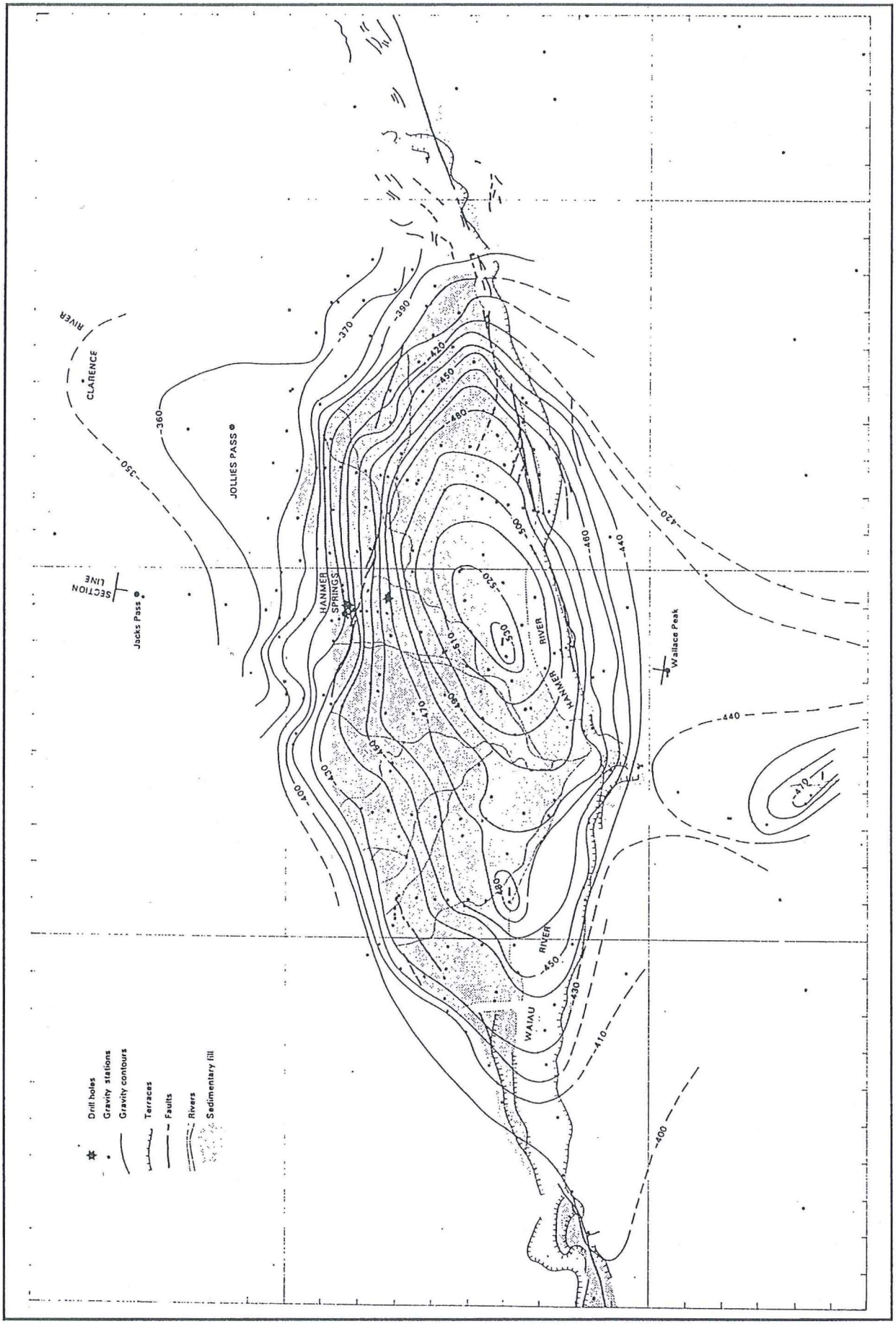

Figure 4.2 Bouguer gravity anomaly map for Hanmer region (Anderson 1987). Locations of faults, terraces and sediment limits from Freund (1971). Scale is indicated by the thousand yard grid. The deepest point in the basin is south of Hanmer Springs township.

at approximately 15° to the west into the basin. An east-west seismic profile (Seismic Profile No.2: Appendix 2) shows that the gravels dip westward into the basin. Projection of these dips into the deepest part of the basin imply a depth of up to 1500 metres, three kilometres west of Leslie Pass Road. This estimate represents a maximum depth because bedding dips may decrease near the deepest part of the basin, which is one kilometre south of the seismic profiles.

4.4 The age of Hanmer Basin

The gravels exposed by the Hanmer River and elsewhere at the east end of the basin, may provide clues to the age of Hanmer Basin. The gravels are moderately well consolidated, moderately to poorly bedded, subangular to angular, and moderately to poorly sorted. Clasts are derived from Torlesse basement and are usually 5 to 10 centimetres in diameter. Layers of carbonaceous and diatomaceous silt occur within the gravels. Carbonaceous mud from an exposure (at grid reference 260 N32 033505) forming a band several centimetres thick was dated and yielded an age of greater than 45 000 years (unpublished data), which is the upper limit for radiocarbon dating. During this study a layer of diatomaceous mud 15 centimetres thick containing *Pinnularia maior* (Broady pers. comm. 1991), was found directly above Freund's carbonaceous layer (Figure 4.4).

Pinnularia maior is a cold water benthic species of diatom. It is slow growing and often lives in nutrient-poor, acidic waters, in a swamp environment (Hawarth pers. comm. 1991). The probable paleoenvironment is a swampy pond formed on an alluvial fan or braided river, during a period of cold climate. This may represent an upper limit of Mid to Late Pleistocene for the age of the diatomaceous horizon, which is approximately 300 metres stratigraphically above the Torlesse/Quaternary gravel unconformity.

A Mid to Late Pleistocene age is consistent with pollen analysis, (Anderson 1987). Pollen types collected from the base of the Pleistocene gravels (grid reference N32 979529) are indicative of a cold climate (sample N32/f20).

Figure 4.3 Exposure in the north bank of Hanmer River in Hanmer Forest, of Pleistocene gravel dipping to the southwest at approximately 25°. Exposure is approximately 20 metres high. Grid reference is 260 N32 0134498.

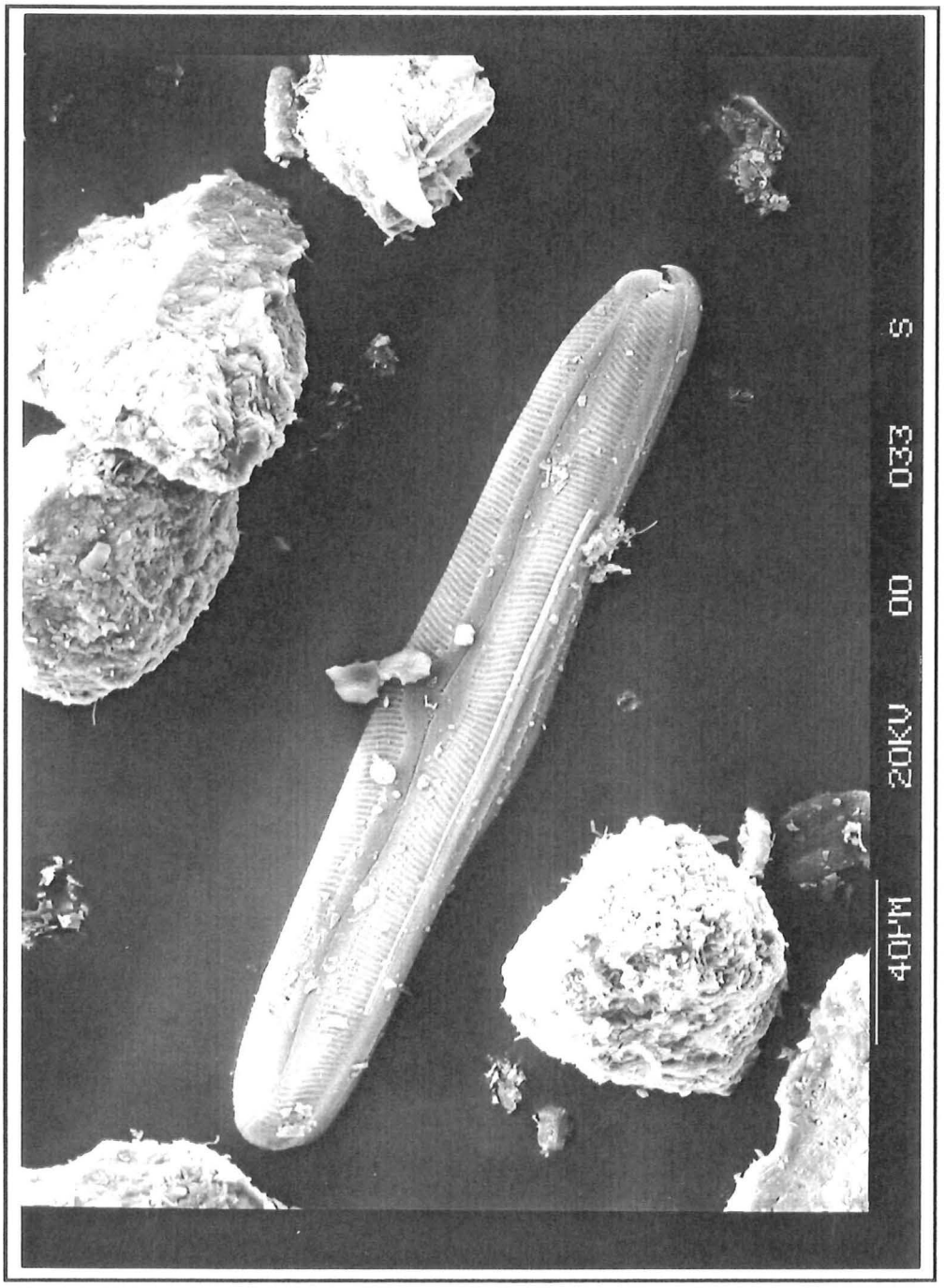

Figure 4.4 Electron micrograph of diatoms found in a silt layer within Pleistocene gravel at Hossack Station. The diatoms are Pinnularia maior, a cold water species consistent with glacial environment for early Hanmer Basin development. Also this species is adapted to life in acidic, nutrient-poor water, again consistent with the carbonaceous mud found in conjunction with the diatoms at the locality. Grid reference 260 N32 033505.

4.5 Active folding of Pleistocene basin-fill deposits

Geological mapping of the Torlesse basement rocks and the overlying Pleistocene gravels revealed a series of folds that plunge west into Hanmer Basin, approximately parallel to the strike of the Hope Fault, (Figures 4.5; 4.6). The most prominent fold is an anticline forming the ridge that runs up to Sunday Hill. The highest point on the crest of this anticline is 200 metres above the level of the surrounding plain. Although the bedding data collected from the gravels is limited, it is clear that folding is complex, particularly to the northeast. This pattern of folding suggests that the east end of the basin has accommodated approximately 5% shortening in a north-south direction (Nicol, pers. comm. 1991), which increases towards the east.

The Hanmer Fault projects into the core of an anticline formed in Pleistocene gravels in Hanmer Forest (Figure 4.5). The presence of a fold rather than a surface trace at this locality may reflect a greater thickness of basin fill for the fault to propagate through, compared to the depth of sediment near Hanmer Springs. Given that shortening is occurring across this corner of the basin, it is likely that the Hanmer Fault is a reverse fault, at least at the east end of the basin.

The folds appear to be propagating westwards into the basin. McKay's Road is visibly warped in the region of the anticlinal ridge adjacent to the Hanmer River. The warping is post-glacial in age.

Relative uplift at the east end of the basin is also indicated by downcutting of the Hanmer River. At Hanmer Forest, the present river level is about 25 metres below the highest postglacial river terraces.

Paleocurrent indicators, such as dipping forset beds within the Pleistocene gravels, suggest that the source area for the gravels was to the east. The presence of occasional, well rounded cobbles that have been eroded from Torlesse conglomerate beds is particularly interesting. The likely source of Torlesse conglomerate cobbles is at Hossack Station to the east. Low hills now separate Hossack Station from Hanmer Basin, and these are inferred to have been uplifted after the gravels were deposited.

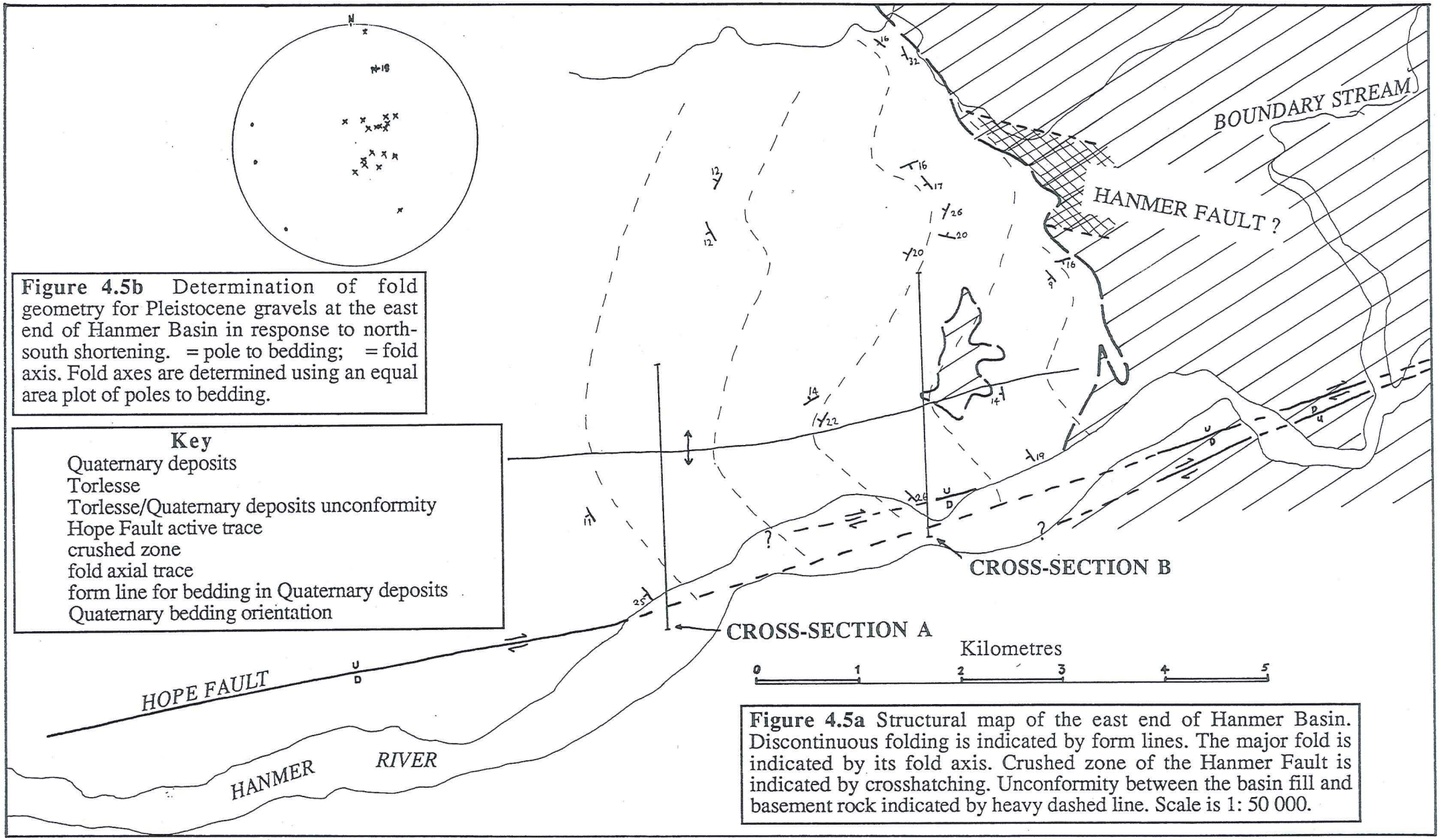

Figure 4.5b Determination of fold geometry for Pleistocene gravels at the east end of Hanmer Basin in response to north-south shortening. = pole to bedding; = fold axis. Fold axes are determined using an equal area plot of poles to bedding.

Figure 4.5a Structural map of the east end of Hanmer Basin. Discontinuous folding is indicated by form lines. The major fold is indicated by its fold axis. Crushed zone of the Hanmer Fault is indicated by crosshatching. Unconformity between the basin fill and basement rock indicated by heavy dashed line. Scale is 1: 50 000.

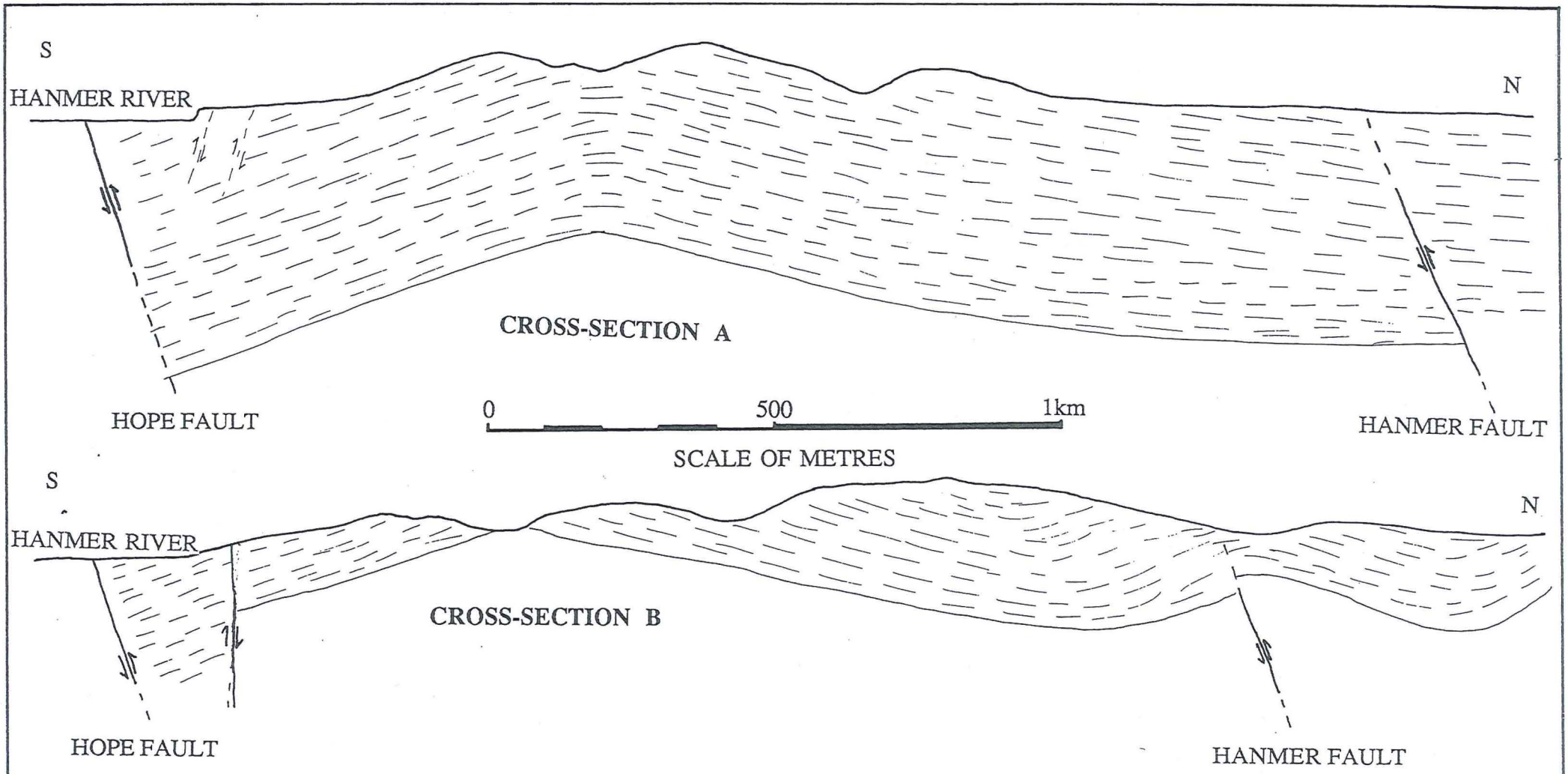

Figure 4.6 Cross-sections of the basin fill at the east end of Hanmer basin. Inferred basin fill-basement contact is indicated by solid line. Folding is inferred from bedding data shown on Figure 4.7. Locations of cross-sections are shown on Figure 4.5. Scale is 1:10 000. No vertical exaggeration.

4.6 Mechanisms for folding of Pleistocene gravel.

Near Sunday Hill, the basal unconformity of Pleistocene gravels is 200 metres above the Hanmer Plain. Therefore uplift of at least 200 metres has occurred since initiation of basin development. The uplift was accompanied by the development of WSW trending folds, due to shortening in an approximately north-south direction (Section 4.5). However, rather than having an *en echelon* relationship (Sylvester 1988) to the Hope Fault, they parallel the main fault. These folds appear to be developing in association with reverse faults propagating up through the basin fill. It is envisaged that the folds have developed above the propagating tips of reverse faults.

Compression across a fault crushed zone can be accommodated by triboplastic deformation (clasts move independently within the crushed zone accommodating deformation along small-scale fractures within the rock mass), (Nicol et. al. 1990). Folding that has occurred in a cover sequence (eg. Quaternary deposits in the Hanmer Basin), is matched by a similar amount of strain in the underlying basement rock. Triboplastic deformation could wholly or partly account for the folding at the east end of Hanmer Basin, in response to north-south compression.

Freund (1971) observed that compressional features are located immediately to the east of the releasing step-overs and bends along the Hope Fault. Freund attributed the development of the compressional bulges to non-parallelism of the master faults. As well as giving rise to extension along the linking oblique fault, localised compression is caused along the eastern bounding segment when strike-slip movement occurs along the Hope Fault Zone (Figure 4.7). The transition from transpression to extension occurs along the Hope Fault between Hossack Station and the Waiau Gorge (Section 4.9).

4.7 Early development of Hanmer Basin

Freund (1971) inferred that Hanmer Basin began developing late in the history of the Hope Fault. He calculated that to have reached its present size, five kilometres of strike-slip movement must have occurred on the Hope Fault. This figure was determined by establishing the amount of fault movement needed to create a "tectonic gap" equal to the volume of the present basin.

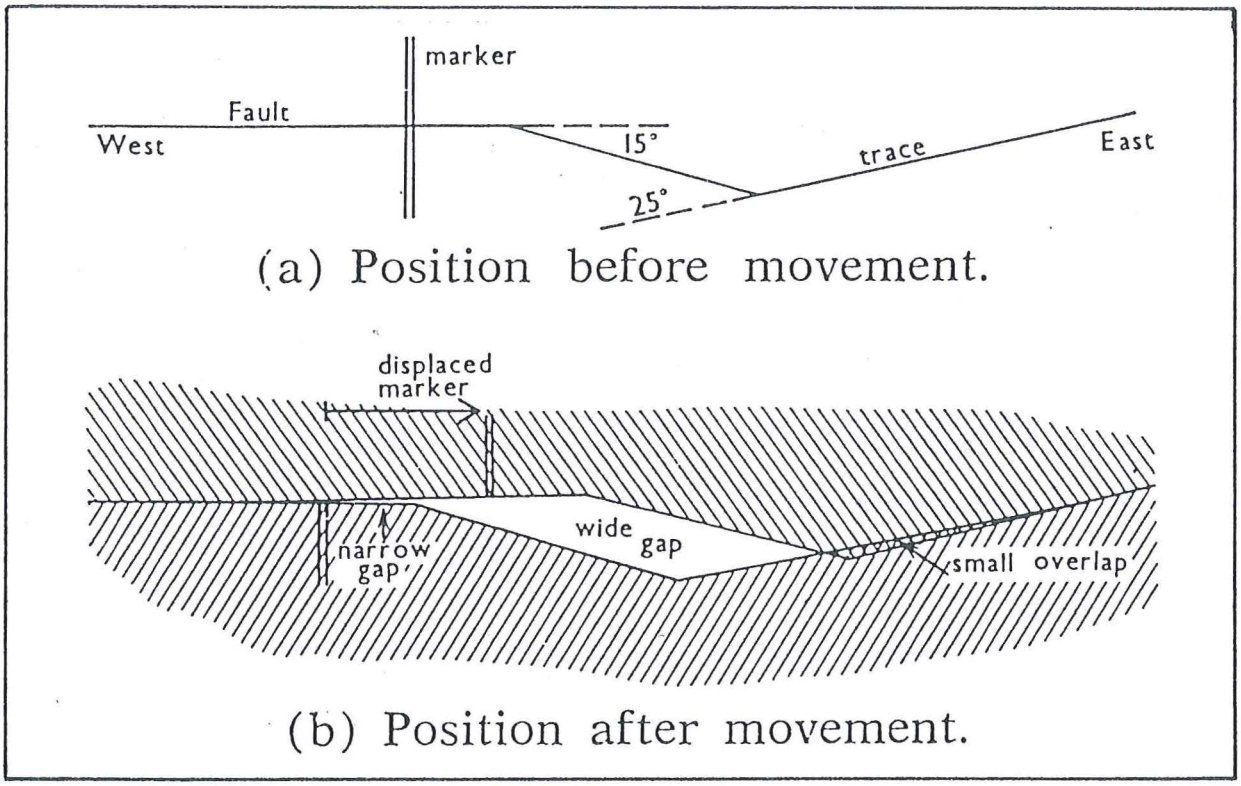

Figure 4.7 Model of the formation by strike-slip movement, of a rhomb-shaped graben with small overlaps at one end. This is the method of formation of the Hanmer Basin and the upwarping of the east end of the basin adopted by Freund. Source-Freund (1971).

Freund's value for the total displacement that had occurred on the Hope Fault was 19 kilometres. His calculation was based on the distinct geomorphological dissimilarity between the smooth, round-topped mountains west, and rugged, sharp-topped mountains east, of Gabriels Gully on the south side, and Hossack Station homestead on the north side of the fault. He attributed the difference in mountain morphology to a variation in Torlesse lithology. If Freund's model for the development of Hanmer Basin is correct, then the basin would have formed during the last quarter of the history of the Hope Fault. This study confirms Freund's estimate of total fault offset. A lithological dissimilarity occurs in Torlesse basement on the north side of the fault, from interbedded mudstones and sandstones west of Hossack Station, to massive sandstones, mudstones and conglomerates, east of Hossack Station homestead (Map 2). This difference was also desribed by Bradshaw and Andrews (1980) on the south side of the basin (Figure 2.5) at Gabriels Gully.

Clayton (1966) proposed an age of 500 000 years for the Hope Fault and Hanmer Basin, calculated from his estimate of total offset on the fault and rate of displacement determined from the Glynn Wye moraine complex. The slip-rate, (18 ± 8 mma^{-1}) determined during this study at the offset stream loops locality (Chapter 3), implies that the Hope Fault could have accommodated 19 kilometres of displacement in less than 900 000 years provided the slip-rate has remained uniform. The age inferred for the Hanmer Basin is less than 250 000 years, assuming Freund's hypothesis that the Hope Fault had already accommodated about 15 kilometres of displacement by the time the basin began to form.

Initial development of Hanmer Basin required an oblique section of the Hope Fault along which subsidence could occur. Freund's theory that Hanmer Basin developed late in the history of the Hope Fault, requires a change in the shape of the fault. The mechanism for the change which resulted in the bend or stepover in the Hope Fault, from which the basin developed, is unknown.

The oblique section of the Hope Fault must have dipped northward (assuming transtension across it) as the basin geometry suggests that the north side of the fault is downthrown. Had the

fault dipped to the south, the basin would have developed southwest of its present locality. The asymmetry of Lake Glynn Wye Graben is consistent with the Hope Fault dipping to the south (Clayton 1966) along the Hope River segment (Cowan 1989) (Figure 4.1b).

4.8 Rate of subsidence of Hanmer Basin

Conditions for the genesis of pull-apart basins occur on oblique-slip faults, whose orientation and sense of movement presumably reflects the stress regime under which the basin is forming (Mann et al. 1983). Prominent examples of such oblique-slip faults include the Hanmer Fault, and the fault along the southwest side of the basin, where maximum postglacial subsidence has occurred. The 60-70 metre high terraces on the south side of the basin are 12-14 000 years old, inferring the rate of subsidence of the Hanmer Plain over that period to be approximately 5 mma^{-1}. At this rate, the Hanmer basin could have formed to a depth of 1000 metres (the estimated basin depth) in 200 000 years.

Faults on the western Hanmer Plain probably dissipate strike-slip movement from the Hope River segment of the Hope Fault. The apparent lack of similar splays on the surface of the Hanmer Plain at the east end of the basin may be due to a greater thickness of basin fill which suppresses the surface expression of faulting in this area. The presence of thrust or reverse faults at the east end of the basin is evident on seismic reflection lines No.1 and No.3 (Wood pers. comm. 1991) and field investigation (Section 2.5). These faults may represent reactivation of old extensional faults, now under compression.

4.9 Migration of Hanmer Basin

Deposition of the gravels that are exposed on Sunday Hill occurred at the eastern margin of the subsiding basin. The basin fill is currently being uplifted, eroded, and redeposited to the west, due to uplift north of the transpressional Conway segment of the Hope Fault.

The point of zero uplift (and subsidence), within the basin is presently between Mackays Road and Leslie Pass Road, and is marked by the presence of folding in the Mackays Road

seismic profile, and the lack of folding in the Leslie Pass Road seismic profile (No.1). This point of inflection has migrated to the west through time along with the centre of maximum subsidence. Both points are inferred to have moved west by approximately five kilometres since deposition began. This figure is also inferred as the total amount of movement that has occurred along the Conway segment of the Hope Fault since Hanmer Basin began to develop perhaps as recently as 250 000 years ago. This indicates that Hanmer Basin has migrated westwards as a result of movement on the Hope Fault.

Pull-apart basins tend to be ephemeral structures when the master faults are non-parallel in either map or cross-section (Hull 1991). In the case of Hanmer Basin, the basin is migrating westwards due to non-parallelism of the master faults, but whether the basin is enlarging or reducing in size, depends upon the relative rates of extension at the west end and uplift at the east end of the basin.

Westward migration of the basin has resulted in the accumulation of an onlapping succession of basin fill units typical of pull-apart basins (Sylvester 1988, Crowell, pers. comm. 1991). It is therefore expected, that the stratigraphic succession in Hanmer Basin is significantly thicker than the 1000 metres exposed in the Hanmer River.

4.10 Difference of slip-rates across Hanmer Basin

Slip-rates for the Hope River segment of the Hope Fault have been determined many times by different authors. The most recent assessment of Late Quaternary displacements of the Hope River segment implies a slip-rate of 14 ± 3 mma^{-1} for the past 17 000$\pm$2000 years, and 10.6 ± 0.3 mma^{-1} for the past 3 500 years (Table 3.3). The different rates may reflect spatial rather than temporal changes in slip-rate (Cowan 1989). The slip-rate for the Conway segment of the Hope Fault determined during this study is 18 ± 8 mma^{-1}. Basin geometry suggests that extension and subsidence resulting from displacement on the Conway segment has been greater than that occurring due to displacement on the Hope River segment. The drop in slip-rate across Hanmer Basin may reflect this.

4.11 Future evolution of the Hanmer Basin

Hanmer Basin is at the "lazy Z" stage of development (Mann et al. 1983), beyond this point, the master faults bounding opposite sides of the basin are likely to overlap, and the basin will become progressively elongated with increasing fault displacement. The lowest point (presently along the south side of the basin) will migrate westwards provided that the rate of extension and subsidence at the west end of the basin exceeds the rate of uplift at the east end of the basin.

4.12 Conclusions

Hanmer Basin has formed in response to strike-slip movement within the Hope Fault Zone. The subsidence has occurred due to the presence of a 5 kilometre releasing bend or right stepover in the Hope Fault Zone, across the Hanmer Basin. The resulting depression is up to approximately one kilometre deep, and the top of the basin fill is approximately 50 square kilometres in area. Assuming a uniform rate of slip, postglacial subsidence has occurred at an average rate of 5 mma^{-1}, which indicates that Hanmer Basin may only be 200 000 years old.

The presence of cold-climate flora and fauna within the lower basin fill stratigraphy, implies that a Pleistocene age is probable for basin inception.

The apparent increase slip-rate on the Hope Fault Zone from west to east across the Hanmer Basin is reflected in the basin geometry. The deepest part of the basin is adjacent to the end of the Conway segment of the fault, indicating that the higher slip-rate has induced more rapid subsidence.

Basin geometry also reflects the non-parallelism of the master faults, in this case the Hope River segment to the west, and the Conway segment to the northeast. The east end of the basin is presently undergoing north-south shortening, resulting in the development of east-west trending folds in Quaternary gravels that parallel the Hope Fault and plunge into the basin. These folds tighten to the east, and imply an higher rate of shortening. North-south shortening occurs in response to transpression across the Hope Fault east of Hanmer Basin and the change in strike

across the basin. The folding evident at the east end of the basin is a manifestation of upward propagation of secondary reverse faults, resulting from the north-south shortening and deformation of the Hope Fault crushed zone.

The subsidence that has resulted in the formation of Hanmer Basin, contrasts with the transpressional features at the east end of the basin. At present, maximum subsidence is occurring at the southwest margin of the basin, 5 kilometres west of the basin axis. Five kilometres of westward basin migration is postulated, being approximately the same amount as the total fault movement required to form the Hanmer Basin.

CHAPTER FIVE

Summary and Conclusions

(1) Hanmer Basin is recognised as a probable segment boundary for the Hope Fault, a major dextral strike-slip fault of the Marlborough Fault System. It is located between the Hope River segment (Cowan 1989,1990),and the Conway segment (Bull et al. in prep.). The Conway segment probably extends as far east as the Charwell Basin, a total length of 50 kilometres.

(2) A wide zone of complex deformation is associated with termination of the Conway segment at Hossack Station and eastern Hanmer Basin. Ongoing deformation is expressed as multiple Late Quaternary fault traces, folding and tilting. Exposures of the active fault plane reveal a dip of greater than 70^{o} to the north, and topographic displacements suggest that the fault is transpressional. Field mapping and seismic reflection profiles confirm that the terminating Conway segment is undergoing cross-fault shortening.

(3) The Hope Fault crushed zone is in excess of one kilometre wide in Torlesse basement at Hossack Station and has a sharp southern contact with intact rock of the footwall. The northern boundary of the crushed zone is gradational into more coherent Torlesse between 0.5 and 1.5 kilometres from the main trace. The active trace of the Hope Fault follows the southern edge of the crushed zone, and dips consistently to the north. The asymmetry of the fault zone about the active trace, may reflect the dip of the Hope Fault, because strain tends to be concentrated against the footwall of the fault.

(4) Dextral displacement across an isolated bend (Sibson 1989) in the Hope Fault active trace, immediately east of Hossack Station homestead, has caused warping of a Late Quaternary degradational river terrace of the Hanmer River. The warping has occurred to the west of the bend,

and is interpreted as being indicative of earthquake propagation from east to west (Sibson 1989). Terrace distortion at this bend may also indicate that the fault motion vector is oriented south of the fault strike.

(5) Sigmoidal distortion of Torlesse bedding shows that the Hope Fault Zone affects a corridor of basement rock at least four kilometres in width. The regional bedding orientation is approximately NE-SW with steep dips to the NW or SE, however within two kilometres of the fault, bedding bends gradually into the fault zone so that at a distance of 500-1000 metres the bedding orientation is subparallel to the Fault. Within 500 metres of the active fault trace, the bedding orientations are irregular (probably due to block rotation within the fault zone), and difficult to measure because only isolated blocks retain intact bedding.

(6) Bedding distortion within the fault zone makes estimation of total fault offset difficult when using displaced features in basement rocks. Freund (1971) estimated the total fault offset to be 19 kilometres based upon the offset of several conglomerate and chert beds within the Torlesse, and a displaced change in mountain morphology, across the fault. This study concords with Freund's estimate by mapping the lithological dissimilarity responsible for the change in mountain morphology. Variations in Torlesse lithology have also been mapped by Bradshaw and Andrews (1980) on the south side of the fault where the matching morphological change occurs. The offset of this dissimilarity in Torlesse lithology is 20±2 kilometres, considering the error due to the distortion of bedding within the fault zone discussed above.

(7) A two kilometre-long pressure ridge occurs adjacent to the end of the main active trace of the Hope Fault at Leslie Pass Road. The active trace is not evident in lower level degradation terraces west of the pressure ridge. The morphology of the pressure ridge suggests that it may be a post-glacial termination bulge.

(8) The channel morphology of the Hanmer River changes where it meets the Hope Fault Zone, immediately east of Hossack Station homestead. The channel form of the Hanmer River changes from a relatively straight, incised channel north of Hossack Station homestead, into a series of incised meanders where it encounters the soft rock of the fault zone. This may reflect uplift of the north side of the fault and the considerable input of sediment resulting from erosion of the fault zone.

(9) The instability of slopes at Hossack Station, reflects the intensely fractured nature of Torlesse within the fault zone. Extensive scree development, deeply incised steam channels, ridge renting and landsliding occurs to the north of the main fault trace, within the crushed zone.

(10) The presence of several, large landslides at Hossack Station, may provide an opportunity to date prehistoric earthquakes. The crushed Torlesse encourages the occurrence of landslides by having a low shear strength and high permeability; deep incision by streams destabilises the slopes by removing toe buttressing. One prominent landslide at Hossack Station may be younger than 1000 years.

(11) The progressive offset of a stream, crossing the main active trace of the Hope Fault one kilometre east of Hossack Station, is recorded by three phases of channel development. Trenching in the two youngest stream channel loops provided preserved wood samples that were radiocarbon dated. Timing of channel abandonment is constrained by the trench stratigraphy and absolute radiocarbon dates, allowing maximum and minimum slip-rates to be inferred. The slip-rate for the stream-loops site over the last 3700 years is inferred to be 18 ± 8 mma^{-1}. Slip-rates determined for the youngest stream loop indicate a maximum slip-rate of about 30 mma^{-1} for the last 1000 years. The discrepancy between these slip-rates may be the result of greater relative uncertainties in the relationship between the history of stream displacement by the fault and deposition of the dated organic material.

(12) Two active traces of the Hope Fault with dextral displacement are evident at the junction of Boundary Stream and Hanmer River. The combined Late Quaternary displacement across the two traces is at least 260 metres. Displaced degradational terrace risers indicate that the active northern trace has accommodated all of the dextral movement and the southern trace has become inactive in the late Holocene. This site, along with two other sites on the fault at Hossack Station, show that locally the active trace has migrated periodically during the Holocene.

(13) Comparison of slip-rates along the Hope Fault suggests three significant trends: (i) the slip-rates are higher on the Conway segment east of Hanmer Basin, than on the Hope River Segment west of the basin; (ii) the Holocene dextral slip-rates on the Hope Fault decrease towards Hanmer Basin from the west and east. Presumably the strike-slip strain is soaked up in Hanmer Basin as a result of extension; and (iii) the dextral slip-rate decreases sharply at the eastern end of the Hope Fault as the fault changes from strike-slip to dominantly oblique-slip and thrust faulting. The slip-rates along the fault are subject to errors resulting from the various methods used in their determination. It is uncertain how much of the above variation in slip-rate is real and how much is due to inaccurate slip-rate calculation or by accommadation of slip on subsidiary fault strands, and hidden fault strands beneath cover strata.

(14) Horizontal/vertical displacement ratios vary along the fault reflecting changes in the character of fault movement. The h/v ratio increases from a minimum of about 1.5-3.0 at the east end of the fault, where the fault motion is strongly oblique, to a maximum of more than 30 at Hossack Station, reflecting the dominantly strike-slip fault motion. The h/v ratio at Manuka Creek on the Hope River segment is 15-17, lower than at Hossack Station, possibly reflecting a component of oblique-normal slip resulting from local transtension.

(15) Fault rupture length associated with an earthquake on the Conway segment, is uncertain

because no historic precedent has occurred and the location of a segment boundary east of Hossack Station is outside the scope of this study. However, Charwell Basin has developed at a releasing bend or right step-over on the Hope Fault, which may constitute a segment boundary (Bull pers. comm. 1991). Rupture from Charwell to Hanmer Basin would give a rupture length of 50 kilometres. The boundary between the strike-slip Kahutara and oblique-reverse slip Mt Fyffe segment is located at Kowhai River (Van Dissen 1989, 1991), rupture from there to Hanmer Basin would be a distance of 67 kilometres. This is considered to be the maximum likely rupture length.

(16) No single-event offsets are recorded at Hossack Station. There are single and multiple-event displacements at Charwell that suggest a 3-5 metre offset associated with earthquake fault rupture (Bull pers. comm. 1991). The lower slip-rate at Hossack Station may suggest that a lower displacement is likely to occur during coseismic rupture. Therefore five metres is considered to be the likely maximum dextral displacement associated with an earthquake at Hossack Station.

(17) Earthquake magnitudes for rupture of the Conway segment have been estimated using empirical relationships from Wyss (1977), Slemmons (1982) and Bonilla et al. (1984). Based on the rupture length, rupture area and maximum fault displacements noted above, the likely magnitude of an earthquake on the Conway segment is between M6.9 and M7.4. Estimated magnitudes for an exceedence probability of 10% are between M7.7 and M7.9. An earthquake of this magnitude is likely to be associated with local felt intensities of MMIX or greater along the fault and in Hanmer Basin, with felt intensities of greater than MMVII in Christchurch. Local aftershocks are likely to be concentrated in Hanmer Basin.

(18) The recurrence interval for earthquakes on the Conway segment is calculated using the inferred slip-rate from the stream-loops locality and the inferred dextral displacements for an earthquake. The inferred recurrence interval is a minimum of 77 years and a maximum of 500 years assuming a constant slip-rate and characteristic event behaviour. Cowan (1989,1990) suggested that the Hope River segment may have experienced characteristic events in the late

Holocene.

(19) Hanmer Basin is a pull-apart basin developed about half way along the Hope Fault Zone. The basin has an asymmetric geometry, the deepest part being south of the east-west centreline of the basin (Anderson 1987). The basin-fill and Hanmer Plain dip towards the actively subsiding, southern edge of the basin. The major rivers follow the south side of the basin, also reflecting the active tilting of the basin floor.

(20) Hanmer Basin is approximately 1000 metres deep at the deepest point, which is 4-5 kilometres south of Hanmer Springs (Anderson 1987). Evidence for the depth comes from gravity anomaly data, seismic reflection surveys and an exposed stratigraphic sequence in north bank of Hanmer River.

(21) Along the south side of Hanmer Basin, a 60 metre high, postglacial terrace has been cut by the Waiau River. No matching terrace occurs on the north side of the Waiau River, suggesting that the elevated terrace has formed in response to vertical displacement associated with an oblique-normal fault hidden beneath the Waiau Riverbed. A minimum of 60 metres vertical, postglacial movement represents a subsidence rate of approximately 5 mma^{-1}. At that rate, Hanmer Basin could have formed to a depth of 1000 metres in 200 000 years.

(22) Analysis of pollen samples from within Quaternary gravels in Hanmer Basin, near the basal unconformity, suggest that the gravels were deposited during a period of cold climate (Anderson 1987). Diatoms found near the Torlesse/Quaternary gravel unconformity also suggest a cold climate at the time of deposition. Cold climate flora and fauna are consistent with a Pleistocene age for the development of Hanmer Basin.

(23) Bedding orientations from the Pleistocene gravels at the east end of Hanmer Basin indicate a

series of non-cylindrical folds, that plunge at 10-15° to the west, into the basin. These folds are parallel to the active trace of the Hope Fault, rather than being *en echelon* to it and suggest that the east end of Hanmer Basin has undergone at least 5% shortening, due to compression in a north-south direction. The folds may be developing over the tips of upward-propagating reverse faults, in response to the shortening. Several, possibly reverse faults, are also exposed in the Pleistocene gravel in Hanmer Forest. North-south compression at the east end of the basin reflects the transpressional character of the Conway segment, influencing basin development.

(24) Subsidence within Hanmer Basin, that occurs in response to movement of the Hope Fault Zone, is presently concentrated on the south-west side of the basin. Gravity anomaly data suggests that the deepest part of the basin is about five kilometres east of the present, actively subsiding margin, possibly indicating that the depocentre has migrated westwards by about 5 kilometres. Uplift at the east end of the basin may also suggest depocentre migration. The non-parallelism of the master faults (in either plan or cross-sectional view) generally leads to basin migration (Hull 1991).

Reference List

* Adams, R.D. and Ware, D.E. 1977: Subcrustal earthquakes beneath New Zealand, location determined with a laterally inhomogeneous velocity model. *New Zealand Journal of Geology and Geophysics, Vol.30, p59-83.*

* Anderson, H.J. 1987: A gravity survey of the Hanmer Depression, North Canterbury. DSIR Research Report No. 214a

* Aydin, A. and Nur, A. 1982: Evolution of pull-apart basins and their scale independence. *Tectonics, Vol. 1, No. 1, p 91-105.*

* Bibby, H.M. 1981: Geodetically determined strain across the southern end of the Tonga-Kermadec-Hikurangi Subduction Zone. *Journal of Geophysical Research, Vol. 66, p513-533.*

* Bishop, D.G.; Bradshaw, J.D. and Landis, C.A. 1985: Provisional Terrain Map of South Island, New Zealand. *In:* Howell, D.G. (ed.) *Tectonostratigraphic terranes of the circum- Pacific region.* Circum- Pacific Council of Energy and Mineral Resources, Houston, Texas. p 515-521.

* Bonilla, M.G., Mark, R.K. and Lienkaemper, J.J. 1984: Statistical relations among earthquake magnitude, surface rupture length, and surface displacement. *Bulletin of the Seismological Society of America, Vol. 74, p2379-2411.*

* Bowman, S.1990: Radiocarbon Dating. British Museum Publications Limited.

* Bradshaw, J.D. and Andrews, P.B. 1980: Torlesse terrane excursion, *in* Weaver, S.D. and Lewis, D.W., Geological Society of New Zealand, 1980 Conference, Christchurch, Field excursions guidebook, p C1-C12.

* Bull, W.B., Cowan, H.A., Pettinga, J.R. and McGlone, M.S. in press: New ways of dating earthquakes on two segments of the oblique-slip Hope Fault, New Zealand.

* Clayton, L.S. 1966: Tectonic depressions along the Hope Fault, A transcurrent fault in North Canterbury, New Zealand. *New Zealand Journal of Geology and Geophysics, Vol. 9, No.1/2.* p95-104.

* Costa, J.E. and Schuster, R.L. 1988: The formation and failure of natural dams. *Geological Society of America Bulletin, Vol. 100, p 1054-1068.*

* Cotton, C.A. 1947: The Hanmer Plain and the Hope Fault. *The New Zealand Journal of science and Technology.B29 p.10-17.*

* Cowan,H.A. 1989: Evaluation of the Late Quaternary displacements associated with the active Hope and Kakapo Faults at Glynnwye. Unpublished Msc. thesis. University of Canterbury.

* Cowan, H.A. 1990: Late Quaternary displacements on the Hope Fault at Glynn Wye, North Canterbury. *New Zealand Journal of Geology and Geophysics, Vol. 33, p 285-293.*

* Cowan, H.A. 1991: The North Canterbury earthquake of September 1, 1888. *Journal of the Royal Society of New Zealand, Vol. 21.*

* Crowell, J.C. 1974: Sedimentation along the San Andreas Fault, California. In *Modern and ancient geosynclinal sedimentation. Eds. Dott, R.H. and Shaver, R.H.*

* Eiby, G.A. 1966: The Modified Mercalli scale of intensity and its use in New Zealand. New Zealand Journal of Geology and Geophysics, Vol.9

* Fitch, T.J. 1972: Plate convergence, transcurrent faults and internal deformation adjacent to southeast Asia and the western Pacific. *Journal of geophyical Research. Vol. 77, p 4432-4460.*

* Freund, R. 1971: The Hope Fault. NZ Geological Survey Bulletin 86

* Freund, R. 1974: Kinematics of transform and transcurrent faults.*Tectonophysics, Vol. 21, p 93-134.*

* Gregg, D.R. 1964: "Geological Map of of New Zealand 1:250 000. Sheet 18, Hurunui" New Zealand Department of Scientific and Industrial Research, Wellington.

* Hempton, M.R. and Dunne, L.A. 1984: Sedimentation in pull-apart basins: Active examples from eastern Turkey. *Journal of Geology, Vol 92, p 513-530.*

* Knuepfer,P.L.K. 1984: The tectonic geomorphology and present day tectonics of the Alpine Shear System, South Island, New Zealand. Unpublished PhD thesis, The University of Arizona.

* Knuepfer, P.K.L. 1988: Estimating ages of late Quaternary stream terraces from analysis of weathering rinds and soils. *Geological Society of America Bulletin, Vol. 100, pp 1224-1236, August 1988.*

* Leech, S.J. 1988: Engineering geology and hydrogeology of Hanmer Springs, North Canterbury. Unpublished MSc. Thesis. University of Canterbury.

* Lensen, G.J. 1958: A method of Horst and graben formation. *Journal of Geology, Vol. 66, p579-587.*

* Mann, P., Hempton, M.R., Bradley, D.C. and Burke, K. 1983: Development of pull-apart basins. *Journal of Geology, Vol. 91, p 529-554.*

* McKay, A. 1890: On the earthquakes of September, 1888, in the Amuri and Marlborough Districts of the South Island. *NZ Geological Survey Report on Geological Exploration 1888-89 20:1-16.*

* Mendenhall, W. 1983: Introduction to probability and statistics. PWS Publishers.

* Nicol, A., Wise, D.U. and Bradshaw, J.D.1990: The Torlesse: New Zealands largest beanbag. Geological Society of New Zealand, Annual Conference.

* Reyners, M 1980: A microeartquake study of the plate boundary, North Island, New Zealand. *Geophysical Journal of the Royal Astronomical Society, Vol. 63, p1-22.*

* Rodgers, D.A. 1980: Analysis of pull-apart basin development produced by *en echelon* strike-slip faults. In *Sedimentation in Oblique-slip mobile zones. Secial publication of the International Association of Sedimentologists 4, p 27-41.*

* Savage, W.Z. and Varnes, D.J. 1987: Mechanisms of gravitational spreading of steep-sided ridges ("sackung"). *Bulletin of the Association of Engineering Geology, No. 35, pp 31-36.*

* Segall, P. and Pollard, D.D. 1980: Mechanics of discontinuous faults. *Journal of Geophysical Research, Vol. 85 p 4337-4350.*

* Slemmons, D.B. 1982: Determination of design earthquake magnitudes for microzonation. Proceedings of the Third International Earthquake Microzonation Conference, Vol. 1 p 119-130.

* Sibson, R.H. 1989: Earthquake faulting as a structural process. *Journal of Structural Geology, Vol. 11, No.1/2, pp 1 - 14, 1989.*

* Silberling, N.J.; Nichols, K.M.; Bradshaw, J.D. and Blome, C.D. 1988: Limestone and chert tectonic blocks from the Esk Head subterrane, South Island, New Zealand.*Geological Society of America Bulletin,*

Vol. 100, p 1213-1223.

* Sylvester, A.G. 1988: Strike-slip faults. *Geological Society of America Bulletin, Vol. 100, p1666-1703.*

* Walcott, R.I. 1978: Geodetic strains and large earthquakes in the axial tectonic belt of the North Island, New Zealand. *Journal of Geophysical Research, Vol. 83 p4429-4429.*

* Walcott,R.I. 1984a: The major structural elements of New Zealand. In An introduction to the Recent crustal movements of New Zealand. The Royal Society of New Zealand Miscellaneous series 7.

* Walcott, R.I. 1984b: The kinematics of the plate boundary zone through New Zealand: a comparison of short and long term deformations. *Geophysical journal of the Royal Astronomical society, Vol. 79, No. 2. p 613-633.*

* Wellman, H.W. 1953: ...Pleistocene faulting in the South Island of New Zealand. *New Zealand Journal of Science and Technology.*

* Whitehouse, I.E. and Bradshaw, J.D. 1988: Reconnaisance bedrock geology of the upper Rakaia River, Canterbury. New Zealand Geological Survey Report G135.

* Wyss, M. 1979: Estimating maximum expectable magnitude of earthquakes from fault dimensions. *Geology Vol. 7 p336-340.*

* Van Dissen, R.J. 1989: Late Quaternary faulting in the Kaikoura Region, Southeastern Marlborough, New Zealand. Unpublished MSc. thesis, University of Canterbury.

Appendix i Radiocarbon dates from Stream Loops locality. Dating and calibrating carried out by the Radiocarbon Dating Laboratory, Waikato University.

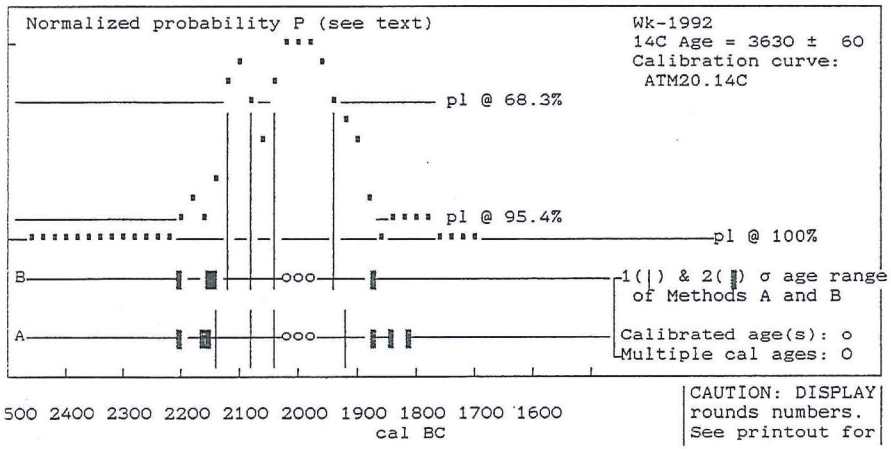

UNIVERSITY OF WASHINGTON
QUATERNARY ISOTOPE LAB
RADIOCARBON CALIBRATION PROGRAM 1987
REV. 2.0

Calibration file(s): ATM20.14C
Listing file: C14FIL.TXT
Plot file: C14FIL.PLT

Wk-1992
Radiocarbon Age BP 3630.0 ± 60.0† Reference(s)
Calibrated age(s) cal BC 2027, 1994, 1987 (Pearson and Stuiver)
cal BP 3976, 3943, 3936
cal AD/BC (cal BP) age ranges obtained from intercepts (Method A):
one Sigma** cal BC 2131-2074(4080-4023) 2045-1921(3994-3870)
two Sigma** cal BC 2192-2160(4141-4109) 2150-1880(4099-3829)
1832-1828(3781-3777)

Summary of above ---
minimum of cal age ranges (cal ages) maximum of cal age ranges:
one sigma cal BC 2131 (2027, 1994, 1987) 1921
cal BP 4080 (3976, 3943, 3936) 3870
two sigma cal BC 2192 (2027, 1994, 1987) 1828
cal BP 4141 (3976, 3943, 3936) 3777

cal AD/BC age ranges (cal ages as above) from probability distribution
(Method B):

% area enclosed	cal BC (cal BP) age ranges	relative area under probability distribution
68.3 (one sigma)	cal BC 2128-2077(4077-4026)	.29
	2043-1931(3992-3880)	.71
95.4 (two sigma)	cal BC 2194-2157(4143-4106)	.03
	2147-1878(4096-3827)	.96

References for datasets [and intervals] used:
Pearson, GW and Stuiver, M, 1986, Radiocarbon, 28, 839-862.

Comments:
†This standard deviation (error) may include a lab error multiplier.
IF SO SPECIFY!
** 1 sigma = square root of (sample std. dev.²+ curve std. dev.²)
2 sigma = 2 x square root of (sample std. dev.²+ curve std. dev.²)
0* represents a "negative" age BP
1955* denotes influence of bomb C-14

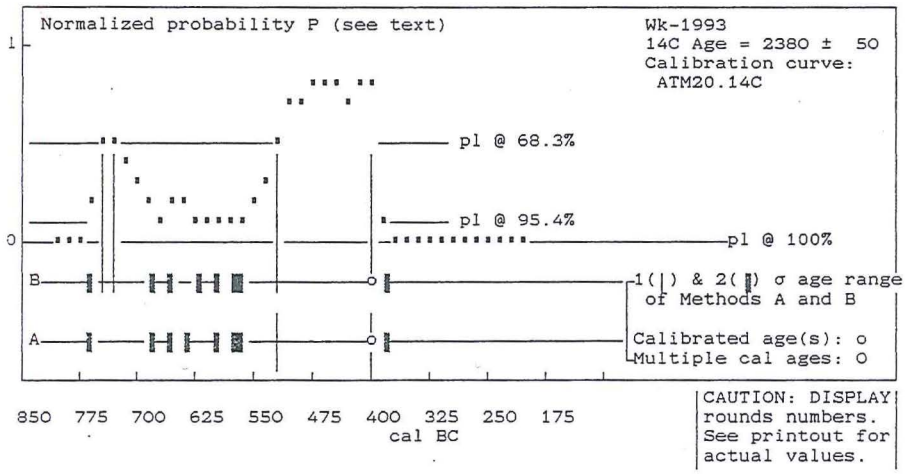

UNIVERSITY OF WASHINGTON
QUATERNARY ISOTOPE LAB
RADIOCARBON CALIBRATION PROGRAM 1987
REV. 2.0

Calibration file(s): ATM20.14C
Listing file: C14FIL.TXT
Plot file: C14FIL.PLT

Wk-1993
Radiocarbon Age BP 2380.0 ± 50.0†
Calibrated age(s) cal BC 405
cal BP 2354

Reference(s)
(Stuiver and Pearson)

cal AD/BC (cal BP) age ranges obtained from intercepts (Method A):
one Sigma** cal BC 517- 397(2466-2346)
two Sigma** cal BC 760- 682(2709-2631) 658- 635(2607-2584)
594- 581(2543-2530) 560- 390(2509-2339)

Summary of above ---
minimum of cal age ranges (cal ages) maximum of cal age ranges:
one sigma cal BC 517 (405) 397
cal BP 2466 (2354) 2346
two sigma cal BC 760 (405) 390
cal BP 2709 (2354) 2339

cal AD/BC age ranges (cal ages as above) from probability distribution (Method B):

% area enclosed	cal BC (cal BP) age ranges	relative area under probability distribution
68.3 (one sigma)	cal BC 750- 731(2699-2680)	.09
	524- 395(2473-2344)	.91
95.4 (two sigma)	cal BC 762- 678(2711-2627)	.21
	661- 631(2610-2580)	.03
	598- 573(2547-2522)	.02
	565- 384(2514-2333)	.74

References for datasets [and intervals] used:
Stuiver, M and Pearson, GW, 1986, Radiocarbon, 28, 805-838.

Comments:
†This standard deviation (error) may include a lab error multiplier.
IF SO SPECIFY!
** 1 sigma = square root of (sample std. dev.²+ curve std. dev.²)
2 sigma = 2 x square root of (sample std. dev.²+ curve std. dev.²)
0* represents a "negative" age BP
1955* denotes influence of bomb C-14

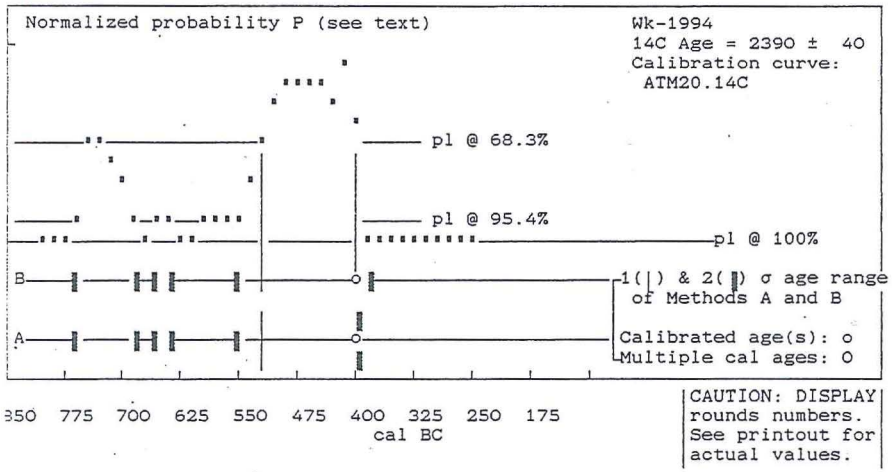

UNIVERSITY OF WASHINGTON
QUATERNARY ISOTOPE LAB
RADIOCARBON CALIBRATION PROGRAM 1987

UNIVERSITY OF WASHINGTON
QUATERNARY ISOTOPE LAB
RADIOCARBON CALIBRATION PROGRAM 1987
REV. 2.0

Calibration file(s): ATM20.14C
Listing file: C14FIL.TXT

Plot file: C14FIL.PLT

Wk-1994
Radiocarbon Age BP 2390.0 ± 40.0†
Calibrated age(s) cal BC 407
cal BP 2356

Reference(s)
(Stuiver and Pearson)

cal AD/BC (cal BP) age ranges obtained from intercepts (Method A):
one Sigma** cal BC 517- 400(2466-2349)
two Sigma** cal BC 758- 687(2707-2636) 653- 644(2602-2593)
546- 393(2495-2342)

Summary of above ---
minimum of cal age ranges (cal ages) maximum of cal age ranges:
one sigma cal BC 517 (407) 400
cal BP 2466 (2356) 2349
two sigma cal BC 758 (407) 393
cal BP 2707 (2356) 2342

cal AD/BC age ranges (cal ages as above) from probability distribution (Method B):

% area enclosed	cal BC (cal BP) age ranges	relative area under probability distribution
68.3 (one sigma)	cal BC 523- 398(2472-2347)	1.00
95.4 (two sigma)	cal BC 761- 681(2710-2630)	.20
	658- 637(2607-2586)	.02
	551- 392(2500-2341)	.77

References for datasets [and intervals] used:
Stuiver, M and Pearson, GW, 1986, Radiocarbon, 28, 805-838.

Comments:
†This standard deviation (error) may include a lab error multiplier.
IF SO SPECIFY!
** 1 sigma = square root of (sample std. dev.²+ curve std. dev.²)
2 sigma = 2 x square root of (sample std. dev.²+ curve std. dev.²)
0* represents a "negative" age BP
1955* denotes influence of bomb C-14

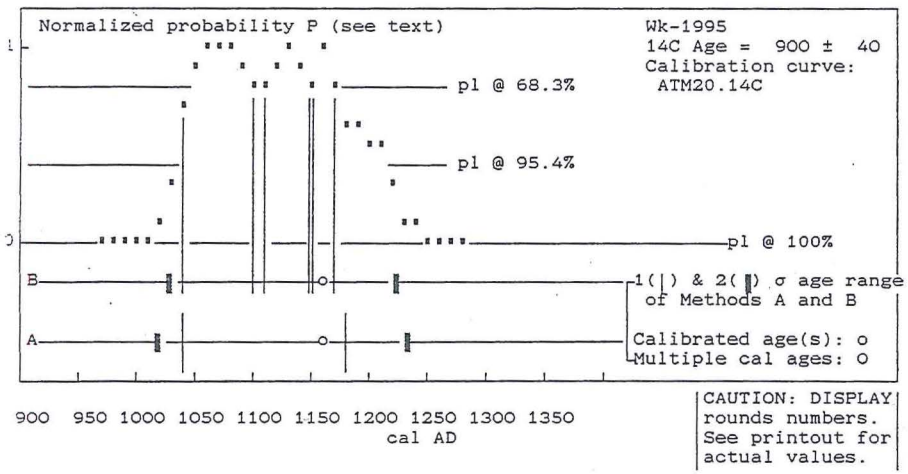

REV. 2.0

Calibration file(s): ATM20.14C
Listing file: C14FIL.TXT
Plot file: C14FIL.PLT

Wk-1995
Radiocarbon Age BP 900.0 ± 40.0†
Calibrated age(s) cal AD 1160
cal BP 790

Reference(s)
(Stuiver and Pearson)

cal AD/BC (cal BP) age ranges obtained from intercepts (Method A):
one Sigma** cal AD 1039-1184(911- 766)
two Sigma** cal AD 1024-1226(926- 724)

Summary of above ---
minimum of cal age ranges (cal ages) maximum of cal age ranges:

one sigma	cal AD 1039 (1160)	1184
	cal BP 911 (790)	766
two sigma	cal AD 1024 (1160)	1226
	cal BP 926 (790)	724

cal AD/BC age ranges (cal ages as above) from probability distribution (Method B):

% area enclosed	cal AD (cal BP) age ranges	relative area under probability distribution
68.3 (one sigma)	cal AD 1044-1103(906- 847)	.52
	1113-1149(887- 801)	.32
	1150-1169(800- 781)	.17
95.4 (two sigma)	cal AD 1032-1215(918- 735)	1.00

References for datasets [and intervals] used:
Stuiver, M and Pearson, GW, 1986, Radiocarbon, 28, 805-838.

Comments:
†This standard deviation (error) may include a lab error multiplier.
IF SO SPECIFY!
** 1 sigma = square root of (sample std. dev.²+ curve std. dev.²)
2 sigma = 2 x square root of (sample std. dev.²+ curve std. dev.²)
0* represents a "negative" age BP
1955* denotes influence of bomb C-14

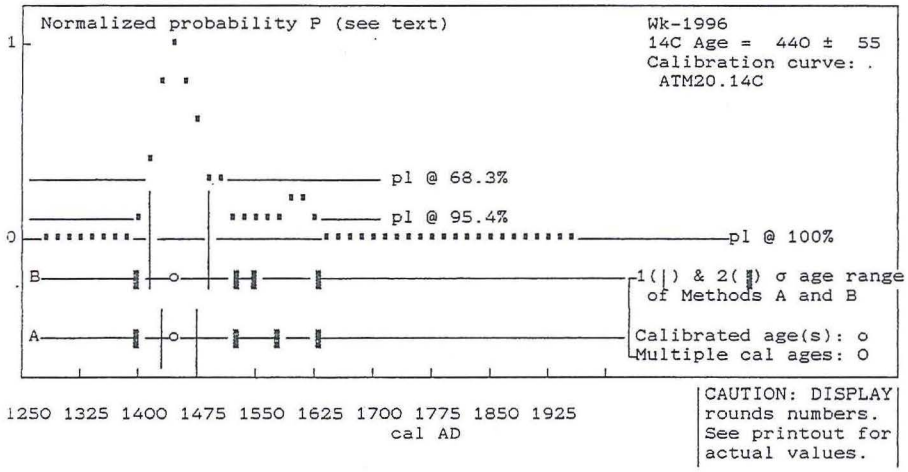

UNIVERSITY OF WASHINGTON
QUATERNARY ISOTOPE LAB
RADIOCARBON CALIBRATION PROGRAM 1987
REV. 2.0

Calibration file(s): ATM20.14C
Listing file: C14FIL.TXT
Plot file: C14FIL.PLT

Wk-1996
Radiocarbon Age BP 440.0 ± 55.0†
Reference(s)
Calibrated age(s) cal AD 1442
cal BP 508
(Stuiver and Pearson)

cal AD/BC (cal BP) age ranges obtained from intercepts (Method A):
one Sigma** cal AD 1424-1472(526- 478)
two Sigma** cal AD 1400-1520(550- 430) 1581-1624(369- 326)

Summary of above ---
minimum of cal age ranges (cal ages) maximum of cal age ranges:

one sigma	cal AD 1424 (1442)	1472
	cal BP 526 (508)	478
two sigma	cal AD 1400 (1442)	1624
	cal BP 550 (508)	326

cal AD/BC age ranges (cal ages as above) from probability distribution (Method B):

% area enclosed	cal AD (cal BP) age ranges	relative area under probability distribution
68.3 (one sigma)	cal AD 1411-1490(539- 460)	1.00
95.4 (two sigma)	cal AD 1398-1527(552- 423)	.85
	1556-1632(394- 318)	.15

References for datasets [and intervals] used:
Stuiver, M and Pearson, GW, 1986, Radiocarbon, 28, 805-838.

Comments:
†This standard deviation (error) may include a lab error multiplier.
IF SO SPECIFY!
** 1 sigma = square root of (sample std. dev.²+ curve std. dev.²)
2 sigma = 2 x square root of (sample std. dev.²+ curve std. dev.²)
0* represents a "negative" age BP
1955* denotes influence of bomb C-14

Appendix ii Seismic reflection profiles of Hanmer Basin. These profiles are included with permission from the Department of Scientific and Industrial Research, Geology and Geophysics. No part of them is to be reprinted without permission from the DSIR.


RANGE
Dog Stream Waterfall 31m
Jollies Pass
LXXII 864m
X No2 1058m
PG No2 631m lookout
Conical Hill 550 lookout
Motor camp
Water tank
Cemetary
Hospital
Golf course
Hanmer Springs
Hanmer Fault
Hope Fault
LINE 1
LINE 2
LINE 3
LINE 4
100
200
300
400
500
600
700
800
900
1000
1100
1200
1300
1367
982
616
Ford
Sawmill
Molesworth Farm
Chatterton
St Helens
Oxidation pond
Ben Nevis
Silos
Water tank
Karaha
Medway
Birch Topping A 1032m
Mt Leslie ML 952m
Leslie Pass 665
Druids Hill
5423 828m
5431 471m
5432
5433 596m
JOLLIES PASS
MULLANS ROAD
ROWAN ROAD
MT ISOBEL RD
MENZIES RD
JOLLIFFE RD
GULLY RD
PAWSON ROAD
MT DUMBLANE RD
CHATTERTON RD
JACKS PASS
McINTYRE RD
SWITCHBACK ROAD
HYDRO ROAD
LARCH RD
ANDREWS ROAD
HEATHERINGTON ROAD
PERCIVAL ROAD
HIGH ROAD
SAWYERS ROAD
HUNTER ROAD
LOOP RD
ROLLS ROAD
RIPPINGALE ROAD
MAIN ROAD
MONTGOMERY ROAD
JUBILEE ROAD
MORRISON ROAD
BURMA ROAD
OLD COACH ROAD
HERDMANS ROAD
PHILLIPS ROAD
FOWLERS LANE
MANSFIELD ROAD
LANE
SHORTCUT ROAD
ROCHE ROAD
DEADMAN RD
McKAYS ROAD
COB ROAD
GUN RD
LESLIE PASS
AVELING ROAD
HOPKINS ROAD
FORBES ROAD
MOORHOUSE AVENUE
CHATTERTON ROAD
HANMER ROAD
RIVER ROAD
Hanmer River
Percival River
Dog Stream
Stream
AMURI

Appendix iii Downcutting rates of the Hanmer River at Boundary Stream. Refer to Section 3.3.

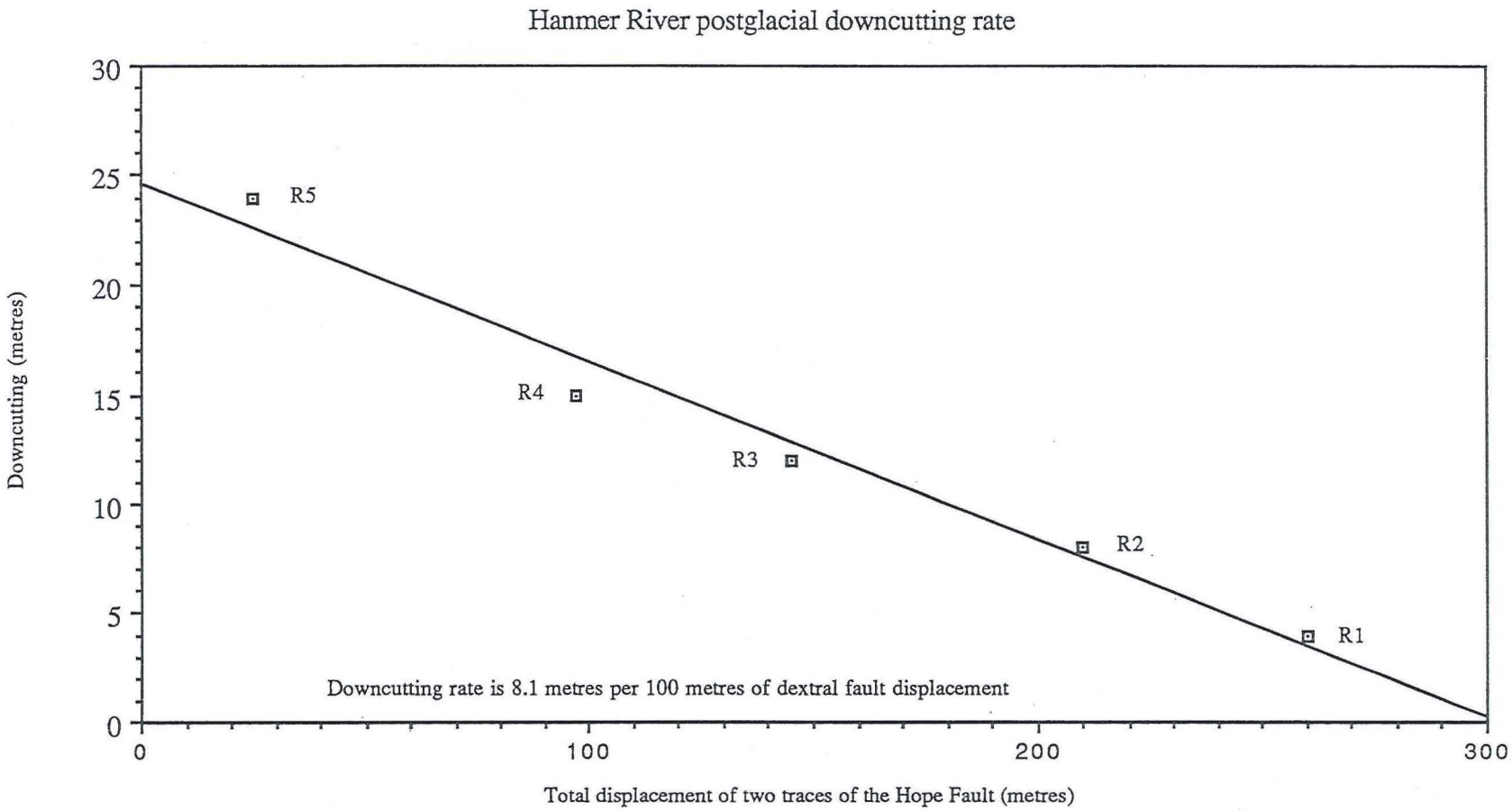

Appendix 3 Graph of the downcutting rate of the Hanmer River at the Boundary Stream site (refer Section 3.3). Downcutting is measured in metres below the height of the top of riser R. Based on the slip-rate inferred from the stream-loops site, the age of the highest surface is 14,400 years.